博士論文

Design, synthesis, and evaluation of fluorogenic cyanine dyes for nucleolar RNA imaging in living cells: effect of regioisomers on probe functions

(生細胞核小体 RNA イメージングのための蛍光性シアニン色素の設計・合成と機能評価：プローブ機能に及ぼす位置異性体の効果)

HE Mengmeng

2023

Acknowledgments

The five-year journey of studying abroad has been full of hardships. I would like to express my deep gratitude to those who have helped me.

First of all, I would like to sincerely thank Prof. NISHIZAWA seiichi and Prof. Sato Yusuke. Three years ago, they gave me the precious opportunity to enter this lab and started my journey to pursue my Ph.D. degree. Prof. NISHIZAWA seiichi and Prof. Sato Yusuke have always been very kind to me, never scolded me harshly, always encouraged me and gave me valuable advice. When I encountered difficulties, they always patiently instructed me and gave me help and guidance. It can be said that without their guidance, I could not have completed my doctoral course so smoothly. Once again, I would like to express my most sincere gratitude to them!

Secondly, I would like to give special thanks to my fellow students in the Nishizawa Lab. Three years ago, my study was switched from theoretical research to experimental research, and I was not good at experimental operations at first. Fortunately, the atmosphere in the Lab. was very harmonious and the members were very friendly, they patiently taught me how to do experiments and explained the principles. Special thanks to Kei Higuchi, Michiyuki Suzuki, Masao Nagaoka and Lee En Ting Tabitha.

In addition, I would like to sincerely thank my family. I come from a small village in China, and my family is not rich, but my parents went out of their way to support my study and life in Japan. Without their support, I would not have been able to receive a better education in Japan.

I would especially like to thank my boyfriend, who has been with me throughout these five years. Like any other person pursuing a doctoral degree, I have been filled with anxiety for graduation and loneliness in a foreign century. He not only waited for me throughout these five years, but also tolerated my little tantrums, comforted me, and provided emotional and financial support. I can't imagine how I would have spent these years in a foreign country without him.

Also I would like to thank my friends who have always given me endless support and encouragement，including but not limited to Tianxue Han, Xinyu Fan, He Luo, Yawen Wu, Ujuagu Akunna Francess, Chioma Uche Okeke. We have had many happy times together and I am so grateful to all of you for your continued companionship and encouragement.

Last but not least, I would like to express my special thanks to CSC (China Scholarship Council) for the financial support, which allowed me to concentrate on my experimental research without worrying about financial problems in the past two years.

Abstract

The thesis consists of **5 chapters.**

Introduction (chapter 1）

RNA-selective small molecular weight probes have been of great interest as a tool for the regulation, inhibition, and/or study of biological RNA functions. Of my particular interest is the design of fluorogenic dyes for the imaging of nucleolar RNA in living cells, given the considerable attention on the role of nucleolus in major physiological functions such as stress response, development and aging, and canceration. While the signaling ability of a commercially available dye (SYTO RNA-select) is promising, it is not applicable to living cells, having a limited use for fixed and permeabilized cells. A variety of chemical scaffolds have therefore been proposed for the imaging of nucleolar RNA in living cells, but the signaling abilities of most probes are only moderate compared to SYTO RNA select. On the other hand, our group has recently developed novel cyanine dyes, including red-emissive BIQ and yellow-emissive BIOP. Both probes are characterized as outstanding off-on signaling ability and inherent RNA selectivity over DNA in solutions and live cells, indicating that cyanine dyes are good candidates as RNA selective dye for nucleolar RNA imaging in living cells.

In this work, three kinds of typical cyanine dyes and their regioisomers were examined for the development of novel RNA selective dyes for nucleolar RNA imaging in living cells. In particular, I examined effect of regioisomers on probe functions.

Results and discussions

Thiazole orange and their derivatives (chapter 2) : First, I focused on thiazole orange (TO, λ_{em} = 532 nm), a typical unsymmetrical monomethine cyanine dye, due to its large fluorescence enhancement when binding with nucleic acid as well as the easily modified structure. In addition, three kinds of TO derivatives, TO-H, TO-C_4, and 2TO were prepared, and their binding and signaling properties were evaluated. It was found that TO showed the response selectivity for RNA over DNA (I_{RNA}/I_{DNA} = 2), and its light up property (I/I_0 = 580-fold, Φ_{bound}/Φ_{free} = 400) even compared with commercial SYTO RNA select (I/I_0 = 500-fold, Φ_{bound}/Φ_{free} = 16). More interestingly, 2TO (λ_{em} = 532 nm), a regioisomer of TO, did work much better as a RNA selective dye (I_{RNA}/I_{DNA} = 3.7) where the value of Φ_{bound}/Φ_{free} reached 1200 (I/I_0 = 430-fold). Furthermore, it was found that TO had a good cell plasma and nuclear membrane permeability in living cells, and was applicable to the imaging of nucleolar RNA in living cells. Significantly, much better image was obtained by 2TO, where the nucleolus was clearly stained with a much higher contrast, revealing the potential of 2TO as RNA-selective dye for live cell imaging. These results may indicate that the isomerization of TO is key to improving RNA selectivity.

Quinoline blue and its regioisomer (chapter 3) : Based on the above-mentioned finding, quinoline blue (QB, λ_{em} = 609.5 nm), the first synthesized cyanine dye, as well as its regioisomer, 2QB (also known as QV, λ_{em} = 578 nm) were developed and examined as RNA selective dyes. It was found that both probes showed RNA selectivity over DNA in solutions (QB, I_{RNA}/I_{DNA} = 1.6; 2QB, I_{RNA}/I_{DNA} = 2.8), and applicable to nucleolar RNA imaging in living cells. Similarly to the TO system, 2QB, the regioisomer worked much better than QB, where 2QB showed remarkable light-up response (I/I_0 = 640-fold), better

than QB (I/I_0 = 320-fold). In fact, 2QB is one of the top level of yellow emissive dye with off-on signaling ability. Additionally, the regioisomer showed relatively good photostability in solutions and cells. The live cell imaging experiment was consistent with the solution-based experiments, demonstrating that the regioisomer 2QB exhibits superior selectivity for nucleolar RNA compared to QB, where 2QB displays higher contrast to the nucleus. This further underscores the effectiveness of isomerization in improving probe functions, such as RNA selectivity, light-up properties, and photostability.

Thiazole red and its regioisomer (chapter 4) : Finally, the representative unsymmetrical trimethine cyanine dye thiazole red (TR, λ_{em} = 661 nm) and its regioisomer 2TR (λ_{em} = 615 nm) were synthesized and their functions were examined. While TR showed pretty good light-up signaling ability (I/I_0 = 200-fold, Φ_{bound}/Φ_{free} = 165), I found that TR showed DNA selectivity over RNA in solution (I_{RNA}/I_{DNA} = 0.9), and its photostability was extremely poor. Furthermore, TR could not be used for nucleolar RNA imaging. On the other hand, 2TR, the regioisomer of TR, was found to work as a promising red-emissive fluorogenic probe for nucleolar RNA imaging in living cells, showing pretty good off-on signaling ability (I/I_0 = 320-fold, Φ_{bound}/Φ_{free} = 35), improved photostability and superior selectivity to RNA (I_{RNA}/I_{DNA} = 1.9) in both solution and living cells.

Conclusions (chapter 5)

In summary, three kinds of typical cyanine dyes and their isomers were examined in this work. Except for TR, the other cyanine dyes were found for the first time to work as nucleolar RNA selective dye in living cell, indicating cyanine dyes are indeed good candidates as RNA selective dye. More significantly, for all cases, the regioisomers did work much better. The isomerization is indeed key to improving RNA selectivity which may provide a helpful strategy for the design of RNA selective dyes.

CONTENT

Chapter 1

General introduction

1. Nucleolus and nucleolar RNA imaging in living ells

The nucleolus is considered one of the most prominent structures in the cell nucleus. It is the site of ribosomal RNA (rRNA) transcription, pre-rRNA processing, and ribosome subunit assembly, playing a crucial role in the synthesis of ribosomal RNA (rRNA) and assembly of nascent ribosomes.[1,2] A typical metazoan nucleolus consists of three major elements, FC (the fibrillar center), DFC (the dense fibrillar component) and GC (the granular component),[3] as the Fig. 1-1-B shown. Transcription of the rDNA repeats mainly occurs at the border between the FC and DFC, with RNA pol I subunits being enriched in the FC region. On the other hand, the processing and modification of the pre-rRNA transcripts take place predominantly in the DFC, where the snoRNPs accumulate. Additionally, most proteins concentrate in the GC region where ribosome subunit assembly is completed.[4]

Following our Lab's previous work on developing fluorescent probes targeting biologically important RNAs, such as an abasic site duplex RNA,[5-8] siRNA,[9-11] the bacterial A-site RNA,[12-15] double-stranded RNA,[16-23] of my particular interest is the design of fluorogenic dyes for the imaging of nucleolar RNA in living cells. Indeed, nucleolus imaging in living cells is an essential tool for real-time detection and monitoring RNA functions, considering the role of nucleolus in major physiological functions such as stress response,[24][25] development and aging,[26] and canceration.[27][28]

(A) (B)

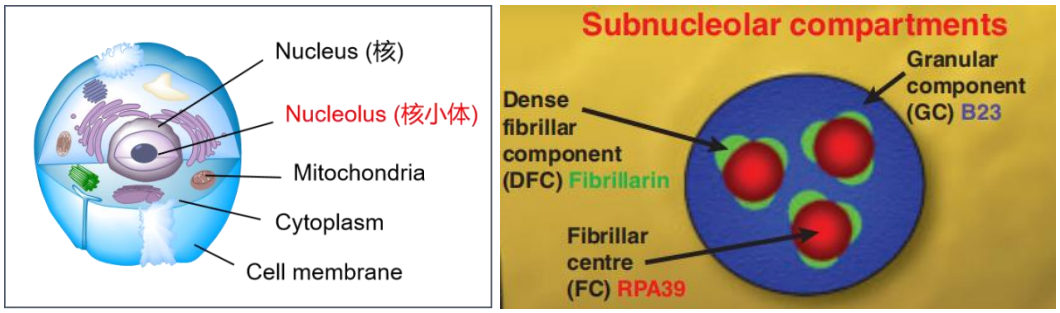

Fig. 1. 1-1 (A) Cell structure and (B) subnucleolar compartment[1].

2. RNA analysis methods

2.1 Molecular beacon

Molecular beacons is a widely used method for RNA imaging in cells by using nucleic acid hybridization techniques.[29-33] It was firstly proposed by Sanjay Tyagi and Fred Russell Kramer in 1996.[34] As illustrated in the Fig. 1.2-1, molecular beacon is a stem-loop structured single-stranded oligonucleotide sequence. A fluorescent molecule and a quencher are attached to the end of the stem, respectively. It is present in the form of a stem ring before the molecular beacons bind with the target RNA. In this situation, it shows almost non-fluorescence because the fluorescence molecule and quencher are close. Here, the emitted fluorescence will be absorbed by the quencher group through fluorescence resonance energy transfer. In sharp contrast, it will gives strong fluorescence when a molecular beacon specifically binding with the target RNA. This is because the molecular beacon and target RNA formed hybrid molecule separates the fluorescent molecule and quencher so that the fluorescence emitted by the fluorescent molecule cannot be absorbed by the quencher group.

However, the large molecular weight structure of molecular beacons does result in poor cell membrane permeability, which makes them difficult to apply to live cell RNA imaging and may have a negative affect on the cell.

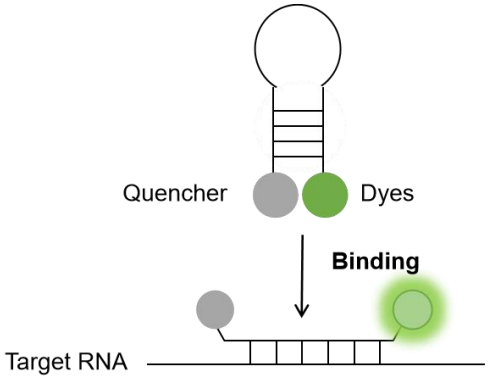

Fig. 1. 2-1 Schematic of molecular beacon bind to the target RNA.

2.2 FISH method

Fluorescent in situ hybridization (FISH) is a commonly used technology for detecting and locating specific nucleic acid by hybridizing a fluorescent probe with the nucleic acid sequence.[35] In general, the fluorescence probe and nucleic acid sequence should have high similarity so that the fluorescent probe could show high selectivity and specificity. But because of this, FISH method is time-consuming to design the specific fluorescence probe. What's more, it was reported that the FISH method is only applicable to fixed and permeablized cells.[36-40]

3. Small molecular weight RNA selective fluorescent probes design

RNA-selective small molecular weight fluorescent probes have been of great interest as a promising tool for the regulation, inhibition, and/or study of biological RNA functions.[41-48] Generally an ideal small molecular weight fluorescent probe for nucleolar RNA imaging in living cells should meet the properties such as RNA selectivity, prominent off-on signaling ability, high binding affinity, good cell permeability, good water solubility, high quantum, good photostability and low cytotoxicity.[49] However, it is not easy to design a perfect fluorescent small molecular weight probe that possess all of the attractive properties. The major challenge in designing fluorescent probes is making the small molecular weight probes selectively bind with nucleolar RNA rather than DNA because of their similar structure. Usually fluorescent probes tend to preferentially bind with the major grooves in DNA because the wider major groove provides a much larger contact area and more interact sites, compared with RNA.

4. Commercially available nucleolus imaging probes in cells

Up to date, only two kinds of dyes are commercially available for nucleolar RNA imaging in cells. One is SYTO RNA select (λ_{em} = 530 nm), while the other is Nucleolus Bright (Green: λ_{em} = 537 nm, Red: λ_{em} = 605 nm). While their chemical structures have been undisclosed. When free in solutions, both dyes are almost non-fluorescent, but their fluorescence is significantly enhanced upon binding to RNA. In the case of SYTO RNA select, the light-up factor (I/I_0, where I and I_0 denote fluorescence intensities at λ_{em} in the presence and absence of 1.0 mM *E. coli* total RNA, respectively) reached 500-fold, which was accompanied by an increase in the fluorescence quantum yield (Φ_{bound} = 0.36).[50] In the case of Nucleolus Bright, it was demonstrated that the nucleolus was clearly stained without any washing steps.[51] Although such signaling and staining abilities are indeed promising, these two dyes do not apply to living cells, having a limited use for fixed and permeabilized cells. Therefore, probes for nucleolar RNA imaging in living cells are desirable.

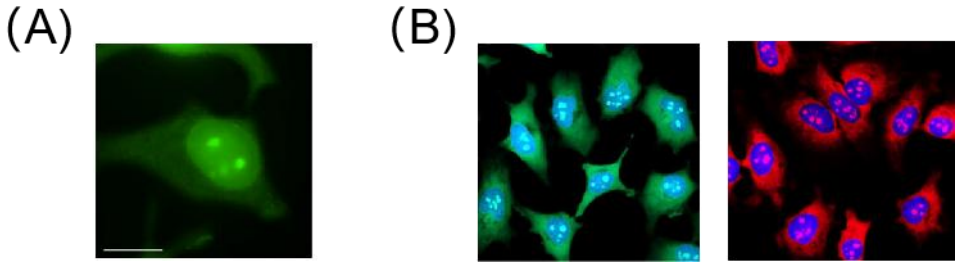

Fig. 1. 4-1 Fixed and permeabilized cell imaging. (A) Fixed and permeabilized MCF7 cell imaging. [SYTO RNA select] = 500 nM. Incubation time: 20 min. Scale bar: 15 μm.[52] (B) Fixed and permeabilized HeLa cell imaging. [Nucleolus bright green/red] = 1 μmol/L. Incubation time: 5 min.[51]

5. Recently researches on designing small molecular weight probes for RNA imaging in cells

Much effort has thus been devoted to developing new small fluorescent molecular probes for the imaging of nucleolar RNA in living cells. Various chemical scaffolds have been proposed to this end, including styryl-based dyes,[53,54,55] trimethine cyanine dye,[56] Nile Blue derivatives,[57] hemicyanine dye,[58] naphthalimide derivatives,[59] coumarin-fused pyronin,[60,61] indole-based cyanine,[62,63] meso-substituted thiazole orange,[64] and thiazole orange derivatives.[65] Unfortunately, the signaling abilities of most probes are only moderate compared to SYTO RNA select, and there are limited reports addressing the light-up property of the probes despite their importance to achieve sensitive and wash-free imaging.[66] In addition, a relatively high concentration of probes was usually required for live-cell imaging experiments probably due to their low membrane permeability in living cells. Imaging under a lower probe concentration should be beneficial because it can significantly reduce the damage caused to the biological systems inside the cells.[53,67,68] What more important is that no strategy is given to design RNA selective dyes among with previous researches.

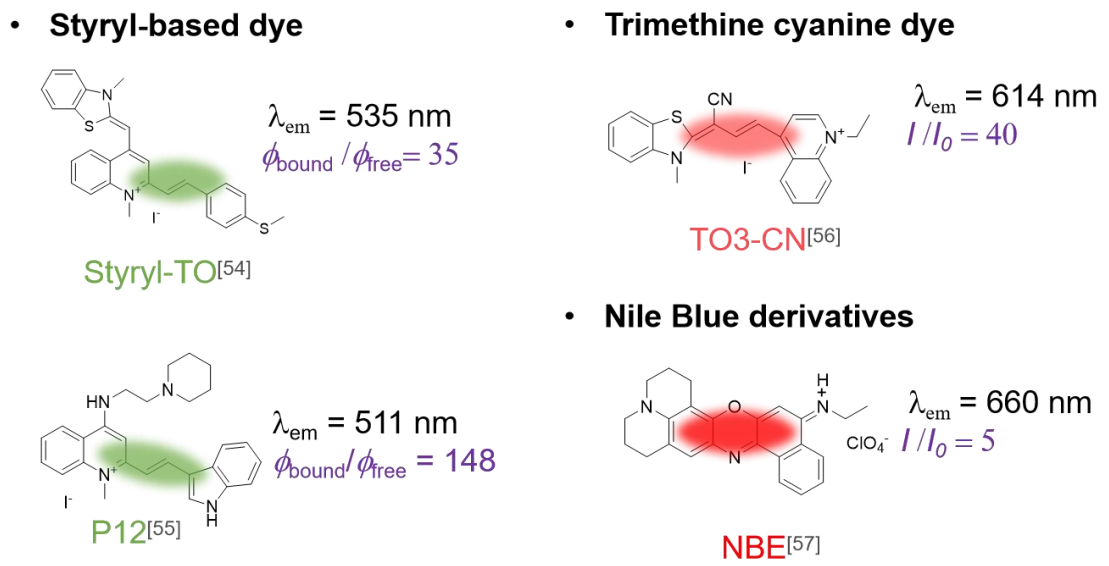

Fig. 1. 5-1 Several representative examples of developed fluorescent small molecular weight probes for nucleolus imaging in living cells.

6. Previous research in our Lab. on developing cyanine dyes

Our laboratory have recently developed novel unsymmetrical monomethine cyanine dyes for nucleolar RNA imaging in living cells, including yellow emissive benzo[c,d]indole-oxazolo[5,4-c]pyridine (BIOP, λ_{em} = 570 nm),[50] and deep-red emissive benzo[c,d]indole-quinoline (BIQ, λ_{em} = 657 nm).[69,70] Both BIQ and BIOP are characterized by the fluorogenic off-on signaling ability upon binding to RNA, which almost compared to SYTO RNA select. Notably, the light up factor (I/I_0) of BIOP (1.0 μM) reached 770-fold (Φ_{free} = 0.00038, Φ_{bound} = 0.52) in the presence of 1.0 mM *E. coli* total RNA. We have demonstrated highly sensitive imaging of nucleolar RNA in living cells, where BIOP was able to stain the nucleolus even at the concentration as low as 50 nM. The nucleolar RNA imaging by such a low concentration and distinguished signaling ability has never been demonstrated for other types of probes,[11-18] indicating the potential of cyanine dyes for nucleolar RNA imaging in living cells.

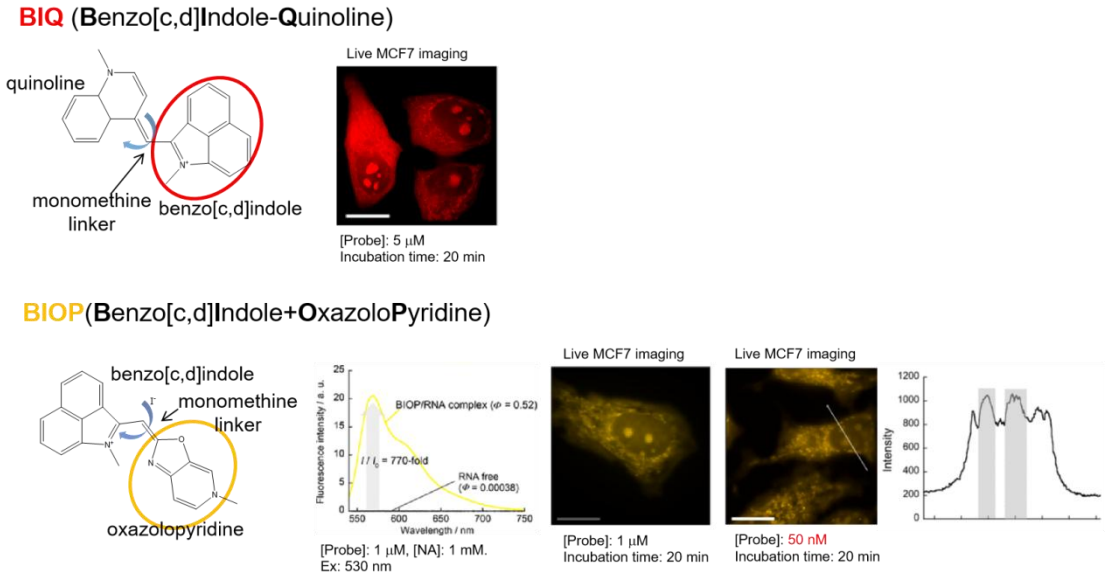

Fig. 1. 6-1 Cyanine dyes developed in our Lab. for nucleolus imaging in living cells.

7. Purpose of my study

The purpose of my study is to design fluorogenic probe with outstanding off-on signaling ability for nucleolar RNA imaging in living cells at a low work concentration. Furthermore, I aim to develop helpful strategy for design RNA selective dyes.

To this end, three kinds of typical cyanine dyes, including the unsymmetrical monomethine dye, TO, the symmetrical monomethine dye, QB, as well as the unsymmetrical trimethine dye, TR, were developed. Their regioisomers, 2TO, 2QB and 2TR as well as TO derivatives, TO-H and TO-C_4 were examined.

8. Reference

1. Y. W. Lam, L. Trinkle, Mulcahy, and A. I. Lamond, *J. Cell Sci.*, **2005**, *118*, 1335-1337.
2. T. Pederson, *Cold Spring Harb Perspect Biol.*, **2011**, *3*, a000638.
3. U. Scheer and R. Hock, *Nucleus and gene expression*, **1999**, *11*, 365-390.
4. F. -M. Boisvert, S. Koningsbruggen, J. Navascués and A. I. Lamond, *Nat. Rev., Mol. Cell Bio.*, **2007**, *8*, 574-585.
5. Y. Sato, T. Ichihashi, S. Nishizawa, N. Teramae, *Angew. Chem. Int. Ed.*, **2012**, *51*, 6369-6372.
6. Y. Sato, Y. Toriyabe, S. Nishizawa, N. Teramae, *Chem. Commun.*, **2013**, *49*, 9983-9985.
7. Y. Sato, M. Kudo, Y. Toriyabe, S. Kuchitsu, C.-X. Wang, S. Nishizawa, N. Teramae, *Chem. Commun.*, **2014**, *50*, 515-517.
8. Y. Sato, H. Saito, D. Aoki, N. Teramae, S. Nishizawa, *Chem. Commun.*, **2016**, *52*, 14446-14449.
9. T. Sato, Y. Sato, K. Iwai, S. Kuge, S. Nishizawa, N. Teramae, *Chem. Commun.*, **2015**, *51*, 1421-1424.
10. T. Sato, Y. Sato, K. Iwai, S. Kuge, N. Teramae, S. Nishizawa, *Anal. Sci.*, **2015**, *31*, 315-320.
11. Y. Sato, M. Kaneko, T. Sato, S. Nakata, Y. Takahashi, S. Nishizawa, *ChemBioChem*, **2019**, *20*, 408-414.
12. Y. Sato, M. Rokugawa, S. Ito, S. Yajima, H. Sugawara, N. Teramae, S. Nishizawa, *Chem. Eur. J.*, **2018**, *24*, 13862-13870.
13. Y. Sato, S. Yajima, A. Taguchi, K. Baba, M. Nakagomi, Y. Aiba, S. Nishizawa, *Chem. Commun.*, **2019**, *55*, 3183-3186.
14. Y. Sato, Y. Aiba, S. Yajima, T. Tanabe, K. Higuchi, S. Nishizawa, *ChemBioChem*, **2019**, *20*, 2752-2756.
15. Y. Ito, Y. Sato, N. Teramae, S. Nishizawa, *BUNSEKI KAGAKU*, **2021**, *70*, 149-157.
16. T. Sato, Y. Sato, S. Nishizawa, *J. Am. Chem. Soc.*, **2016**, *138*, 9397-9400.
17. T. Sato, Y. Sato, S. Nishizawa, *Chem. Eur. J.*, **2017**, *23*, 4079-4088.
18. T. Chiba, T. Sato, Y. Sato, S. Nishizawa, *Org. Biomol. Chem.*, **2017**, *15*, 7765-7769.
19. T. Tanabe, T. Sato, Y. Sato, S. Nishizawa, *RSC Adv.*, **2018**, *8*, 42095-42099.
20. Y. Sato, Y. Takahashi, T. Tanabe, S. Nishizawa, *Org. Biomol. Chem.*, **2020**, *18*, 4009-4013.
21. E. T. T. Lee, Y. Sato, S. Nishizawa, *Chem. Commun.*, **2020**, *56*, 14976-14979.
22. T. Sato, Y. Sato, S. Nishizawa, *Biopolymers*, **2021**, e23474.

23. Y. Sato, H. Miura, T. Tanabe, C. U. Okeke, A. Kikuchi, S. Nishizawa, *Anal. Chem.*, **2022**, *94*, 7814-7822.

24. M. O. J. Olson, *Science's STKE*, **2004**, *224*, pe10.

25. S. Boulon, B. J. Westman, S. Hutten, F. M. Boisvert, and A. I. Lamond, *Molecular Cell*, **2010**, *40*, 216-227.

26. N. O. Kalinina, S. Makarova, A. Makhotenko, A. J. Love and M. Taliansky, *Front. Plant Sci.*, **2018**, *9*.

27. V. Tiku, A. Antebi, *Tends in cell biology*, **2018**, *28*, 662-672.

28. L. B. Maggi Jr., C. L. Winkeler, A. P. Miceli, A. J. Apicelli, S. N. Brady, M. J. Kuchenreuther, J. D. Weber, *Biochimica et Biophysica Acta*, **2014**, *1842*, 831-839.

29. P. J. Santangelo, B. Nix, A. Tsourkas, G. Bao, *Nucleic Acids Research*, **2004**, *32*, No. 6 e57.

30. P. J. Santangelo, N. Nitin, G. Bao, *Journal of Biomedical Optics*, **2005**, *10 (4)*, 044025.

31. W. J. Rhee, P. J. Santangelo, H. Jo, and G. Bao, *Nucleic Acids Research*, **2008**, *36*, No. 5 e30.

32. M. Chen, Z. Ma, X. Wu, S. Mao, Y. Yang, J. Tan, C. J. Krueger and A. K. Chen, *Scientific Reports*, **2017**, *7*, 1550.

33. Y. Kam , A. Rubinstein , S. Naik, I. Djavsarov, D. Halle , I. Ariel, A. O. Gure, A. Stojadinovic, H. Pan, V. Tsivin, A. Nissan, E. Yavin, *Cancer Letters*, **2014**, *352*, 90-96.

34. S. Tyagi, F. Kramer, *Nat Biotechnol.*, **1996**, 14, 303-308.

35. J. G. Bauman, J. Wiegant, P. Borst, P. V. Duijn, *Exp. Cell Res.*, **1980**, *128*, 485-490.

36. C. Meyer, A. Garzia, T. Tuschl, *Methods*, **2017**, *118-119*, 101-110.

37. J. Y. Kishi, S. W. Lapan, B. J. Beliveau, E. R. West, A. Zhu, H. M. Sasaki, S. K. Saka, Y. Wang, C. L. Cepko and P. Yin, *Nature Methods*, **2019**, *16*, 533-544.

38. J. R. Sinnamon, K. Czaplinski, *RNA*, **2014**, *20*, 260-266.

39. M. O. Urbanek, W. J. Krzyzosiak, *Methods*, **2016**, *98*, 115-123.

40. D. W. Hwang, Y. Choi, D. Kim, H. Y. Park, K. W. Kim, M. Y. Kim, C. Park, D. S. Lee, *Nanomedicine: Nanotechnology, Biology, and Medicine*, **2019**, *16*, 162-172.

41. C. S. Chow and F. M. Bogdan, *Chem. Rev.*, **1997**, *97*, 1489-1513.

42. J. R. Thomas and P. J. Hergenrother, *Chem. Rev.*, **2008**, *108*, 1171-1224.

43. S. L. Wicks and A. E. Hargrove, *Methods*, **2019**, *167*, 3-14.

44. A. U. Juru and A. E. Hargrove, *J. Biol. Chem.*, **2021**, *296*, 100191.

45. Y. Xia, R. Zhang, Z. Wang, J. Tian and X. Chen, *Chem. Soc. Rev.*, **2017**, *46*, 2824-2843.

46. S. H. Alamudi and Y.-T. Chang, *Chem. Commun.*, **2018**, *54*, 13641-13653.

47. N. Köcker, F. P. Weissenboeck and A. Rentmeister, *Chem. Soc. Rev.*, **2020**, *49*, 8749-8773.

48. G. Yang, T. Song, M. Wang, M. Li, Q. Su, Z. Xie, X. Xie, H. Zhang, Y. Feng, C. Wu, Y. Liu and H. Yang, *ACS Appl. Nano Mater.*, **2022**, *5*, 3065-3086.

49. Y. V. Suseela, N. Narayanaswamy, S. Pratihar and T. Govindaraju, *Chem. Soc. Rev.*, **2018**, *47*, 1098.

50. K. Higuchi, Y. Sato, N. Togashi, M. Suzuki, Y. Yoshino and S. Nishizawa, *ACS Omega*, **2022**, *7*, 23744-23748.

51. https://www.dojindo.eu.com/Nucleolus-Bright-Green.aspx.

52. K. Higuchi, Master thesis, **2021**.

53. Q. Li, Y. Kim, J. Namm, A. Kulkarni, G. R. Rosania, Y.-H. Ahn and Y.-T. Chang, *Chem. Biol.*, **2006**, *13*, 615-623.

54. Y. Lu, Q. Deng, D Hu, Z. Wang, B. Huang, Z. Du, Y. Fang, W. Wong, K. Zhang and C. Chow, *Chem. Commun.*, **2015**, *51*, 15241-15244.

55. C. Wang, Y. Lu, S. Cai, W. Long, Y. Zheng, J. Lin, Y. Yan, X. Huang, W. Wong, K. Zhang and C. Chow, *Sens. Actuators, B*, **2018**, *262*, 386-394.

56. S. Zhang, J. Fan, Z. Li, N. Hao, J. Cao, T. Wu, J. Wang and X. Peng, *J. Mater. Chem. B*, **2014**, *2*, 2688-2693.

57. Q. Yao, H. Li, L. Xian, F. Xu, J. Xia, J. Fan, J. Du, J. Wang and X. Peng, *Biomaterials*, **2018**, *177*, 78-87.

58. Z. Li, S. Sun, Z. Yang, S. Zhang, H. Zhang, M. Hu, J. Cao, J. Wang, F. Liu, F. Song, J. Fan and X. Peng, *Biomaterials*, **2013**, *34*, 6473-6481.

59. C. Cao, P. Wei, R. Li, Y. Zhong, X. Li, F. Xue, Y. Shi and T. Yi, ACS Sens., 2019, 4, 1409-1416.

60. B. Zhou, W. Liu, H. Zhang, J. Wu, S. Liu, H. Xu and P. Wang, *Biosens. Bioelectron.*, **2015**, *68*, 189-196.

61. W. Liu, B. Zhou, G. Niu, J. Ge, J. Wu, H. Zhang, H. Xu and P. Wang, *ACS Appl. Mater. Interfaces*, **2015**, *7*, 7421-7427.

62. G. Song, Y. Sun, Y. Liu, X. Wang, M. Chen, F. Miao, W. Zhang, X. Yu and J. Jin, *Biomaterials*, **2014**, *35*, 2103-2112.

63. L. Guo, M. S. Chan, D. Xu, D. Y. Tam, F. Bolze, P. K. Lo and M. S. Wong, *ACS Chem. Biol.*, **2015**, *10*, 1171-1175.

64. L. Guan, A. Li, Y. Song, M. Yan, D. Gao, X. Zhang, B. Li and L. Wang, *J. Org. Chem.*, **2016**, *81*, 6303-6313.

65. D. Aristova, V. Kosach, S. Chernii, Y. Slominsky, A. Balanda, V. Filonenko, S. Yarmoluk, A. Rotaru, H. G. Özkan, A. Mokhir and V. Kovalska, *Methods Appl. Fluoresc.*, **2021**, 9, 045002.

66. F. Hövelmann, I. Gaspar, J. Chemiolo, M. Kasper, J. Steffffen, A. Ephrussi and O. Seitz, *Chem. Sci.*, **2016**, 7, 128-135.

67. W. Sun, J. Fan, C. Hu, J. Cao, H. Zhang, X. Xiong, J. Wang, S. Cui, S. Sun and X. Peng, *Chem. Commun.*, **2013**, *49*, 3890-3892.

68. C. G. Guzman, A. Fernandez, N. Avlonitis, M. Bradley and M. Vendrell, *Comb. Chem. High Throughput Screening*, **2016**, *19*, 353-361.

69. Y. Yoshino, Y. Sato and S. Nishizawa, *Anal. Chem.*, **2019**, *91*, 14254-14260.

70. Y. Sato, Y. Igarashi, M. Suzuki, K. Higuchi and S. Nishizawa, *RSC Adv.*, **2021**, *11*, 35436-35439.

Chapter 2

The classical thiazole orange and its regioisomer as fluorogenic probes for nucleolar RNA imaging in living cells

(M. He, Y. Sato, S. Nishizawa, *Analyst*, **2023**, *148*, 636-642)

1. Introduction

Indeed, unsymmetrical monomethine cyanine dyes have been widely used for nucleic acid detection (DNA and RNA) in solutions. Thiazole orange (TO, Fig. 1-1), consisting of benzothiazole and quinoline heterocycles via a monomethine bridge, is a representative of this class of dyes, and its off-on signaling ability is outstanding as a DNA staining dye (Φ_{free} = 0.0002, Φ_{bound} for calf thymus DNA = 0.11).[1] In addition to being used for staining DNA in gels,[2] TO has been utilized in reticulocyte analysis to stain residual RNA of blood cells.[3] TO was also utilized as an indicator in fluorescence indicator displacement (FID) assay to characterize small molecule-RNA interactions.[4,5] Furthermore, DNA-selective dyes have been successfully developed based on the structural modification of the TO framework for the imaging of nucleus[6] or for the selective detection of G-quadruplex DNA.[7,8] As far as we know, however, no reports have been focusing on TO itself as the dye for nucleolar RNA imaging in living cells while three kinds of TO derivatives have been reported for this purpose.[9,10,11]

In particular, the interesting work by Wang et al[10] reported on the imaging of living cells with TO itself and meso-substituted TO (Fig. 1-1), but they preferred the discussion on the change in the staining patterns in cells, which was caused by the incorporation of a benzyl group at the meso-position of the methine chain of parent TO.

We also note that the structural modification of parent TO often made the resultant probes lose the affinity for RNA[6,7,8] and/or the membrane permeability in living cells,[12] which should be an issue to be addressed in our research direction.

In this chapter, I focus and report on TO (4TO) itself and it's derivatives, TO-H, TO-C_4, as well as it's regioisomer structure, 2TO (Fig. 1-1), comparing their binding ability to RNA and ability to stain nucleolar RNA in living cells.

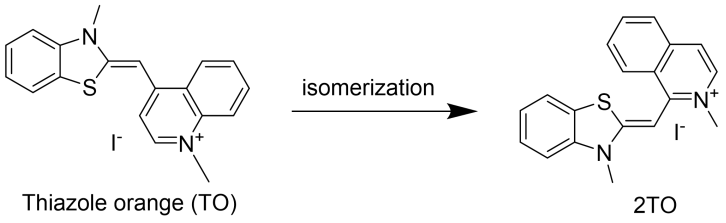

Fig. 1-1 Structure of TO (4TO) and meso-substituted TO (2TO).

2. Synthesis of TO (4TO), 2TO, and TO derivatives

2.1 (Z)-1-methyl-4-((3-methylbenzo[d]thiazol-2(3H)-ylidene) methyl)quinolin-1-ium iodide (4TO):

This compound was prepared according to the literature.[13]

2.2 Synthetic scheme for the preparation of TO-H.

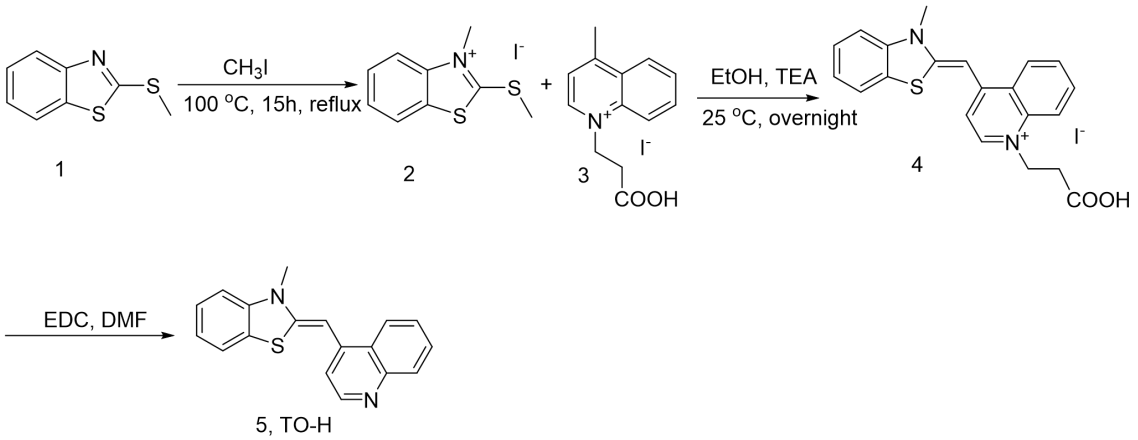

2.3 Synthetic scheme for the preparation of TO-C_4.

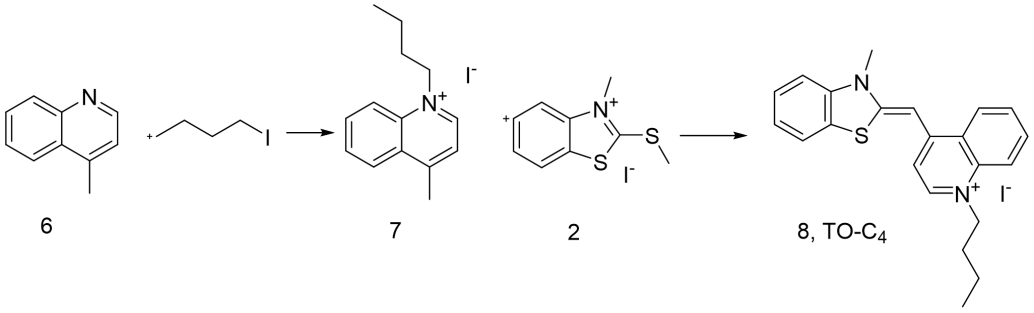

2.4 Synthetic scheme for the preparation of 2TO.

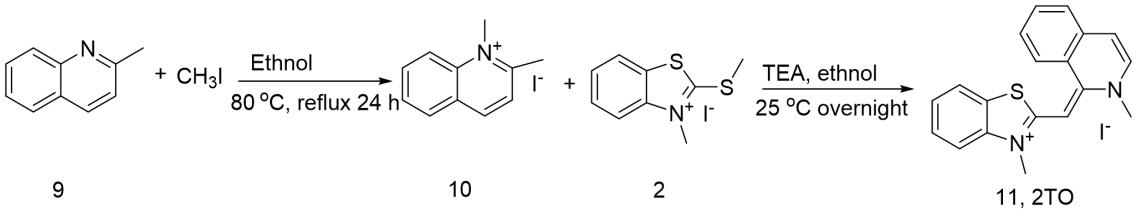

TO (4TO), 2TO and TO derivatives were prepared essentially according to literature.[14,15,16,17] These probes were characterized by ^{1}H NMR, ^{13}C NMR and HRMS. For experimental details on synthesis and characterization, see Supplementary information in this chapter.

3. Photophysical properties and fluorescence signaling abilities of TOs for RNA sensing

3.1 Absorption spectra of TOs to biological nucleic acid

Absorption spectra of TOs in the absence and presence of 1.0 mM calf thymus DNA or 1.0 mM *E. coli* total RNA at 25 ℃ in 10 mM sodium phosphate buffer (pH 7.0) containing 100 mM NaCl and 1.0 mM EDTA were determined as Figure 3.1-1. A red shift absorption band of the four TOs was observed in the presence of nucleic acid, implying the intercalative binding mode of TOs.[1]

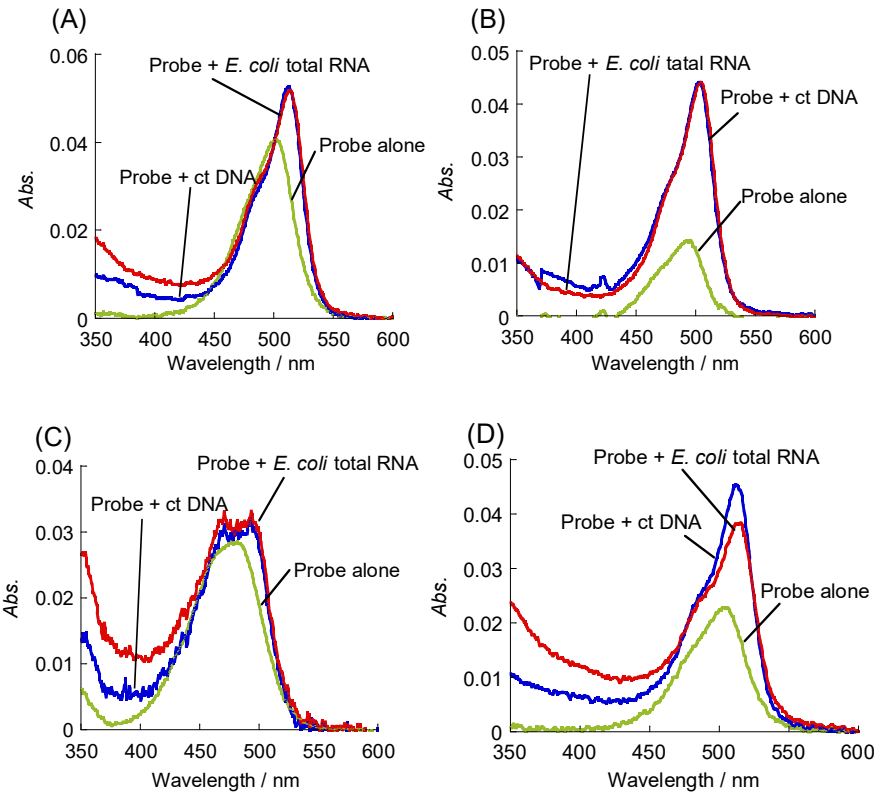

3.1-1 Absorption spectra of TOs (1.0 μM) in the absence and presence of 1.0 mM calf thymus DNA or 1.0 mM *E. coli* total RNA : (A) TO, (B) TO-H, (C) 2TO and (D) TO-C_4.

Experimental condition: [probe] = 1.0 μM in 10 mM sodium phosphate buffer (pH 7.0) containing 100 mM NaCl 1.0 mM EDTA. Before the measurement, sample solutions were incubated for 30 min. Sensitivity: medium, data interval: 0.5 nm, scan rate: 100 nm/ min, temperature: 25 ℃, cell: 1.0 × 0.2 cm, optical path: 10 mm. [*Analyst*, **2023**, *148*, 636-642] -Reproduced by permission of The Royal Society of Chemistry.

3.2 Fluorescence response to nucleic acid

3.2.1 Fluorescence response to biological nucleic acid

Fluorescence response of four TOs to biological nucleic acid, calf thymus DNA and *E. coli* total RNA, were measured as Figure 3.2.1-1. It's obviously that all four TOs exhibit almost no fluorescence in the absence of nucleic acid ($\Phi < 0.001$), which is caused by the non-radiative energy loss owing to the free rotation around the monomethine linker between benzothiazole and quinoline rings.[18] While the addition of *E. coli* total RNA significantly enhanced the fluorescence intensity for TOs in the green spectral region (λ_{em}: TO, 532 nm; TO-H, 523 nm; 2TO, 532 nm; TO-C_4, 532.5 nm), where the fluorescence intensity boosted more than 100 times. Together with the absorption spectra results, it is therefore considered that the light-up response comes from the restricted rotation of TOs because of the intercalation into the base pair in RNA.

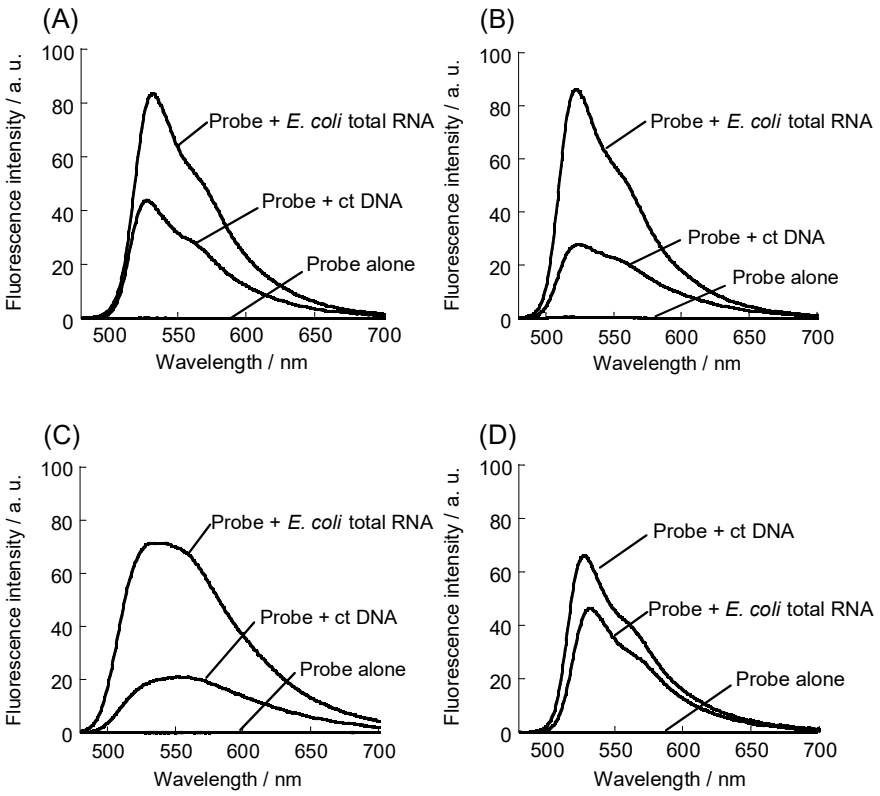

Figure 3.2.1-1 Fluorescence spectra of TOs (1.0 μM) in the absence and presence of 1.0 mM *E. coli* total RNA or 1.0 mM calf thymus DNA: (A) TO, (B) TO-H, (C) 2TO and (D) TO-C_4. Measurements were performed in 10 mM sodium phosphate buffer solution (pH 7.0) containing 100 mM NaCl and 1.0 mM EDTA. Before the measurement, sample solutions were incubated for 30 min. Excitation: 470 nm. Ex band: 3 nm, Em band: 3 nm, senseitivity: medium. Scan rate: 100 nm / min, response : 0.5 s, 3 × 3 nm quartz cell. Temperature: 25 ℃. [*Analyst*, **2023**, *148*, 636-642] -Reproduced by permission of The Royal Society of Chemistry.

It is surprising that TO shows the fluorescence response selectivity for RNA over DNA (Fig. 3.2.1-1-A, I_{RNA}/I_{DNA} = 2), considering the challenge of designing RNA-selective small molecules.[20,21,22]

Interestingly, the response selectivity of TOs toward RNA depends on a slight change in the chemical structure. The attachment of a butyl chain at N1 of the quinoline ring caused the probe (TO-C_4) to lose RNA selectivity, where a larger response was observed for DNA over RNA (Fig. 3.2.1-1-D, I_{RNA}/I_{DNA} = 0.7). However, in the case of TO-H where the CH_3 substituent at N1 of the quinoline ring was removed, the selectivity became better (3.2.1-1-B, I_{RNA}/I_{DNA} = 3.1) compared to parent TO. The selectivity for RNA further improved in the case of 2TO (Fig. 3.2.1-1-C, I_{RNA}/I_{DNA} = 3.7), a regioisomer of TO, where the benzothiazole unit was connected to position 2 in the quinoline ring. Although the reason for this is unclear now, the inherent preference for RNA is apparently improved by the regioisomer of TO.

3.2.2 Fluorescence response to synthetic nucleic acid

In order to investigate the reason for better RNA selectivity of regioisomer, the fluorescence response to synthetic nucleic acid were firstly examined as the Fig. 3.2.3-1. As we can see from these spectra, TO prefers double stranded RNA (rG/rC and rA/rU) over its DNA counterpart. The response of TO is significant to single stranded rG (13-mer) that could adopt a G-quadruplex structure, in which again TO prefers RNA (13-mer rG) over DNA (13-mer dG). TO likely has an inherent binding preference for RNA over DNA. Of particular interest is that 2TO shows an almost specific response to double stranded RNA (rG/rC) and single stranded rG over others. Again, here we can draw the conclusion that TO has an binding preference to RNA over DNA and the preference for RNA is improved by the regioisomer of TO. These results agree well with the examination using biological DNA and RNA.

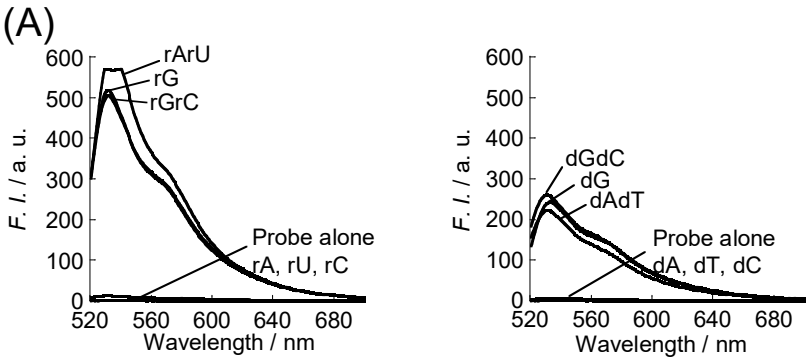

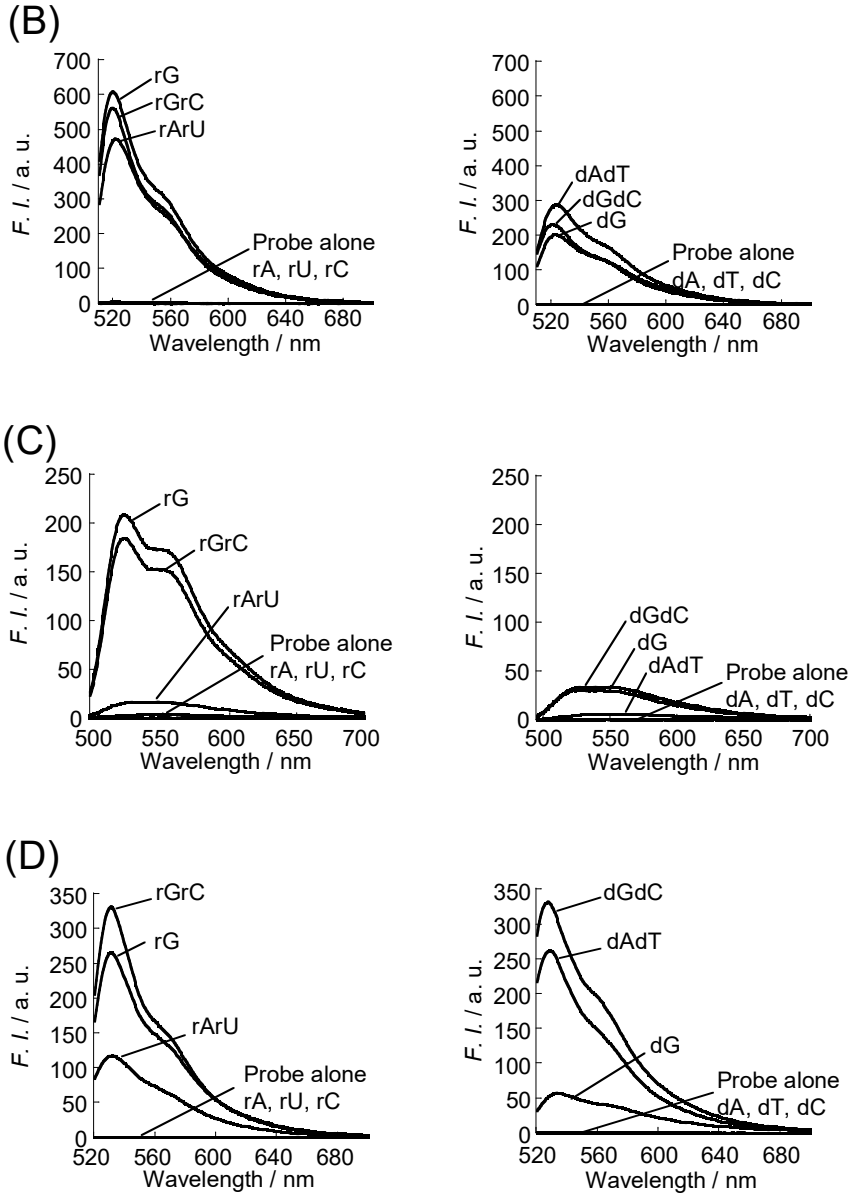

Fig. 3.2.2-1 Fluorescence response of TOs (1.0 μM) to synthetic nucleic acids (20 μM): (A) TO, (B) TO-H, (C) 2TO and (D) TO-C_4.

Experimental condition: Excitation: (A) 503 nm, (B) 493.5 nm, (C) 479 nm, (D) 503 nm. [dye] = 1.0 μM in 10 mM sodium phosphate buffer solution (pH 7.0) containing 100 mM NaCl and 1.0 mM EDTA. Ex band: 3 nm, Em band: 3 nm, senseitivity: medium. Scan rate : 100 nm / min, response : 0.5 s, temperature: 25 ℃, 3 × 3 nm quartz cell. Data were obtained after mixing TOs with nucleic acid solutions and subsequent incubation for 30 min. [*Analyst*, **2023**, *148*, 636-642] -Reproduced by permission of The Royal Society of Chemistry.

The nucleic acid sequences:

rG: 5'- r(GGG GGG GGG GGG G)-3' dG: 5'- d(GGG GGG GGG GGG G)-3'

rC: 5'- r(CCC CCC CCC CCC C)-3' dC: 5'- d(CCC CCC CCC CCC C)-3'

rA: 5'- r(AAA AAA AAA AAA A)-3' dA: 5'- d(AAA AAA AAA AAA A)-3'

rU: 5'- r(UUU UUU UUU UUU U)-3' dT: 5'- d(TTT TTT TTT TTT T)-3'

3.2.3 TO binding to DNA

In previous research conducted in 1998, Jan Nygren et al.,[1] reported the binding of thiazole orange (TO) to DNA. They proposed that TO binds to nucleic acids by intercalation, but in several modes. For double-stranded DNA, such as calf thymus DNA, TO binds as a monomer. However, for single-stranded poly dG, TO can bind both as a monomer and as a dimer.

As shown in Figure 3.2.4-1, when TO binds as a monomer, a red-shift peak can be observed in the excitation spectra. On the other hand, when TO binds as a dimer, a blue-shift peak is observed. These spectroscopic shifts provide valuable insights into the different binding modes of TO to nucleic acid.

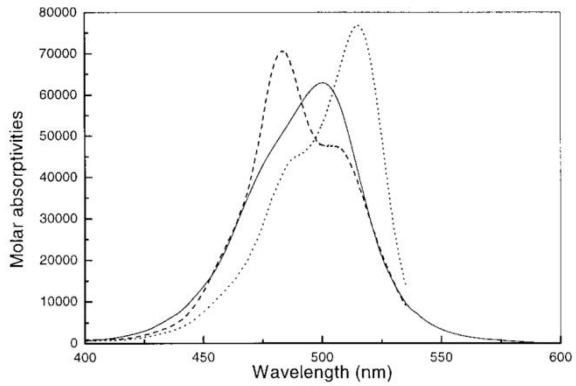

Fig. 3.2.3-1 Absorption spectra of free TO monomer (—) and fluorescence excitation spectra of bound TO monomer (.....) and dimer (----) normalized to the same area as the absorption spectrum.[1]

3.2.4 Comparison of binding modes between TO and 2TO

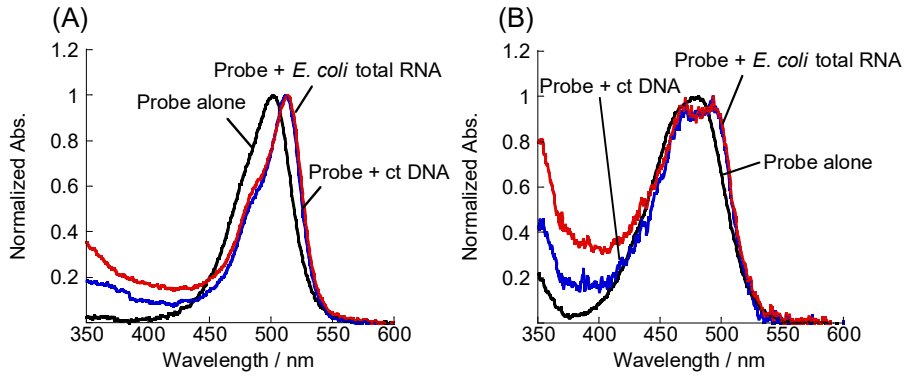

Fig. 3.2.4-1 Normalized absorption spectra of (A)TO (1.0 μM) and (B) 2TO (1.0 μM) in the absence and presence of 1.0 mM calf thymus DNA or 1.0 mM *E. coli* total RNA. Before the measurement, sample solutions were incubated for 30 min. Experimental condition: [probe] = 1.0 μM in 10 mM sodium phosphate buffer (pH 7.0) containing 100 mM NaCl 1.0 mM EDTA, temperature: 25 ℃, cell: 1.0 × 0.2 cm, optical path: 10 mm. [*Analyst*, **2023**, *148*, 636-642] -Reproduced by permission of The Royal Society of Chemistry (partially modified).

In my case, as we can see from the normalized absorption spectra of TO and 2TO to calf thymus DNA and *E. coli* total RNA (Fig. 3.2.4-1), a red-shift is visible both in TO and 2TO, indicate that the two probes bind to nucleic acid as a monomer. The difference is that a little bit TO bind to nucleic acid as a dimer where we can see a small shoulder around 490 nm (Fig. 3.2.4-1-A). In the case of 2TO, the peak around 470 nm is more visible (Fig. 3.2.4-1-B) indicate binding as a dimer is more significant for 2TO. The fluorescence spectra gives a same result where 2TO shows a broader spectra than TO (Fig. 3.2.2-1-A and -C) because much more 2TO bind to nucleic acid as a dimer, which maybe key exhibiting RNA selectivity.

3.2.5 Calculation of quantum yield

Fluorescence quantum yield is a physical quantity that measures the efficiency with which a fluorescent substance is converted to fluorescence. It represents the efficiency with which a molecule or substance in the excited state releases the energy of the excited state in the form of light through the fluorescence process. The symbol Φ is usually used to denote fluorescence quantum yield.

Quantum yield of TOs was determined relative to fluorescein in 0.1 M NaOH (Φ = 0.93, Ex: 470 nm).[23] The calculation equation is as follows:

$$\Phi_x = \Phi_{st} \bullet \left(\frac{A_{st}(\lambda_{ex})}{A_x(\lambda_{ex})} \right) \bullet \left(\frac{F_x}{F_{st}} \right) \bullet \left(\frac{n_x^2}{n_{st}^2} \right) \bullet \left(\frac{D_x}{D_{st}} \right)$$

Where Φ is the quantum yield, A (λ_{ex}) is the absorption value at the excitation wavelength, F is the area of fluorescence spectra, n is the refractive index of the solvent, D is dilution rate, the subscripts x and st denote detection samples and standard samples respectively.

Here, it's necessary to use the same sample to measure absorption spectra and also fluorescence spectra (Fig. 3.1-1 and Fig. 3.2.1-1). Finally, the quantum yield and signaling ability of all four TOs were calculated as the following table 3.2.5-1.

Probes	Samples	ϕ_{bound}	ϕ_{RNA}/ϕ_{free}	ϕ_{RNA}/ϕ_{DNA}	Light-up factor (I/I_0)
TO	Probe alone	0.0004	380	1.6	580
	ct DNA	0.098			
	E coli. total RNA	0.16			
TO-H	Probe alone	0.002	80	2.8	190
	ct DNA	0.057			
	E coli. total RNA	0.16			
2TO	Probe alone	0.00009	1200	3.1	430

	ct DNA	0.035			
	E coli. total RNA	0.11			
TO-C_4	Probe alone	0.001	100	0.6	760
	ct DNA	0.16			
	E coli. total RNA	0.10			

Table 3.2.6-1 Quantum yield and light-up factor of TOs.

Notably, the fluorogenic off-on signaling ability of TOs (Table 3.2.2-1) is good enough compared with the probes developed for nucleolar RNA imaging in living cells.[24-32] In particular, the light-up property of TO (I/I_0 = 580-fold, ϕ_{RNA}/ϕ_{free} = 380) compares with commercial SYTO RNA select (I/I_0 = 500-fold).[24] TO even compares with styryl-based green-emissive dye P12 (λ_{em} = 511 nm, ϕ_{RNA}/ϕ_{free} = 148)[25] because is currently one of the leading RNA-selective dyes with high ϕ_{RNA} values for RNA (ϕ_{RNA} = 0.577). Furthermore, 2TO performs much better when the value of ϕ_{RNA}/ϕ_{free} reaches 1200 (I/I_0 = 430-fold).

In conclusion, the remarkable light-up property of TO and 2TO is indeed promising as RNA staining dyes.

3.3 Photostability of TOs

The photostability of probes is another issue to be addressed in imaging studies. As has been reported in the literature,[24,33,34] commercial SYTO RNA select has very low photostability. Our previous study showed that its emission intensity bound to *E. coli* total RNA decreased by as much as 75 % under continuous irradiation for 160 min.[24] Fortunately, both TO and 2TO were found to have relatively good photostability. As shown in Fig. 3.3-1, the decrease in the fluorescence intensities of these two probes was moderate after 180 min of continuous irradiation (< 20 %), whereas the decrease was significant for TO-H (45 %) and TO-C_4 (36 %).

Researches reveals that cyanine dyes usually shows low photostability because the typical bridge structure in cyanine dyes tend to react with singlet oxygen form oxides. Singlet oxygen is a high-energy excited state of oxygen molecules with strong oxidizing properties and highly reactive with electron-rich substrates.[35,36] It seems that the butyl group at N1 of the quinoline ring performs as a stronger electron-donating group than the methyl group does, which makes TO-C_4 more photo-reactive. The reverse is also true for TO-H, where the methyl group is absent at the N1 of the ring.

Therefore, both TO and 2TO are relatively robust in solutions, which is desirable for use in the long-term observation of living cells.

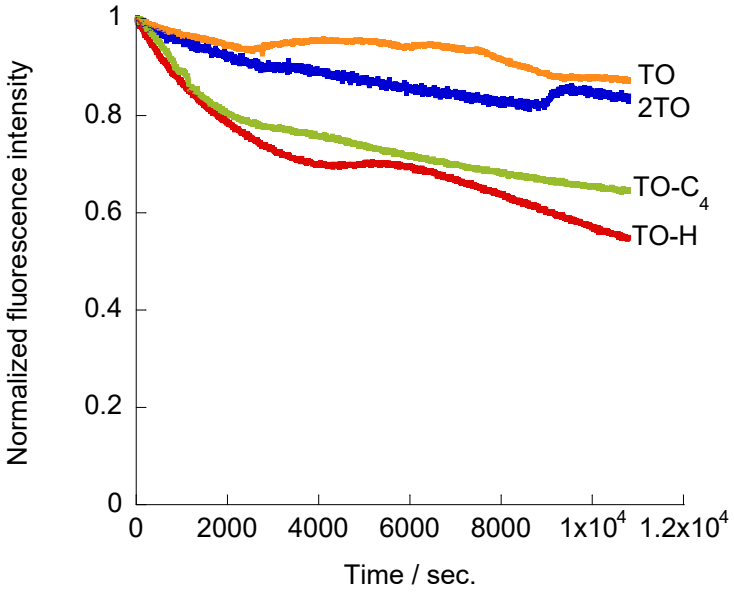

Figure 3.3-1 Changes in fluorescence intensity of four TOs when bound to E. coli total RNA under continuous irradiation (3 h). [Probe] = 1.0 μM, [*E. coli* total RNA] = 100 μM in solutions buffered at pH 7.0 (10 mM sodium phosphate) containing 100 mM NaCl and 1.0 mM EDTA. Before the measurement, sample solutions were incubated for 30 min. Excitation: 503 nm (TO), 493.5 nm (TO-H), 479 nm (2TO), 503 nm (TO-C_4). Ex band: 3 nm, Em band: 3 nm, sensitivity, medium. Temperature: 25 ℃. [*Analyst*, **2023**, *148*, 636-642] -Reproduced by permission of The Royal Society of Chemistry.

4. Application to cells

MCF7 and HeLa cells were obtained from the Cell Resource Center for Biomedical Research at Tohoku University. As for fluorescence live-cell and fixed-cell imaging, DNase and RNase digestion experiments, cell toxicity tests (AlamarBlue® assay), all measurements were performed based on our previous reports.[24,33] The details are also provided in the supporting information in this chapter.

4.1 Living cell imaging

Given the sensing properties in the solution, as aforementioned, all of TOs were applied to RNA imaging in living MCF7 cells. It can be found that all TOs had good cell plasma and nuclear membrane permeability in living cells, but the degree depended on the probes. The working concentration were optimized for each probe as follows: TO, 0.5 μM; TO-H, 2 μM; 2TO, 0.5 μM; and TO-C_4, 0.3 μM in RPMI 1640 media or in D-PBS buffer.

Fig. 4.1-1-A shows typical fluorescence images of living MCF7 cells after the incubation of TO (0.5 μM) for 20 min. Here, the nucleus was co-stained by Hoechst 33342, a conventional blue-emissive DNA staining dye. With a high contrast to the blue emission from the nucleus (emission filter: 435/48 nm), a strong emission in the green region (emission filter: 545/48 nm) was observed in the nucleolus, indicating good cell plasma and nuclear membrane permeability of TO in living cells. The nucleolus was stained because of the binding of TO to RNAs that were abundant in this region.

Importantly, much better images were obtained by TO-H and 2TO (Fig. 4.1-1-B and -C), where green emission was clearly observed in the nucleolus with higher contrast to the blue emission from the nucleus.

However, TO-C_4 has a poor ability to stain the nucleolus in living cells (Fig. 4.1-1-D).

These results are well agree with the sensing properties in solutions.

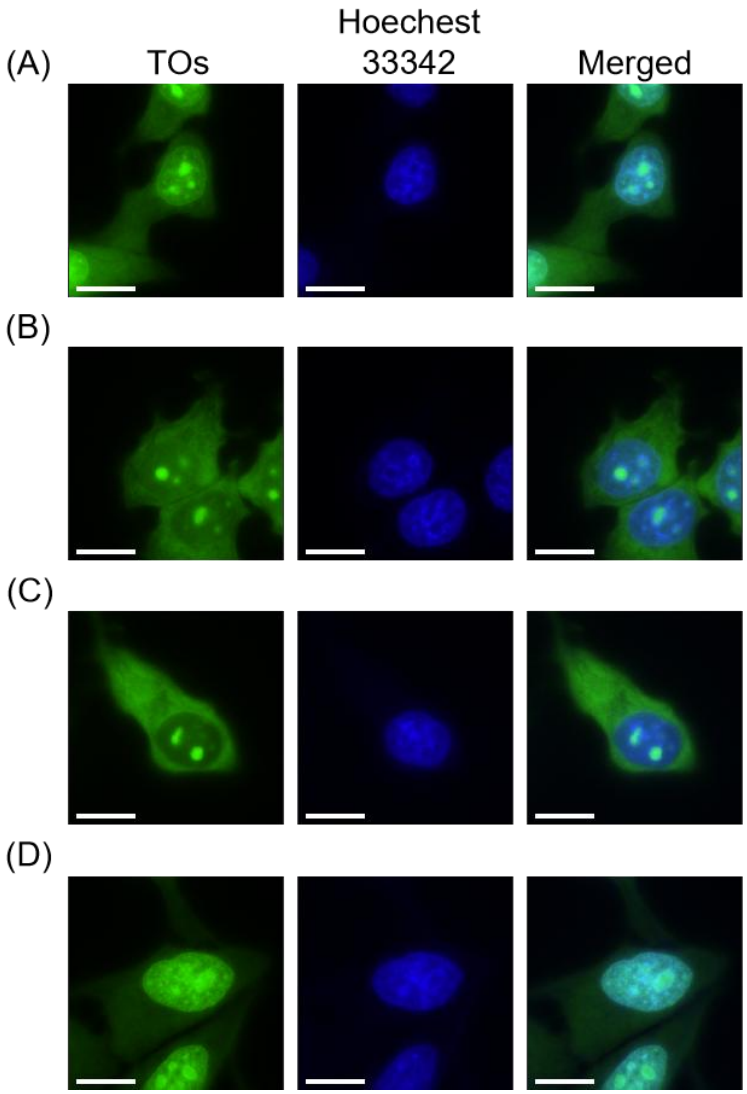

Figure 4.1-1 Fluorescence images of living MCF7 cells stained by TOs with Hoechst 33342 (176 nM). [TO]=0.5 μM, [TO-H]=2 μM, [2TO]=0.5 μM, [TO-C_4]=0.3 μM. The cells were incubate with Hochest for 20 min firstly, after remove the co-satin probe solutions, the cells were further incubate with work concentration of TOs for 20 min. Incubation time : 20 min. Parameters: FITC, 32 %, 0.1 s for all images. Scale bar: 15 μm. The cells were imaged in HBSS buffer after washing with HBSS buffer twice. [*Analyst*, **2023**, *148*, 636-642] -Reproduced by permission of The Royal Society of Chemistry.

4.2 Digestion experiment

To further explore the signal from the nucleolus, digestion experiments in fixed and permeabilized MCF7 cells by using deoxyribonuclease (DNase) and ribonuclease (RNase) were carried out. The control group was also set up.

Fig. 4.2.1-A shows strong emission remained observed in the nucleolus after DNase treatment. In contrast, the nucleolar emission decreased in the case of RNase treatment, which reveals that the observed emission at the nucleolus originated from TO bound to the nucleolar RNA. Apparently, TO performs as a fluorogenic dye for nucleolar RNA imaging in living cells.

Moreover, Fig. 4.2-1-B and -C suggest that RNase digestion led to the disappearance of the emission in the nucleolus, whereas the nucleolar emission remained almost unaffected by treatment with DNase. This result reveals that both TO-H and 2TO have high selectivity for RNA over DNA in cells, which is much superior to TO because considerable emission was still observed after RNase treatment (Fig. 4.2-1-A).

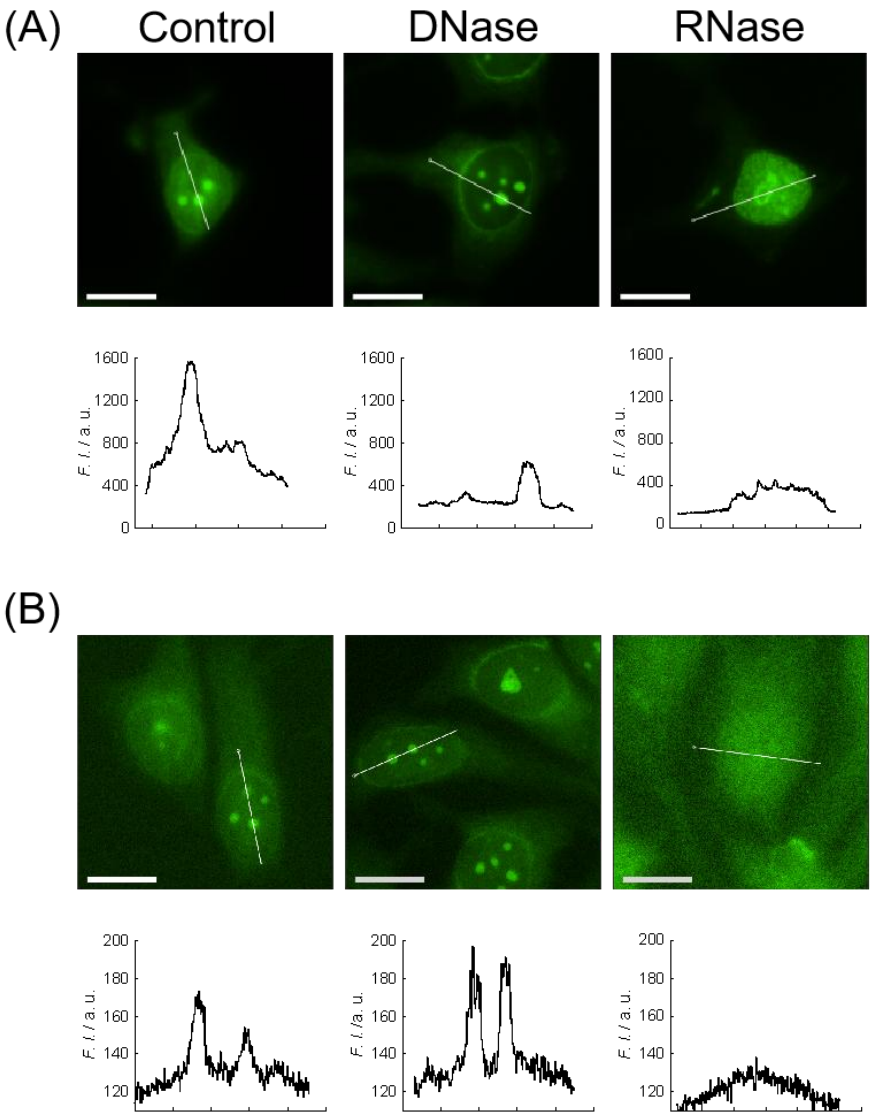

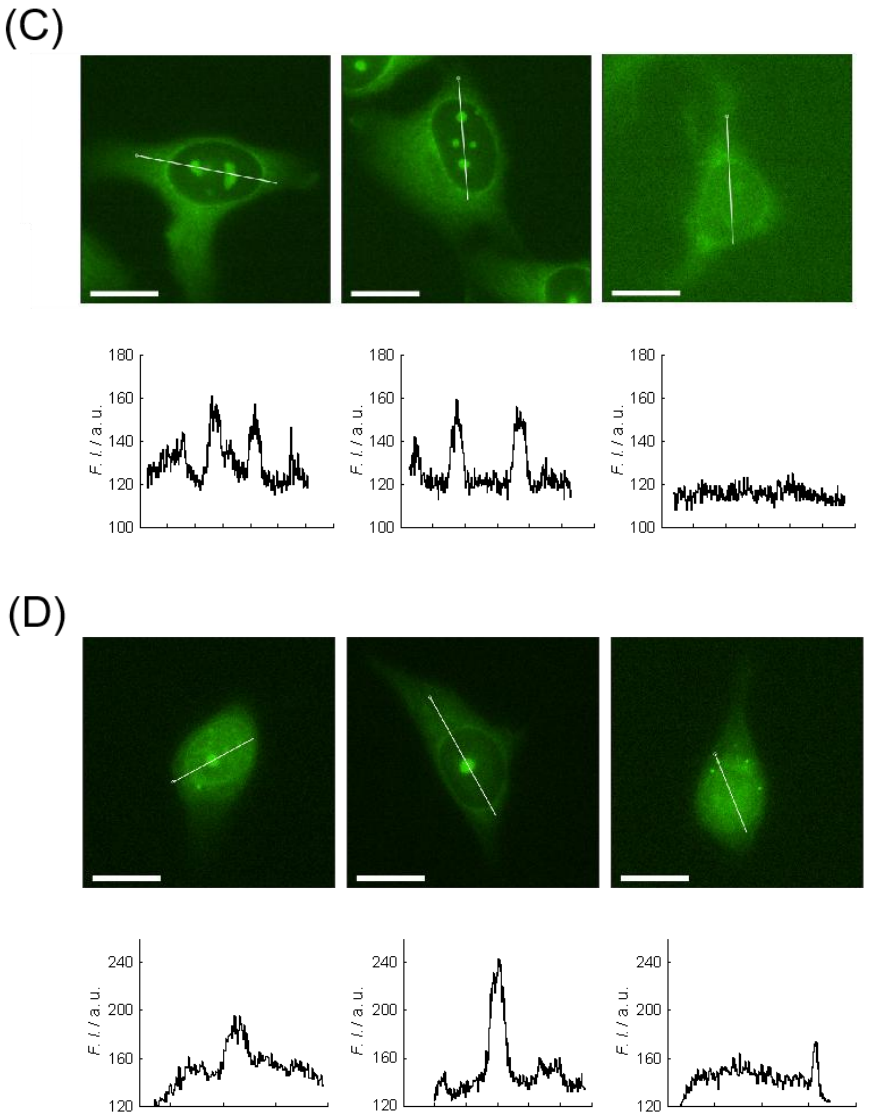

Figure 4.2-1 Fluorescence images of fixed and permeabilized MCF7 cells stained by TOs (1 μM) before (control) and after treatment with DNase or RNase for 3 hours. Parameters: FITC, 32 %, 0.2 s for all images. Scale bar: 15 μm. The cells were imaged in D-PBS buffer after washing with D-PBS buffer twice. [*Analyst*, **2023**, *148*, 636-642] -Reproduced by permission of The Royal Society of Chemistry.

4.3 Co-stain with mitochondria staining probe

I also remarked on the localization of probes in the mitochondria, which may be an issue to be addressed for the next design of nucleolar RNA-selective dyes. As has been observed for other monomethine cyanine dyes,[24,33,37,38] 2TO seems to accumulate to some extent in the mitochondria. This was revealed by colocalization experiments using a mitochondria staining probe (Fig. 4.3-1-C, Pearson's correlation coefficient: 0.76). This could be due to the possible interaction of cationic dyes with a negative mitochondrial membrane. In addition, the emission from mitochondria originates from binding to mitochondrial RNA because the emission almost disappeared after the RNase treatment (Fig. 4.2-1). Besides, the mitochondria accumulation of TO and TO-H seems less compared with 2TO (Pearson's correlation coefficient: 0.58, 0.56, respectively). Especially in the case of TO-C_4, the accumulation in the mitochondria seems no longer negligible (Fig. 4.3-1-D, Pearson' s correlation coefficient: 0.27). Although TO-C_4 fails to keep the RNA selectivity from the parent TO, the increase in hydrophobicity is a simple but effective way to control the membrane permeability in living cells, which then leads to nucleolar RNA-selective dyes.

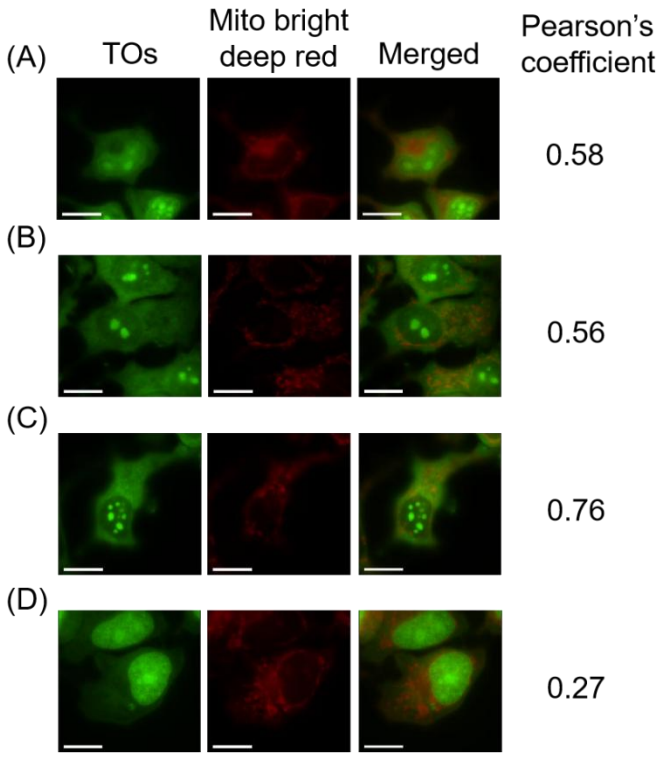

Figure 4.3-1 Co-staining of living MCF7 cells with each probe (TO, 2TO and TO derivatives) and mitochondria-staining probe (MitoBrigtht LT Deep Red). (A) [TO] = 0.5 μM, (B) [TO-H] = 2 μM, (C) [2TO] = 0.5 μM, and (D) [TO-C_4] = 0.3 μM. The cells stained with TO and TO derivatives (20 min) were further incubated in media containing co-staining probe for 20 min. Parameters: FITC, 32 %, 0.1 s for all images. Scale bar: 15 μm. After washing with HBSS buffer twice, the cells were imaged in HBSS buffer.

4.4 Fixed and permeabilized cell imaging

Except for live cell imaging, fixed and permeabilized MCF7 cells imaging were also conducted by using methanol and Toriton-X reagent. The situation is, however, totally different with living MCF7 cells. Under the same working concentration for live cell imaging, the nucleolus was highly selectively stained, and the emission from the cytoplasm was negligible (Fig. 4.4-1) for TO, TO-H and 2TO because fixed cells have better cell membrane permeability. This again reminds us that membrane permeability is key to designing probes for live cell imaging.

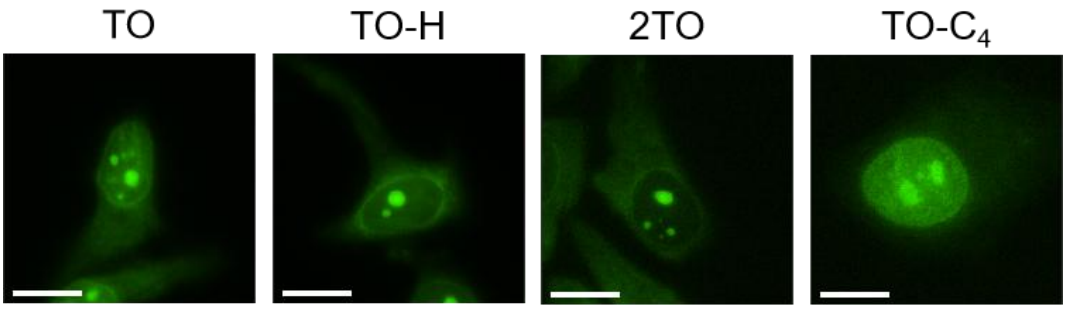

Figure 4.4-1 Fluorescence images of fixed and permeabilized MCF7 cells stained by TO, 2TO or TO derivatives after 20 min incubation. [TO] = 0.5 μM, [TO-H] = 2 μM, [2TO] = 0.5 μM, [TO-C_4] = 0.3 μM. Parameters: FITC, 32 %, 0.05 s for all images. Scale bar: 15 μm. After washing with D-PBS buffer twice, the cells were imaged in D-PBS buffer. [*Analyst*, **2023**, *148*, 636-642] -Reproduced by permission of The Royal Society of Chemistry.

4.5 Living cell imaging without washing protocol

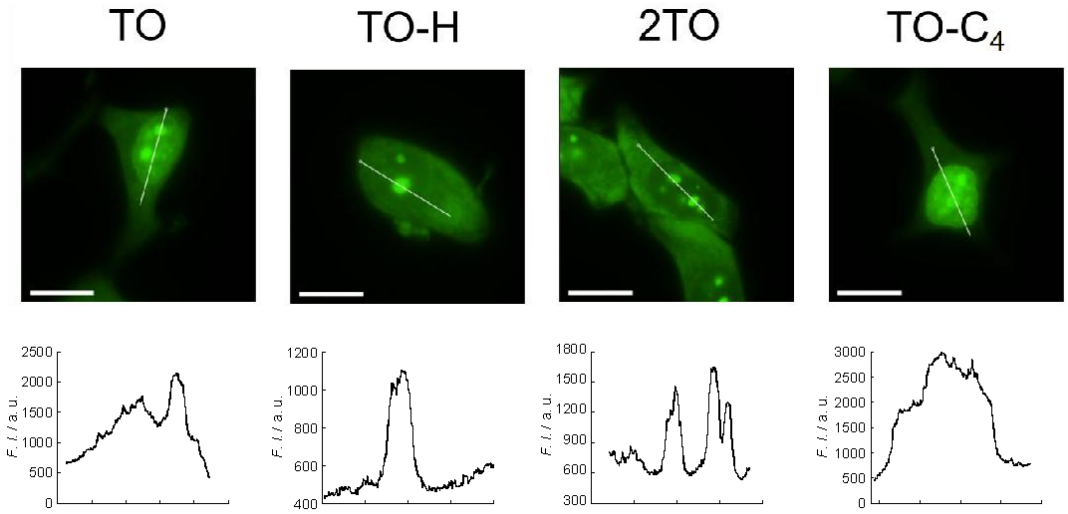

Figure 4.4-1 *No-washing* fluorescence imaging of living MCF7 cells stained by TO (0.5 μM), TO-H (2.0μM), 2TO (0.5 μM) or TO-C_4 (0.3 μM) after 20 min incubation. Fluorescence intensity profiles along the white line are also shown. Scale bar: 15 μm. The cells were imaged in HBSS buffer. [*Analyst*, **2023**, *148*, 636-642] -Reproduced by permission of The Royal Society of Chemistry.

Usually in cell imaging experiments, cells need to be washed twice with HBSS buffer (for live cells) or D-PBS buffer (for fixed and permeabilized cells) before observation with the fluorescence microscope to obtain a clearer image. However, this step is somewhat cumbersome. Therefore, I also tested the staining ability of TOs without washing step, and the results (Fig. 4.5-1) showed that TO is even applicable to wash-free live-cell imaging. The nucleolus was clearly stained after 20 min of incubation, and the signal-to-background ratio was comparable to the image obtained with the washing step (Fig. 4.1-A). Evidently, TO has been demonstrated to function as a fluorogenic dye for the visualization of nucleolar RNA in living cells.

Fig. 4.5-1 further highlighted the usefulness of TO-H and 2TO. Compared with TO, the nucleolus was clearly stained with much higher contrast, again revealing its potential as a dye for live cell imaging specifically targeting RNA within the nucleolus.

4.6 Living cell imaging after 24 h incubation

Prior to this, the staining ability of probes with 20 minutes incubation were performed, and next, all four TOs were incubated in live MCF7 cells for 24 hours to explore the possibility of long-time observation experiment in live cells.

No any morphological changes was observed even after 24 h of incubation (Fig. 4.5-1), indicating no influence on cell viability in the long-term experiment. Again, both TO-H and 2TO were found to perform

better than TO, where both probes clearly stained the nucleolus with excellently high contrast, as can be observed for the case after 20 min of incubation (Fig. 4.1-1).

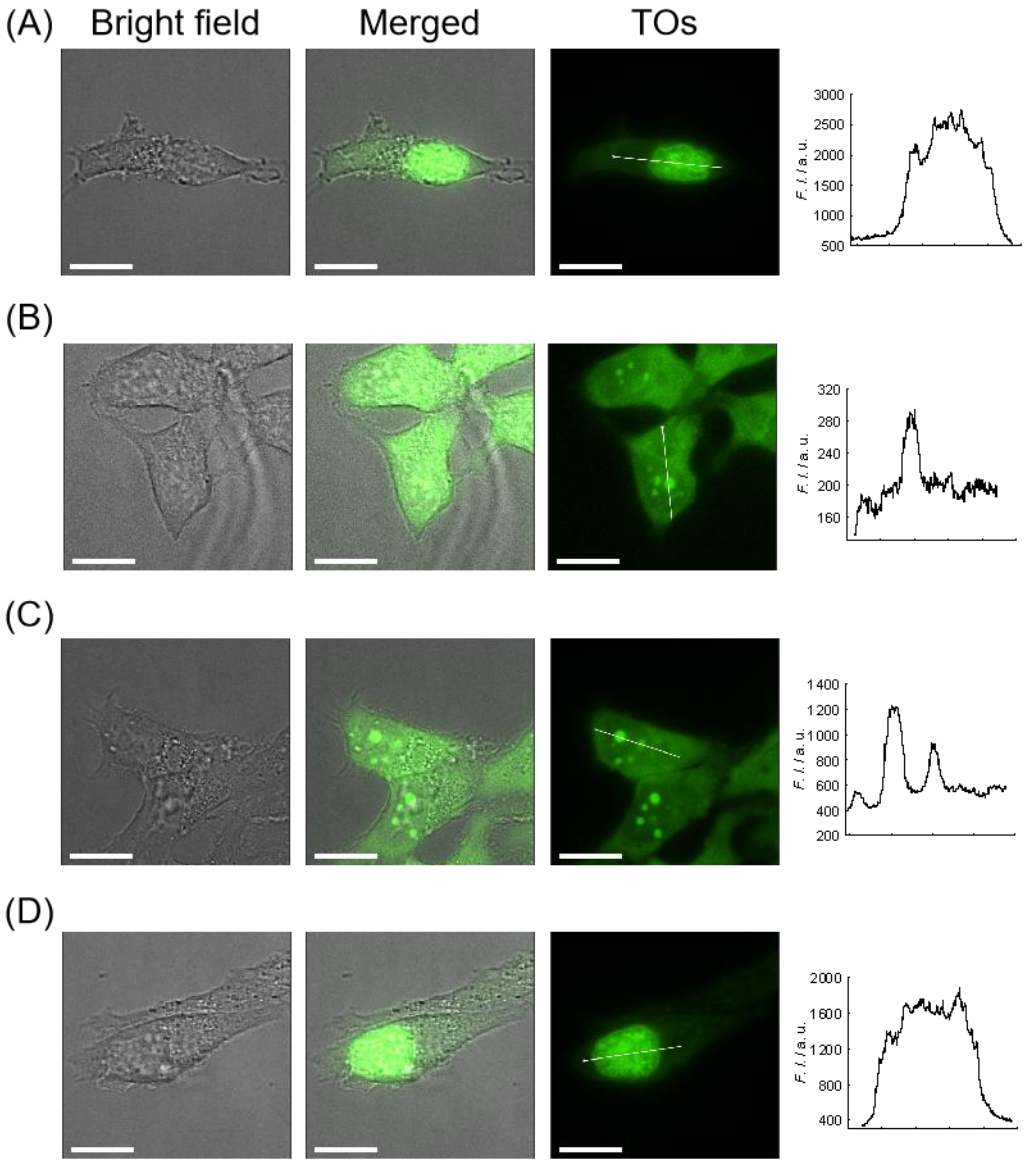

Figure 4.5-1 Images of living MCF7 cells stained by (A) TO (0.5 μM), (B) TO-H (2.0 μM), (C) 2TO (0.5 μM), or (D) TO-C_4 (0.3 μM) after 24 h incubation. Fluorescence intensity profiles along the white line are also shown. Scale bar: 15 μm. After washing with HBSS buffer twice, the cells were imaged in HBSS buffer. [*Analyst*, **2023**, *148*, 636-642] -Reproduced by permission of The Royal Society of Chemistry.

4.7 The other cell line imaging

Now, I want to study how well these probes stain in other cell lines, not limited to live MCF7 cells. Therefore, all of four TOs were also applied to living HeLa cell with 20 min incubation. As depicted in the Fig 4.6-1, four TOs keep their staining ability as in the living MCF7 cells. TO demonstrates its efficiency as a fluorogenic dye for visualizing nucleolar RNA also in living HeLa cells. Again, in comparison to TO, the staining ability of 2TO to the nucleolus exhibited enhanced contrast, underscoring its potential as a dye with nucleolar RNA-selective properties for live cell imaging.

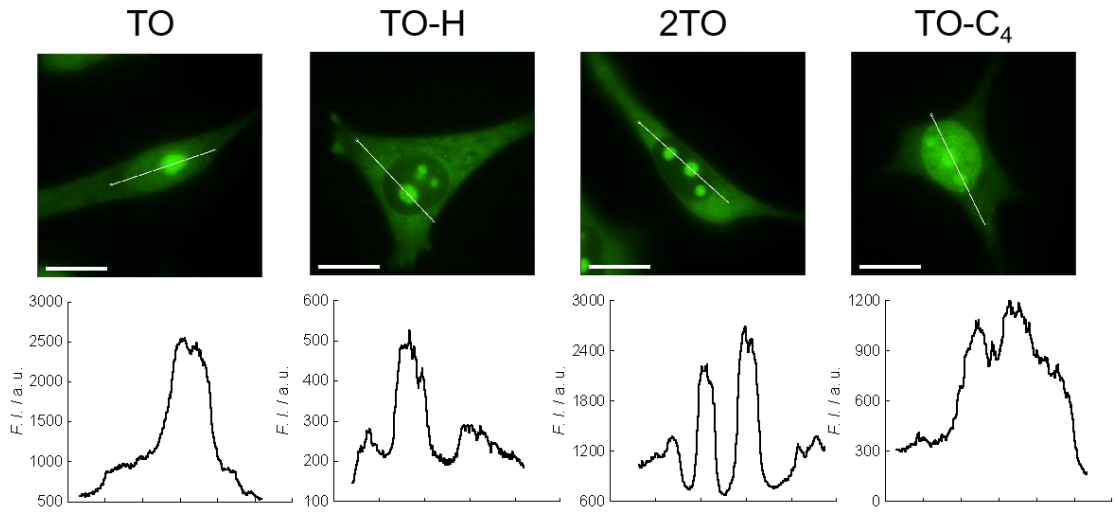

Figure 4.6-1 Fluorescence imaging of living HeLa cells stained by TO (0.5 μM), TO-H (2.0 μM), 2TO (0.5 μM) or TO-C_4 (0.3 μM) after 20 min incubation. Fluorescence intensity profiles along the white line are also shown. Parameters: FITC, 32 %, 0.05 s for all images. Scale bar: 15 μm. After washing with HBSS buffer twice, the cells were imaged in HBSS buffer. [*Analyst*, **2023**, *148*, 636-642] -Reproduced by permission of The Royal Society of Chemistry.

4.8 Cell toxicity

Toxicity of dyes is also an important factor in live cell imaging experiments. In this experiment, AlamarBlue® reagent was used to detect cell toxicity. As illustrated in Fig. 4.8-1, AlamarBlue® reagent contains resazurin, which is originally a blue and non-fluorescent substance. However, when AlamarBlue® is added to the cell culture medium, metabolic activity within the cells produces metabolites. These metabolites undergo a redox reaction with resazurin, reducing resazurin to highly red fluorescent resorufin.[39] Therefore, we can indirectly know the metabolic activity of cells to the reagent and the survival status of cells by measuring the fluorescence intensity of probe solutions containing AlamarBlue® using a fluorescence-based micro-plate reader.

Fig. 4.8-1 Schematic of AlamarBlue®

Generally speaking, if the cells are metabolically active and have more metabolites, it will lead to the enhancement of the redox reaction of AlamarBlue®, producing more red fluorescent resorufin and thus increasing the fluorescence intensity. Whereas, in cases where cells are affected by toxic substances, the metabolic activity of the cells will be reduced, leading to a weakening of the redox reaction of AlamarBlue® and thus a decrease in fluorescence intensity. In this way, we were able to assess the effect of the probes on the cells and understand its impact on the survival state of cells.

The Fig.4.8-2 shows the cytoxicity of four TOs in the living MCF7 cells with different concentration after 20 min incubation by using AlamarBlue® assay. As shown in the figure, less cell viability and more cytotoxicity as concentration increases. Fortunately, the four TOs exhibited almost no toxicity towards living MCF7 cells at the working concentrations (TO, 0.5 μM; TO-H, 2 μM; 2TO, 0.5 μM; TO-C_4, 0.3 μM) where the cell viability remained over 95 % after 20 min incubation.

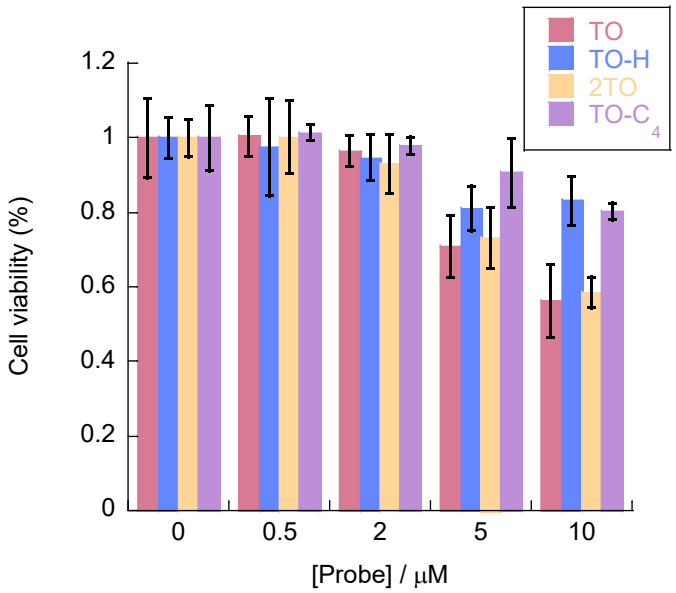

Figure 4.8-2 Evaluation of probe cytotoxicity after 20 min incubation. Buffer treatment served as a positive control. Values are means ± standard deviation of six independent experiments (N = 6). [TOs] = 0~10 μM. Ex: 570 nm, Em: 610 nm, cut off: 590 nm. Incubation time: 20 min for probes; 3 hours for AlamarBlue® assay. [*Analyst*, **2023**, *148*, 636-642] -Reproduced by permission of The Royal Society of Chemistry.

5. Summary

I described the signaling and staining abilities of thiazole orange (TO) and its derivatives as RNA-selective dyes for live cell imaging. We found that the slight change in the TO framework significantly affected RNA selectivity, photostability and membrane permeability. Significantly, TO was good enough to work as a fluorogenic probe for nucleolar RNA imaging in living cells, where the nucleolus was clearly stained after incubation with 0.5 μM TO for 20 min. TO was even applicable to wash-free imaging of living cells. If necessary, TO was, of course, applicable to fixed and permeabilized cells, where TO performs much better than in living cells. Because TO is commercially available, TO would now be the first choice for the study of nucleolar RNA imaging in biological processes, such as stress response, development and aging, and canceration.[40]

More significantly, a much better image was obtained with 2TO, a regioisomer of TO (4TO). Compared to TO, 2TO showed superior selectivity for RNA in both solution and living cells, and its off–on signaling function (I/I_0 = 430-fold and ϕ_{RNA}/ϕ_{free} = 1200) was the top level among the probes developed so far for nucleolar RNA imaging in living cells. Together with our previous study, this study demonstrates the potential of cyanine dyes for living cell imaging.[41,42,43] In particular, this study demonstrates that the isomerization of TO is key to improving RNA selectivity, which is adapted to fit other cyanine dyes.

6. Reference

1. J. Nygren, N. Svanvik and M. Kubista, *Biopolymers*, **1998**, *46*, 39-51.
2. I. Lubitz, D. Zikich and A. Kotlyar, *Biochemistry*, **2010**, *49*, 3567-3574.
3. L. G. Lee, C.-H. Chen and L. A. Chiu, *Cytometry*, **1986**, *7*, 508-517.
4. S. L. Wicks and A. E. Hargrove, *Methods*, **2019**, *167*, 3-14.
5. Y. Ito, Y. Sato, N. Teramae and S. Nishizawa, *Bunseki Kagaku*, **2021**, *70*, 149-157.
6. K. Uno, T. Sasaki, N. Sugimoto, H. Ito, T. Nishihara, S. Hagihara, T. Higashiyama, N. Sasaki, Y. Sato and K. Itami, *Chem. - Asian J.*, **2017,** *12*, 233 – 238.
7. Y. Lu, Q. Deng, J. Hou, D. Hu, Z. Wang, K. Zhang, L. G. Luyt, W.-L. Wong and C.-F. Chow, *ACS Chem. Biol.*, **2016**, *11*, 1019-1029.
8. L. Guan, J. Zhao, W. Sun, W. Deng and L. Wang, *ACS Omega*, **2020**, *5*, 26056-26062.
9. Y. Lu, Q. Deng, D. Hu, Z. Wang, B. Huang, Z. Du, Y.- Fang, W.-L. Wong, K. Zhang and C.-F. Chow, *Chem. Commun.*, **2015**, *51*, 15241-15244.
10. L. Guan, A. Li, Y. Song, M. Yan, D. Gao, X. Zhang, B. Li and L. Wang, *J. Org. Chem.*, **2016**, *81*, 6303-6313.
11. D. Aristova, V. Kosach, S. Chernii, Y. Slominsky, A. Balanda, V. Filonenko, S. Yarmoluk, A. Rotaru, H. G. Özkan, A. Mokhir and V. Kovalska, *Methods Appl. Fluoresc.*, **2021**, *9*, 045002.

12. N. I. Shank, H. H. Pham, A. S. Waggoner and A. Armitage, *J. Am. Chem. Soc.*, **2013**, *135*, 242-251.

13. A. Abdelhameed, X. Liao, C. A. McElroy, A. C. Joice, L. Rakotondraibe, J. Li, C. Slebodnick, P. Guo, W. D. Wilson, K. A. Werbovetz, *Bioorg. Med. Chem. Lett.*, **2020**, *30*, 126725.

14. M. V. Sonar, M. E. Wampole, Y-Y. Jin, C-P. Chen, M. L. Thakur, E. Wickstrom, *Bioconjug. Chem.*, **2014**, *25*, 1697−1708.

15. S. Ikeda, A. Okamoto, *Photochem. Photobiol. Sci.*, **2007**, *6*, 1197–1201.

16. C. T. Martins, M. S. Lima, O. A. E. Seoud, *J. Phys. Org. Chem.*, **2005**, *18*, 1072–1085.

17. J. Sun, M. Tian and W. Lin, *Analyst*, **2019**, *144*, 2387-2392.

18. V. Karunakaran, J. L. P. Lustres, L. Zhao, N. P. Ernsting and O. Seitz, *J. Am. Chem. Soc.*, **2006**, *128*, 2954-2962.

19. C. S. Chow and F. M. Bogdan, *Chem. Rev.*, **1997**, *97*, 1489-1513

20. J. R. Thomas and P. J. Hergenrother, *Chem. Rev.*, **2008**, *108*, 1171-1224.

21. S. L. Wicks and A. E. Hargrove, *Methods*, **2019**, *167*, 3-14.

22. A. U. Juru and A. E. Hargrove, *J. Biol. Chem.*, **2021**, *296*, 100191.

23. R. Sjoback, J. Nygren and M. Kubista, *Spectrochim. Acta, Part A*, **1995**, *51*, L7-L21.

24. K. Higuchi, Y. Sato, N. Togashi, M. Suzuki, Y. Yoshino and S. Nishizawa, *ACS Omega*, **2022**, *7*, 23744-23748.

25. C. Wang, Y. Lu, S. Cai, W. Long, Y. Zheng, J. Lin, Y. Yan, X. Huang, W. Wong, K. Zhang and C. Chow, *Sens. Actuators, B*, **2018**, *262*, 386-394.

26. L. Fang, W. Shao, S. Zeng, G. Tang, J. Yan, S. Chen, Z. Huang, J. Tan, X. Chen, *Molecules*, **2022**, *27*, 6927.

27. Q. Li,1 Y. Kim, J. Namm, A. Kulkarni, G. R. Rosania, Y.-H. Ahn, and Y.-T. Chang, *Chemistry & Biology*, **2006**, *13*, 615-623.

28. R. Feng, L. Li, Bing Li, J. Li, D. Peng, Y. Yu, Q. Mu, N. Zhao, X. Yu and Z. Wang, *RSC Adv.*, **2017**, *7*, 16730.

29. Z. Wang, Y. Liu, W. Wang, C. Zhao and W. Lin , *New J. Chem.*, **2021**, *45*, 2614.

30. L. Guo, M.- S. Chan, D. Xu, D. Y. Tam, F. Bolze, P. K. Lo, and M.-S. Wong, *ACS Chem. Biol.*, **2015**, *10*, 1171-1175.

31. B. Zhou , W. Li , H. Zhang, J. Wu, S. Liu, H. Xu, P. Wang, *Biosensors and Bioelectronics*, **2015**, *68*, 189-196.

32. C. Cao, P. Wei, R. Li, Y. Zhong, X. Li, F. Xue, Y. Shi, and T. Yi, *ACS Sens.*, **2019**, *4*, 1409-1416.

33. Y. Yoshino, Y. Sato and S. Nishizawa, *Anal. Chem.*, **2019**, *91*, 14254-14260.

34. Jun Liu, Shilu Zhang, Chenghua Zhang, Jun Dong, Chengyi Shen, Jiang Zhu, Huajun Xu, Mingkai Fu, Guoqiang Yang and Xiaoming Zhang, *Chem. Commun.*, **2017**, *53*, 11476.

35. https://www.chem-station.com/odos/2013/01/-singlet-oxygen.html.

36. J. Al-Nu'airat, I. Oluwoye, N. Zeinali, M. Altarawneh and B. Z. Dlugogorski, *Chem.Rec.*, **2021**, *21*, 315-34.

37. J. R. Carreon, K. M. Stewart, K. P. Mahon, Jr., S. Shin and S. O. Kelley, Bioorg. *Med. Chem. Lett.*, **2007**, *17*, 5182-5185.

38. A. Kurutos, I. Orehovec, D. Saftić, L. Horvat, I. Crnolatac, I. Piantanida and T. Deligeorgiev, *Dyes Pigm.*, **2018**, *158*, 517-525.

39. J. O'Brien, I. Wilson, T. Orton and F. Pognan, *Eur. J. Biochem.*, **2000**, *267*, 5421-5426.

40. V. Tiku and A. Antebi, *Trends Cell Biol.*, **2018**, *28*, 662-672.

41. K. Higuchi, Y. Sato, N. Togashi, M. Suzuki, Y. Yoshino and S. Nishizawa, *ACS Omega*, **2022**, *7*, 23744-23748.

42. Y. Yoshino, Y. Sato and S. Nishizawa, Anal. Chem., 2019, 91, 14254-14260

43. Y. Sato, Y. Igarashi, M. Suzuki, K. Higuchi and S. Nishizawa, *RSC Adv.*, **2021**, *11*, 35436-35439.

Supporting information for chapter 2

1. Material & Method

All materials and measurements required for the experiments were based on the previous work in Nishizawa Lab.[S1-S3]

1.1 Materials

All of the synthetic RNAs and DNAs were custom synthesized and HPLC purified by GeneDesign Inc. (Osaka, Japan) and Nihon Gene Research Laboratories Inc. (Miyagi, Japan), respectively. Calf thymus DNA and *E. coli* total RNA were purchased from Sigma-Aldrich (Darmstadt, Germany) and Thermo Fisher Scientific (Tokyo, Japan), respectively. The other reagents were commercially available and of analytical grade. NMR spectra were recorded on a Bruker Avance III 500 spectrometer. High-resolution mass spectra (HRMS) were recorded on a JEOL JMS-T100CS or JMS-T100GCV instrument. The concentrations of calf thymus DNA and *E. coli* total RNA were determined from the absorbance at 260 nm at 85 ℃ using a molar absorption coefficient of 6600 $M^{-1}cm^{-1}$ and 9250 $M^{-1}cm^{-1}$ (M = mol/L per nucleotide), respectively.[S4] The concentrations of synthetic RNAs were determined from the absorbance at 260 nm measured at 80 ℃, using the molar extinction coefficient provided by the manufacturer. The concentrations of synthetic DNAs were determined according to the literature.[S5] Water was deionized (≥18.0 MΩ cm specific resistance) by an Elix 5 UV water purification system and a Milli-Q Synthesis A10 system (Millipore Corp., Bedford, MA, USA), followed by filtration through a BioPak filter (Millipore Corp., Bedford, MA, USA) in order to remove RNase.

Unless otherwise mentioned, all of the probes were dissolved in DMSO to obtain the stock solutions. The stock solutions were kept at 4 ℃ in the dark before their use. Final DMSO concentration in sample solutions containing the probes was below 0.1 % (v/v).

1.2 Method

1.2.1 UV-visible and fluorescence spectra measurements

Absorption and fluorescence spectra were measured using a JASCO model V-570 UV–vis sectrophotometer and FP-6500 spectrofluorophotometer (Japan Spectroscopic Co. Ltd., Tokyo, Japan), respectively. Both instruments were equipped with thermoelectrically temperature-controlled cell holders. Measurements of absorption and fluorescence spectra were done using a 2 × 10 mm quartz corvette (optical path length: 10 mm) and a 3 × 3 mm quartz corvette, respectively.

1.2.2 Fluorescence live cell imaging

MCF7 cells were cultured in RPMI 1640 media supplemented with 10% fetal bovine serum and 2% penicillin/streptomycin at 37 °C in a 5 % CO_2 incubator. For the fluorescence imaging experiments, MCF7 cells were seeded in a 8-well glass plate (Iwaki, Tokyo, Japan) at a density of about 0.5×10^4 cells/ well and maintained for 24 h. The cells were then incubated in the RPMI medium containing appropriate concentration of probes for 20 min or 24 h at 37 ℃ in a 5 % CO_2 incubator. After washing with HBSS buffer twice, the cells were imaged in HBSS buffer using a Deltavision Elite microscopy system (GE Healthcare Japan, Tokyo, Japan). In the co-staining experiments, the cells stained with probes were incubated in media containing co-staining probe (100 nM MitoBrigtht LT Deep red or 176 nM Hoechst 33342) for 20 min according to the manufacturer's protocol, respectively. The following filter sets were equipped in our Lab.: DAPI filter set (Ex 390/18; Em 435/48); FITC filter set (Ex 475/28; Em 545/48); TRITC set (Ex 545/27; Em 597/45); Cy5 filter set (Ex 632/22; Em 679/34). The obtained images were processed with the softWoRx software.

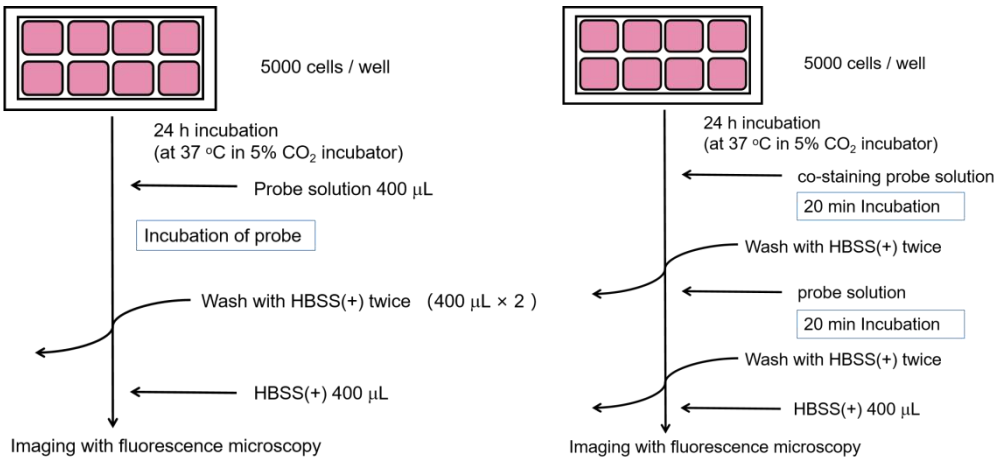

Fig. S 1.2.2-1 Protocols for live cell imaging (left) and co-staining (right) live cell imaging.

1.2.3 DNase and RNase digestion experiments

Digestion experiment need to be performed in the fixed and permeabilized cells. MCF7 cells were fixed in pre-chilled methanol at -20 ℃ for 1 min. The cell membrane was then permeablized with 1% Triton X-100 in MilliQ for 2 min at room temperature. After rinsing with D-PBS twice, the cells were incubated with suitable probes concentration in D-PBS buffer for 20 min at 37 ℃ in a 5 % CO_2 atmosphere, followed by washing with D-PBS buffer twice. Then DNase (100 U/mL), RNase (20 μg/mL), or D-PBS (control) were added into each of the three wells, which was then incubated at 37 ℃ in a 5 % CO_2 atmosphere for 3 h. Cells were rinsed again by D-PBS buffer twice before imaging. The fluorescent imaging pictures were obtained in D-PBS buffer by using an equal exposure time for control, DNase, and RNase experiments. Or add the suitable probe solution and the digestion solution in reverse order.

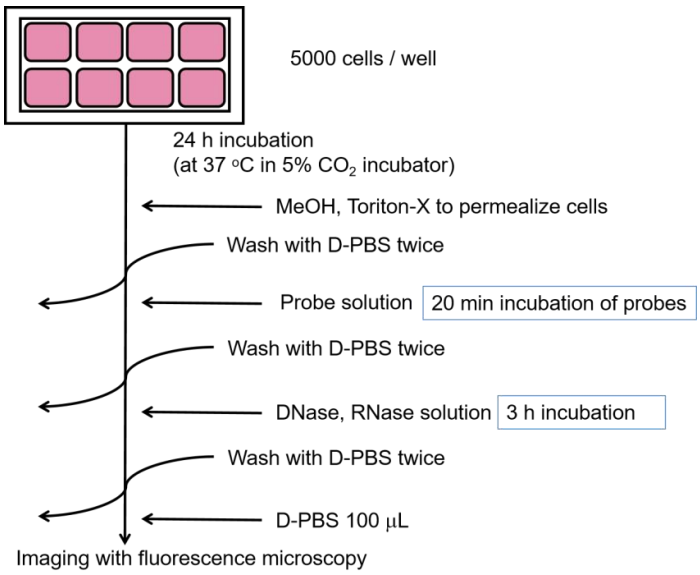

Fig. S 1.2.3-1 Protocols for digestion experiment

1.2.4 Cell toxicity Test (AlamarBlue® assay)

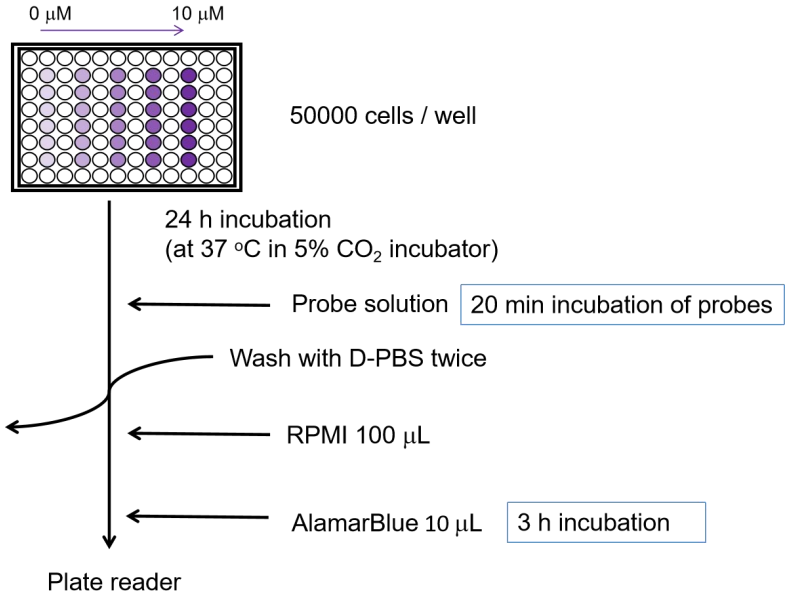

Fig. S 1.2.4-1 Protocols for cell toxicity test experiment.

Stock solution of probes was diluted by fresh medium into four desired concentration. MCF7 cells were seeded in 96-well microplates (Thermo Fisher Scientific, Tokyo, Japan) at a density of 5.0×10^4 cells/well in medium. After 24 h of cell attachment, the cell medium was exchanged by different concentrations of probes-containing medium solutions. They were then incubated at 37 ℃ in 5 % CO_2 for

20 min. After rinsing with D-PBS twice, fresh medium (100 μL) was added to each well, followed by the addition of 10 μL AlamarBlue® stock solution (Invitrogen, Carlsbad, CA) to each well. After incubation for 3 h where the microplates were covered with aluminum foil, the fluorescence intensity of each cell plate at 610 nm (Excitation: 540 nm, cut off: 590 nm) was measured with a microplate reader (SpectraMax M5, Molecular Devices, CA).

2. Synthesis and characterize of TOs

2.1 (Z)-1-methyl-4-((3-methylbenzo[d]thiazol-2(3H)-ylidene) methyl)quinolin-1-ium iodide (4TO):

This compound was prepared according to the literature.[S6]

^{1}H-NMR (500 MHz, DMSO-d_6): δ 8.81 (d, J = 8.5 Hz, 1H), 8.62 (d, J = 7.3 Hz, 1H), 8.08-8.01 (m, 3H), 7.80-7.77 (m, 2H), 7.62 (t, J = 7.8 Hz, 1H), 7.44-7.38 (m, 2H), 6.95 (s, 1H), 4.18 (s, 3H), 4.02 (s, 3H); 13C-NMR (500 MHz, DMSO-d_6): δ 159.6, 148.3, 144.9, 140.3, 137.9, 133.1, 128.0, 126.8, 125.4, 124.3, 123.9, 123.7, 122.7, 118.1, 112.8, 107.7, 87.8, 42.3, 33.8; ESI-MS for $C_{19}H_{17}N_2S$ ($[M]^+$): calcd, 305.11; found, 305.11.

2.2 Synthetic scheme for the preparation of TO-H.

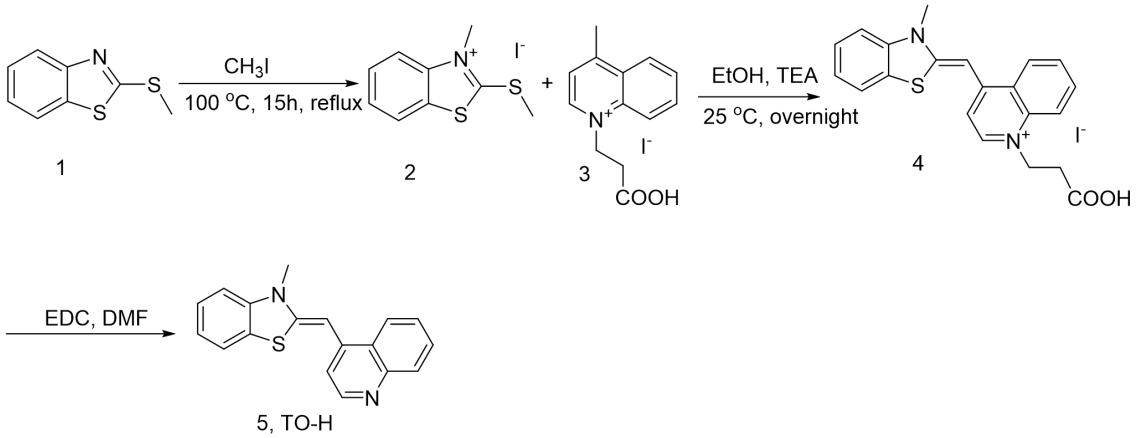

3-methyl-2-(methylthio)benzo[*d*]thiazol-3-ium iodide (2):[S7] To a dry 50 mL round bottom flask 2-(methylthio)benzothiazole (**1**) (4.0 g, 22 mmol) and iodomethane (29.79 mL, 45 mmol) were added. The flask was heated at 50 ℃ for 4 h. The reaction mixture became a white solid. After cooling to room temperature, MeOH (150 mL) and Et_2O (120 mL) were added to ensure that the product had fully precipitated. The precipitate was collected via vacuum filtration, washed with Et_2O (3 × 20 mL), and dried under reduced pressure to yield a white solid (0.42 g, 6%).

^{1}H-NMR (500 MHz, MeOH-d_4): δ 8.16-8.14 (m, 1H), 8.01 (d, J = 8.5 Hz, 1H), 7.79-7.75 (m, 1H), 7.65 (dd, J = 8.2, 7.3 Hz, 1H), 4.08 (s, 3H), 3.06 (s, 3H).

***(Z)*-1-(2-carboxyethyl)-4-((3-methylbenzo[d]thiazol-2(3*H*)-ylidene)methyl)quinolin-1-ium iodide (4):**[S5] The crude compound **2** (1.48 g, 5.0 mmol) and 2-methylmercapto-3-methyl benzothiazolium iodide

(1.62 g, 5.0 mmol) were suspended in ethanol (50 mL). Triethylamine (7.0 mL, 50 mmol) was added to the suspension, and the resultant red solution was stirred at 25 ℃ overnight. Diethyl ether (100 mL) was added, and the resultant suspension was stirred for 10 min. The precipitate was filtered, washed with diethyl ether, and dried under reduced pressure. Water (50 mL) was added to the resultant red solid and the suspension was stirred for 10 min. The precipitate was filtered, washed with water, and dried under reduced pressure. The product **4** was obtained as a red solid (1.92 g, 78%).

^{1}H-NMR (500 MHz, DMSO-d_6): δ 8.87 (d, J = 8.9 Hz, 1H), 8.68 (d, J = 7.3 Hz, 1H), 8.20 (d, J = 8.9 Hz, 1H), 8.12 (d, J = 7.3 Hz, 1H), 8.05 (t, J = 7.8 Hz, 1H), 7.87 (d, J = 8.2 Hz, 1H), 7.82 (t, J = 7.8 Hz, 1H), 7.69 (t, J = 7.8 Hz, 1H), 7.50 (t, J = 7.6 Hz, 1H), 7.42 (d, J = 7.3 Hz, 1H), 7.01 (s, 1H), 4.86 (t, J = 6.9 Hz, 2H), 3.36 (t, J = 7.0 Hz, 2H), 2.75 (s, 3H); ESI-MS for $C_{21}H_{19}N_2O_2S$ ([M]$^+$): calcd, 363.12; found, 363.15.

(Z)-3-methyl-2-(quinolin-4-ylmethylene)-2,3-dihydrobenzo[*d*]thiazole (5, TO-H):[S8] **4** (443 mg, 1.0 mmol) and 1-ethyl-3- (3-dimethylaminopropyl)carbodiimide hydrochloride (383 mg, 2.0 mmol) were suspended in DMF (10 mL). The suspension was stirred at 25 ℃ for 24 h. After addition of 1-ethyl-3-(3-dimethylaminopropyl)carbodiimide hydrochloride (192 mg, 1.0 mmol), it was further stirred at 25 ℃ overnight. The reaction mixture was diluted with chloroform (100 mL) and washed with water (100 mL). The aqueous layer was extracted with chloroform (50 mL) twice. The combined organic layer was dried with Na_2SO_4 and evaporated in vacuo. The product was purified by silica gel column chromatography (5 % MeOH – CH_2Cl_2), giving the product **5** as an orange powder (70 mg, 48%).

^{1}H-NMR (500 MHz, DMSO-d_6): δ 8.73 (d, J = 4.9 Hz, 1H), 8.42 (d, J = 8.2 Hz, 1H), 7.93 (d, J = 8.5 Hz, 1H), 7.73-7.70 (m, 1H), 7.65 (d, J = 7.0 Hz, 1H), 7.57 (t, J = 7.0 Hz, 1H), 7.41 (d, J = 5.2 Hz, 1H), 7.36-7.28 (m, 2H), 7.07 (t, J = 7.5 Hz, 1H), 6.46 (s, 1H), 3.65 (s, 3H); ^{13}C-NMR (500 MHz, DMSO-d_6): δ 149.6, 149.4, 147.9, 142.4, 141.5, 129.2, 128.9, 126.9, 125.3, 125.2, 123.9, 122.4, 121.8, 121.3, 112.9, 109.5, 84.9, 32.0; ESI-MS for C18H15N2S ([M+H]$^+$): calcd, 291.0955; found, 291.0940.

2.3 Synthetic scheme for the preparation of TO-C_4.

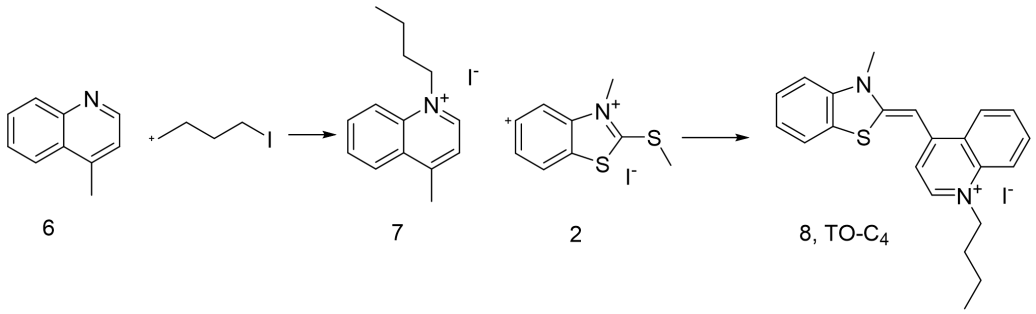

1-butyl-4-methylquinolin-1-ium iodide (7):[S9] Equimolar amounts of the compound **6** and the alkyl iodide (10 mmol each) were heated with stirring for 3 h at 85 ℃. After cooling to room temperature, the solidified crude product was suspended in tetrahydrofuran for 10 min. Precipitation of quaternary ammonium salt was improved by adding diethyl ether. The crude product was collected, washed several times with diethyl ether, and dried in a vacuum. The compound **7** was finally obtained as yellow oils (1.8

g , 55 %).

^{1}H-NMR (500 MHz, DMSO-d_6): δ 9.41 (d, J = 6.1 Hz, 1H), 8.60-8.54 (m, 2H), 8.26 (t, J = 7.3 Hz, 1H), 8.08-8.04 (m, 2H), 5.00 (t, J = 7.6 Hz, 2H), 2.98-3.03 (3H), 1.95-1.89 (m, 2H), 1.39 (td, J = 15.1, 7.4 Hz, 2H), 0.92 (t, J = 7.3 Hz, 3H).

(Z) **-1-butyl-4-((3-methylbenzo[*d*]thiazol-2(3H)-ylidene)methyl)quinolin-1-ium iodide (8, TO-C$_4$):**[S5] The crude compound **7** (832.80mg, 2.5 mmol) and compound **2** (802.62 mg, 2.5 mmol) were suspended in ethanol (25 mL). Triethylamine (3.5 mL, 25 mmol) was added to the suspension, and the resultant red solution was stirred at 25 ℃ overnight. Diethyl ether (50 mL) was added, and the resultant suspension was stirred for 10 min. The precipitate was filtered, washed with diethyl ether, and dried under reduced pressure. Water (25 mL) was added to the resultant red solid and the suspension was stirred for 10 min. The precipitate was filtered, washed with water, and dried under reduced pressure. The product **8** was obtained as a red solid (1.92 g, 78%).

^{1}H-NMR (500 MHz, DMSO-d_6): δ 8.81 (d, J = 8.2 Hz, 1H), 8.64 (d, J = 7.0 Hz, 1H), 8.15 (d, J = 8.5 Hz, 1H), 8.06 (d, J = 7.3 Hz, 1H), 8.00 (t, J = 7.8 Hz, 1H), 7.81-7.75 (m, 2H), 7.63 (t, J = 7.8 Hz, 1H), 7.43 (t, J = 7.3 Hz, 1H), 7.38 (d, J = 7.0 Hz, 1H), 6.94 (s, 1H), 4.61 (t, J = 7.3 Hz, 2H), 4.03 (s, 3H), 1.87-1.81 (m, 2H), 1.38 (td, J = 15.0, 7.5 Hz, 2H), 0.93 (t, J = 7.5 Hz, 3H); ^{13}C-NMR (500 MHz, DMSO-d_6): δ 160.0, 148.5, 144.3, 140.4, 137.0, 133.2, 128.1, 126.7, 125.8, 124.4, 124.2, 123.8, 122.8, 118.1, 112.9, 107.8, 88.1, 53.9, 33.8, 30.8, 19.2, 13.5; ESI-MS for $C_{22}H_{23}N_2S$ ([M]$^+$): calcd, 347.16; found, 347.16.

2.4 Synthetic scheme for the preparation of 2TO.

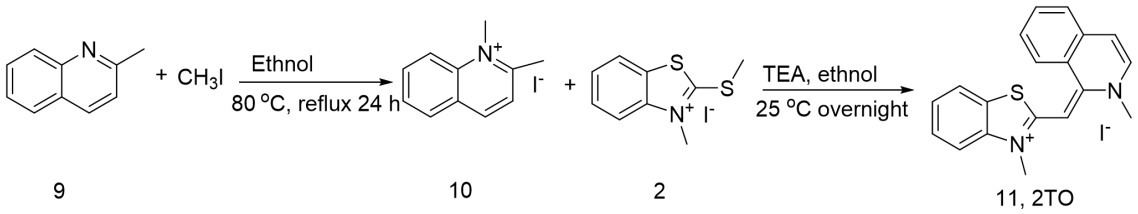

1,2-dimethylquinolin-1-ium iodide (10):[S10] Toward a round-bottom flask with 5 mL ethanol, 1.0 mL (7.4 mmol) of 2-methylquinoline and 0.46 mL (7.4 mmol) iodomethane were added. The mixture was stirred evenly and heated to reflux at 80 ℃ for 24 h. The system was then cooled down to room temperature, and dark yellow powder was precipitated. The product was filtered and washed with ethanol three times, and was used for the next step without further purification (0.61 g, 28%).

^{1}H-NMR (500 MHz, DMSO-d_6): δ 9.10 (d, J = 8.5 Hz, 1H), 8.59 (d, J = 8.9 Hz, 1H), 8.40 (d, J = 8.2 Hz, 1H), 8.23 (t, J = 7.2 Hz, 1H), 8.12 (d, J = 8.5 Hz, 1H), 7.99 (t, J = 7.5 Hz, 1H), 4.45 (s, 3H), 3.08 (s, 3H).

(*E*)-3-methyl-2-((2-methylisoquinolin-1(2*H*)-ylidene)methyl)benzo[*d*]thiazol-3-ium iodide (11, 2TO):[S5] The crude 1,2-dimethylquinolin-1-ium (148 mg, 0.5 mmol) and 2-methylmercapto-3-methyl

benzothiazolium iodide (162 mg, 0.5 mmol) were suspended in ethanol (5 mL). Triethylamine (0.7 mL, 5 mmol) was added to the suspension, and the resultant red solution was stirred at 25 ℃ overnight. Diethyl ether (10 mL) was added, and the resultant suspension was stirred for 10 min. The precipitate was filtered, washed with diethyl ether, and dried under reduced pressure. Water (5 mL) was added to the resultant red solid and the suspension was stirred for 10 min. The precipitate was filtered, washed with water, and dried under reduced pressure. The product **11** was obtained as a red solid (40 mg, 16 %).

^{1}H-NMR (500 MHz, DMSO-d_6): δ 8.45 (d, J = 9.2 Hz, 1H), 8.14 (d, J = 8.9 Hz, 1H), 8.09 (d, J = 9.5 Hz, 1H), 8.03 (q, J = 3.8 Hz, 2H), 7.93-7.90 (m, 1H), 7.79 (d, J = 8.2 Hz, 1H), 7.63-7.60 (m, 2H), 7.43 (t, J = 7.6 Hz, 1H), 6.17 (s, 1H), 4.13 (s, 3H), 3.94 (s, 3H); ^{13}C-NMR (500 MHz, DMSO-d_6): δ 161.6, 153.4, 140.7, 139.8, 133.4, 129.4, 128.1, 125.6, 124.8, 124.0, 123.4, 122.8, 118.5, 117.3, 113.1, 86.6, 37.7, 33.9; ESI-MS for for $C_{19}H_{17}N_2S$ ([M]$^+$): calcd, 305.11; found, 305.11.

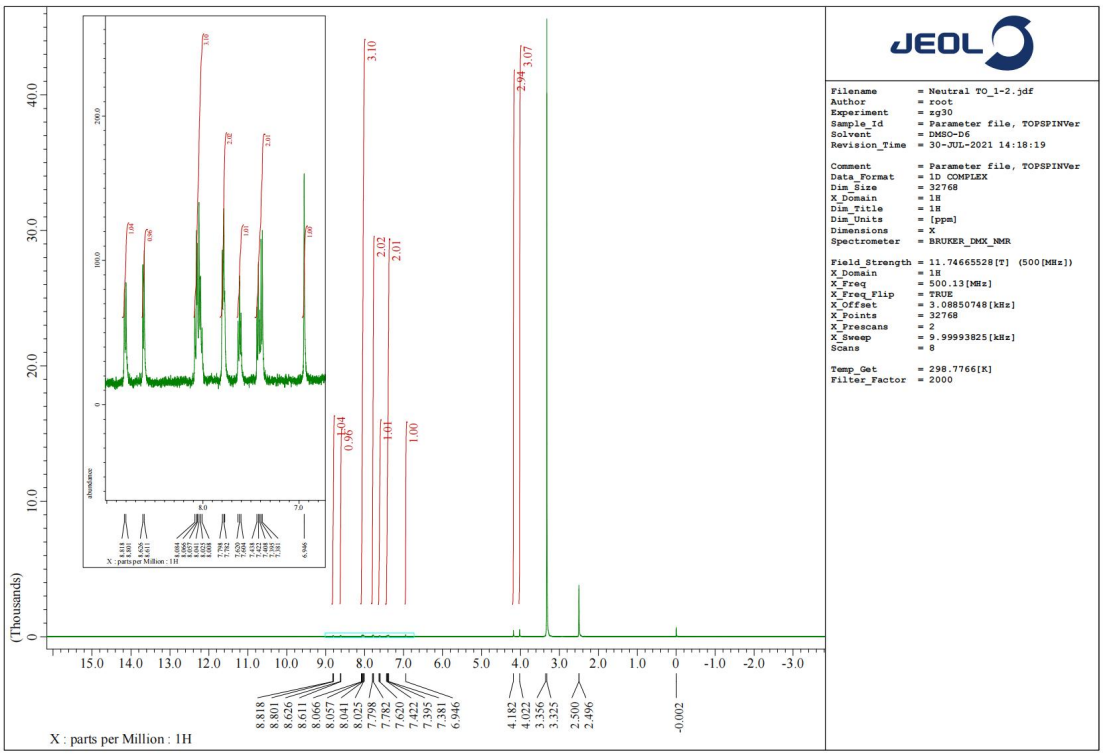

Fig. S 2.1-1 ^{1}H NMR of common TO (4TO) in DMSO-d_6.

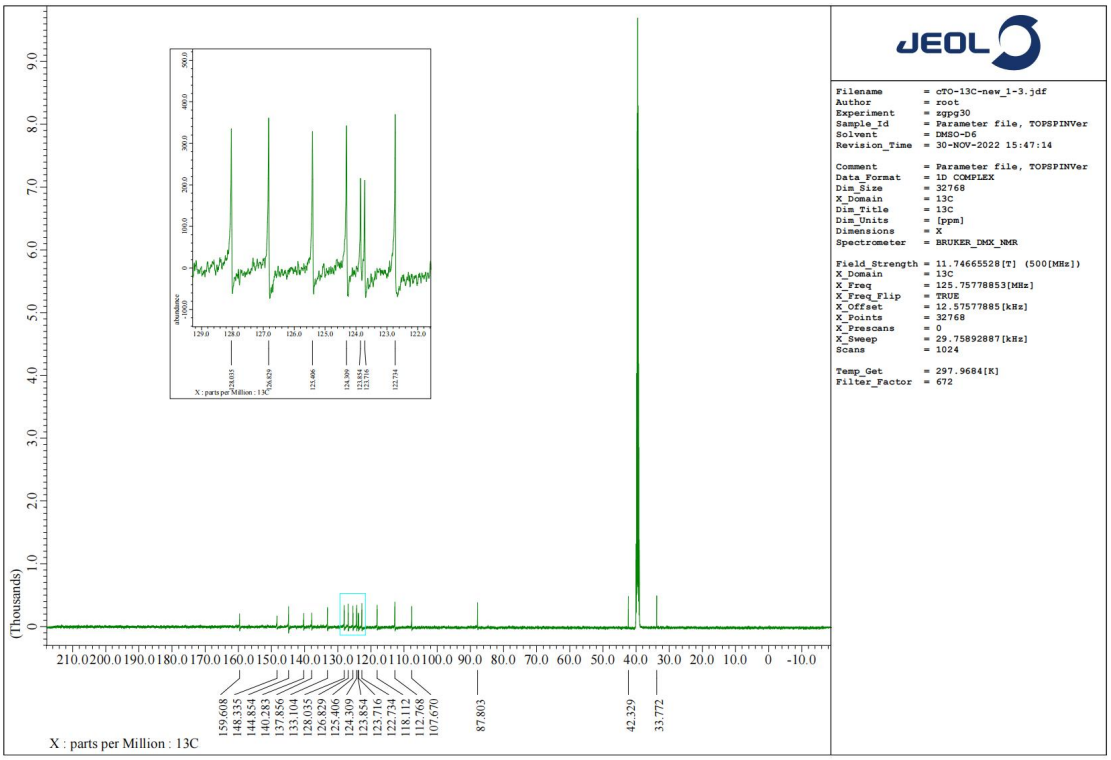

Fig. S 2.1-2 ^{13}C NMR of common TO (4TO) in DMSO-d_6.

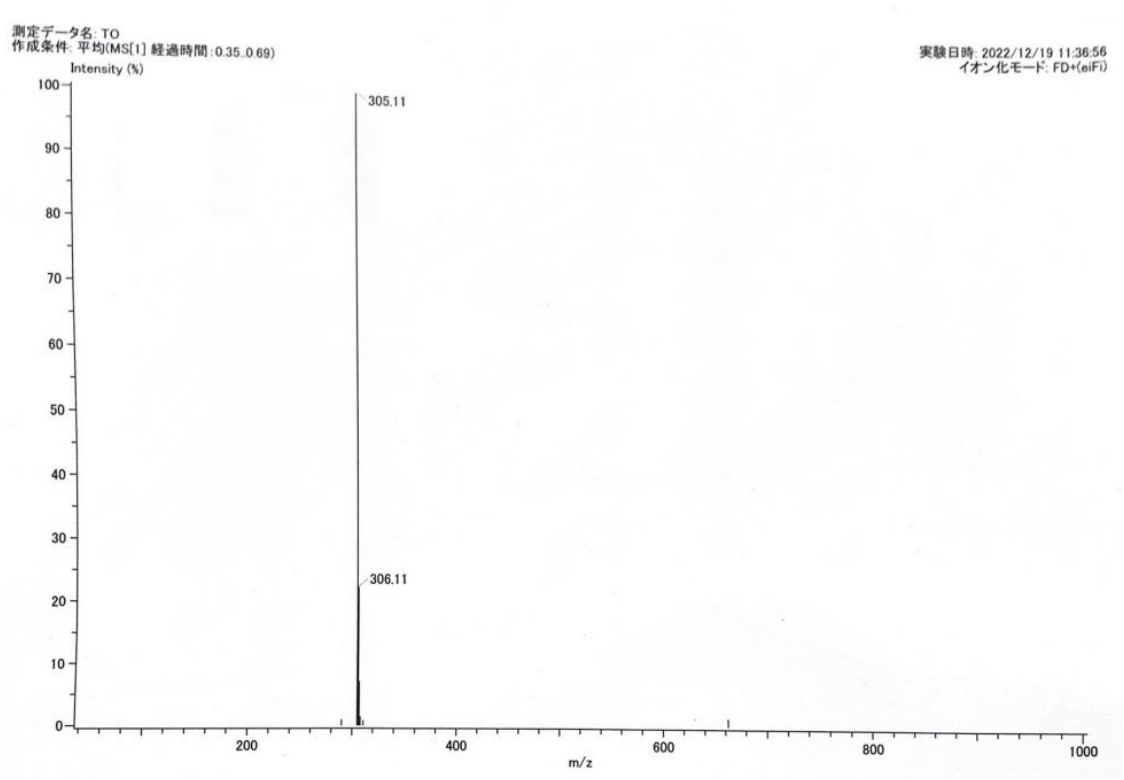

Fig. S 2.1-3 ESI-MS spectrum of TO (4TO) in MeOH.

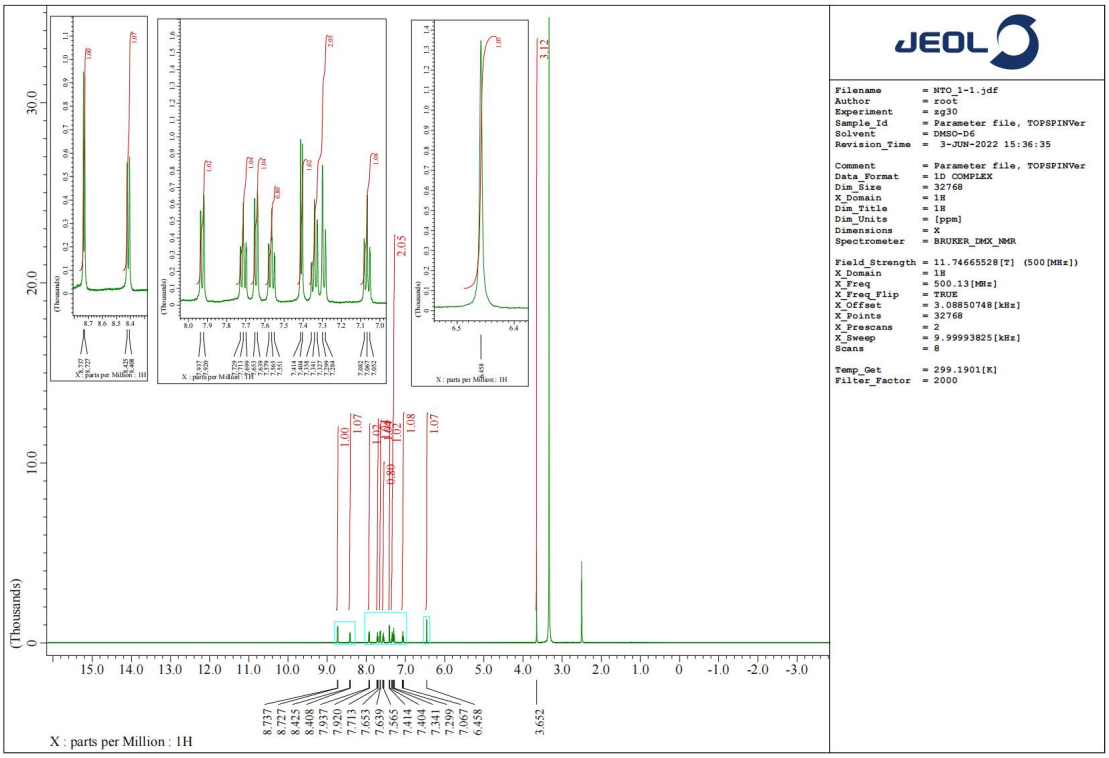

Fig. S 2.2-1 ^{1}H NMR of TO-H in DMSO-d_6.

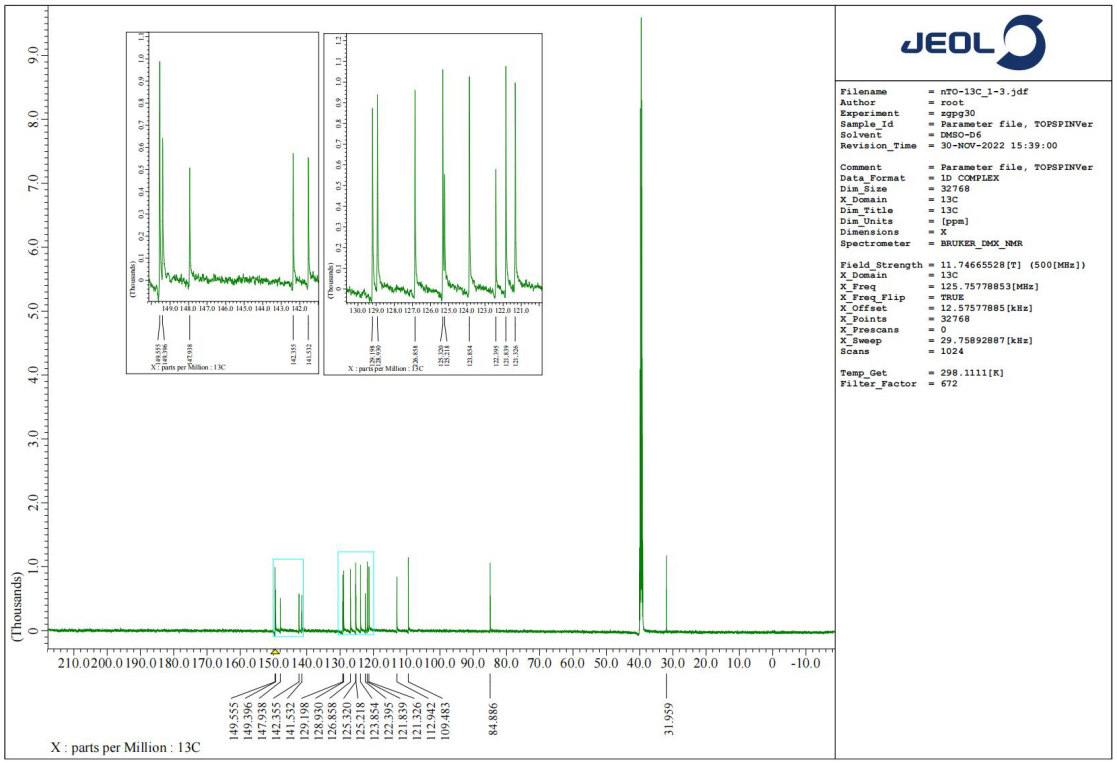

Fig. S 2.2-2 ^{13}C NMR of TO-H in DMSO-d_6.

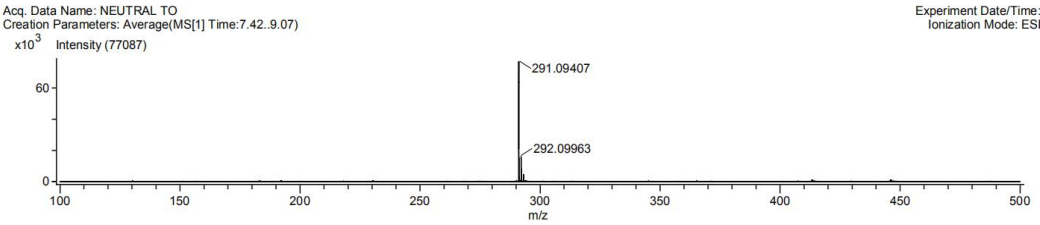

Fig. S 2.2-3 ESI-MS spectrum of TO-H in MeOH.

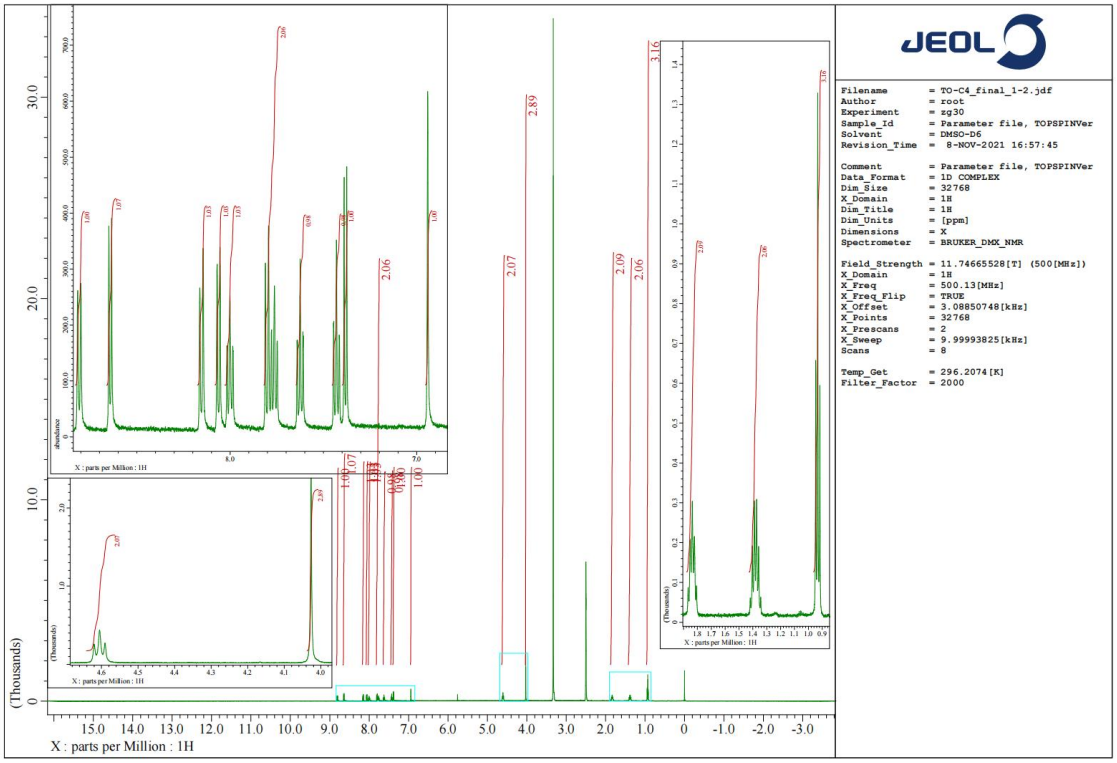

Fig. S 2.3-1 ^{1}H NMR of TO-C$_4$ in DMSO-d_6.

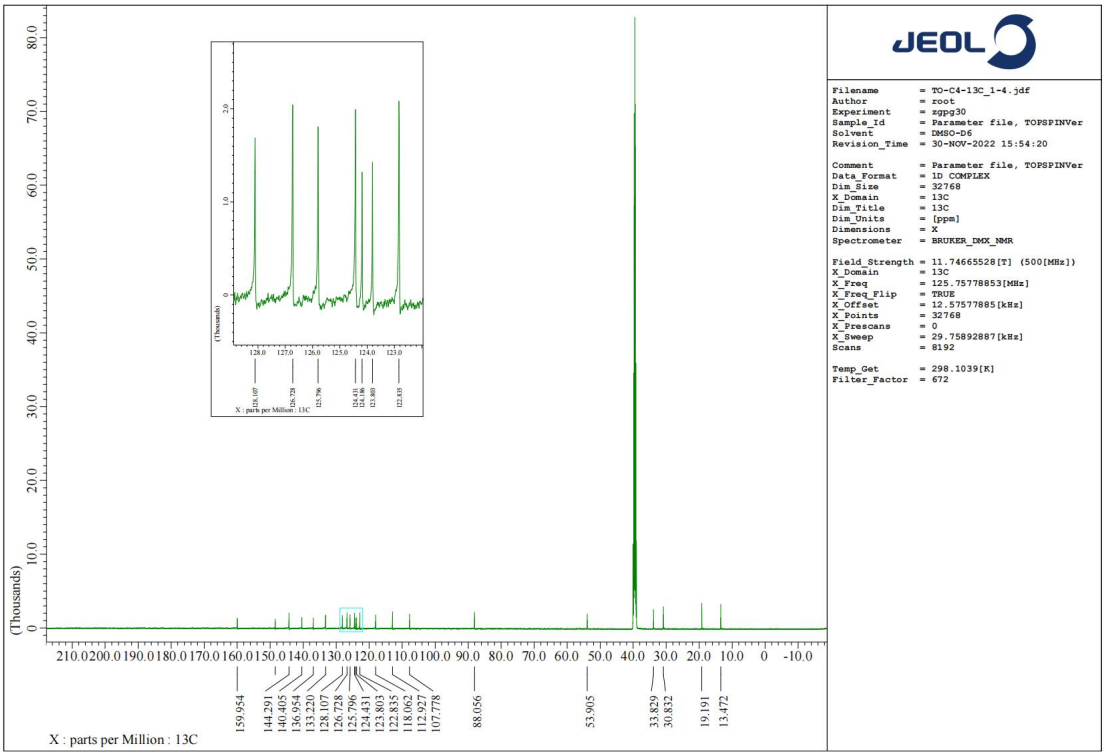

Fig. S 2.3-2 ^{13}C NMR of TO-C_4 in DMSO-d_6.

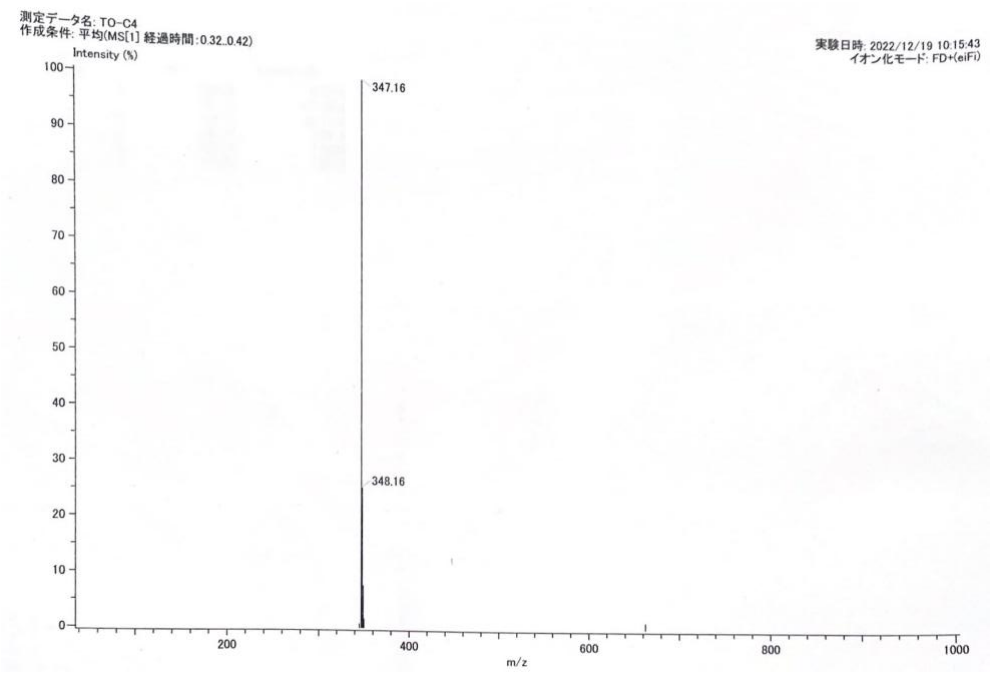

Fig. S 2.3-3 ESI-MS spectrum of TO-C_4 in MeOH.

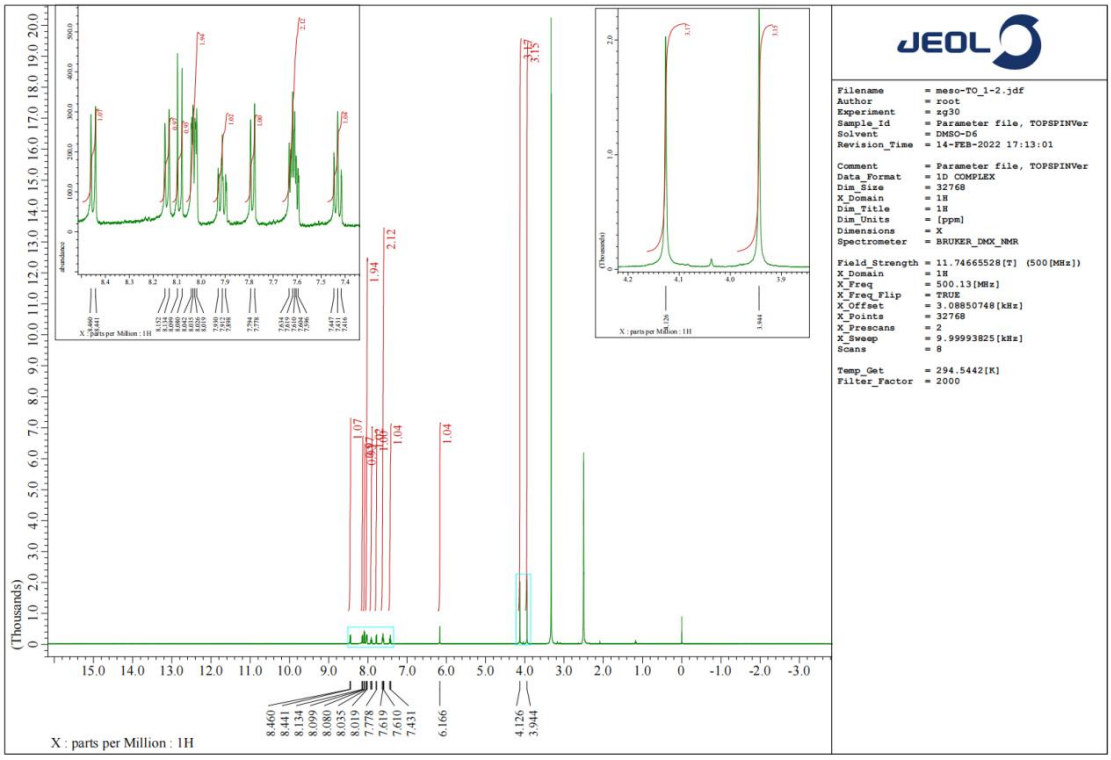

Fig. S 2.4-1 ^{1}H NMR of 2TO in DMSO-d_6.

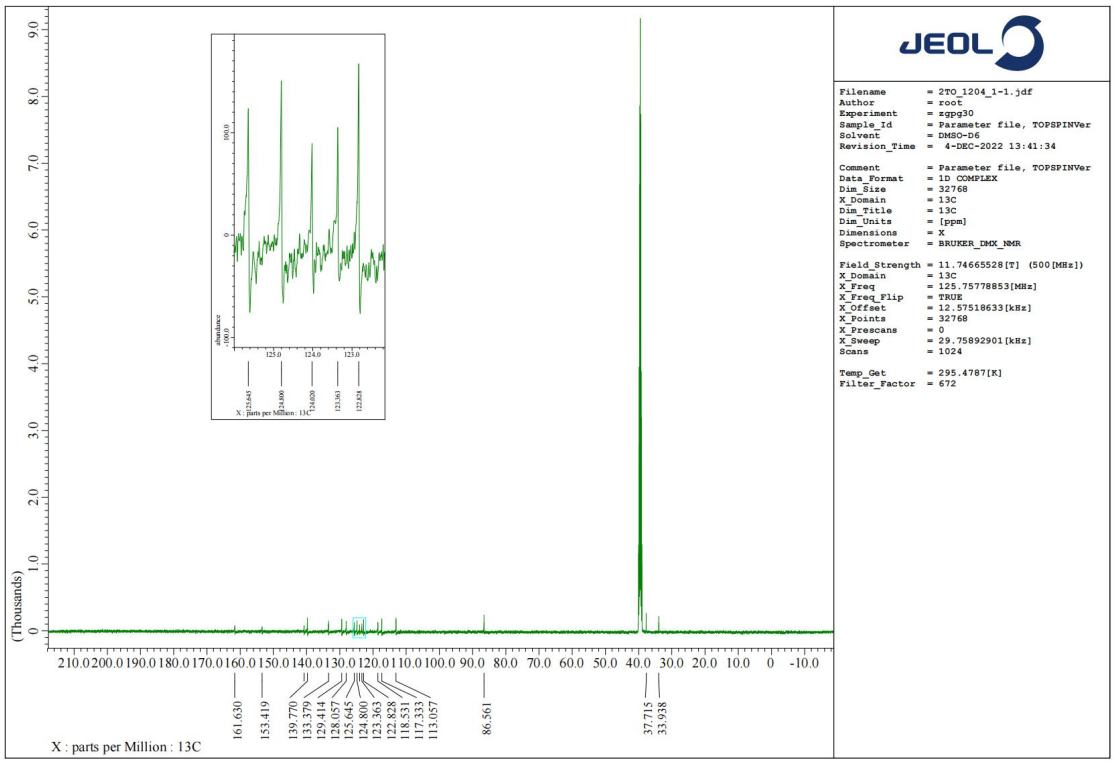

Fig. S 2.4-2 ^{13}C NMR of 2TO in DMSO-d_6.

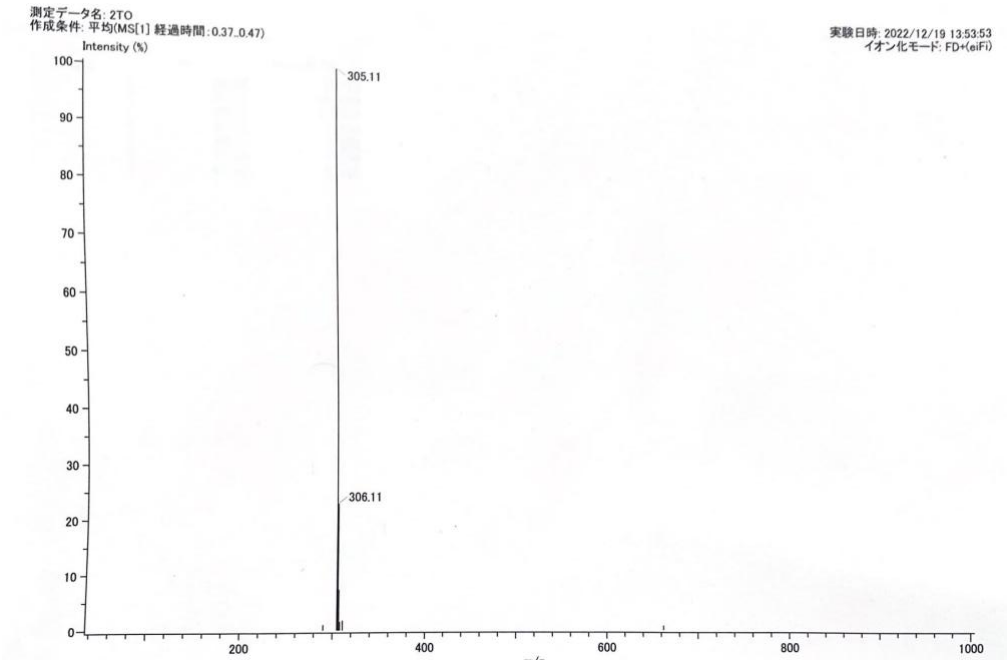

Fig. S 2.4-3 ESI-MS spectrum of 2TO in MeOH.

3. Absorption spectra

3.1 Absorption spectra of TOs in DMSO

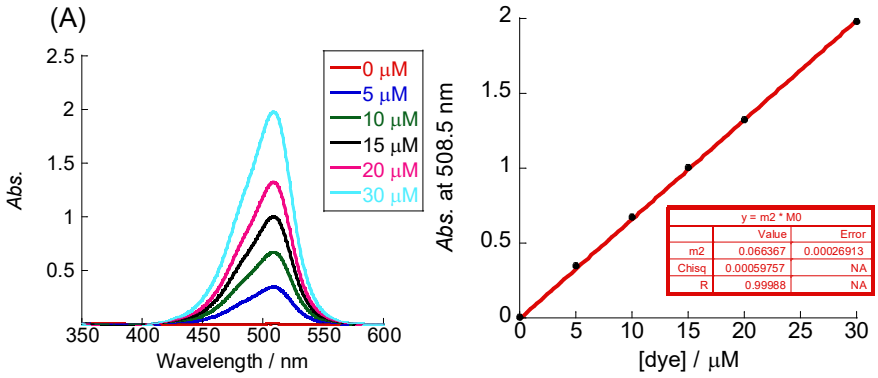

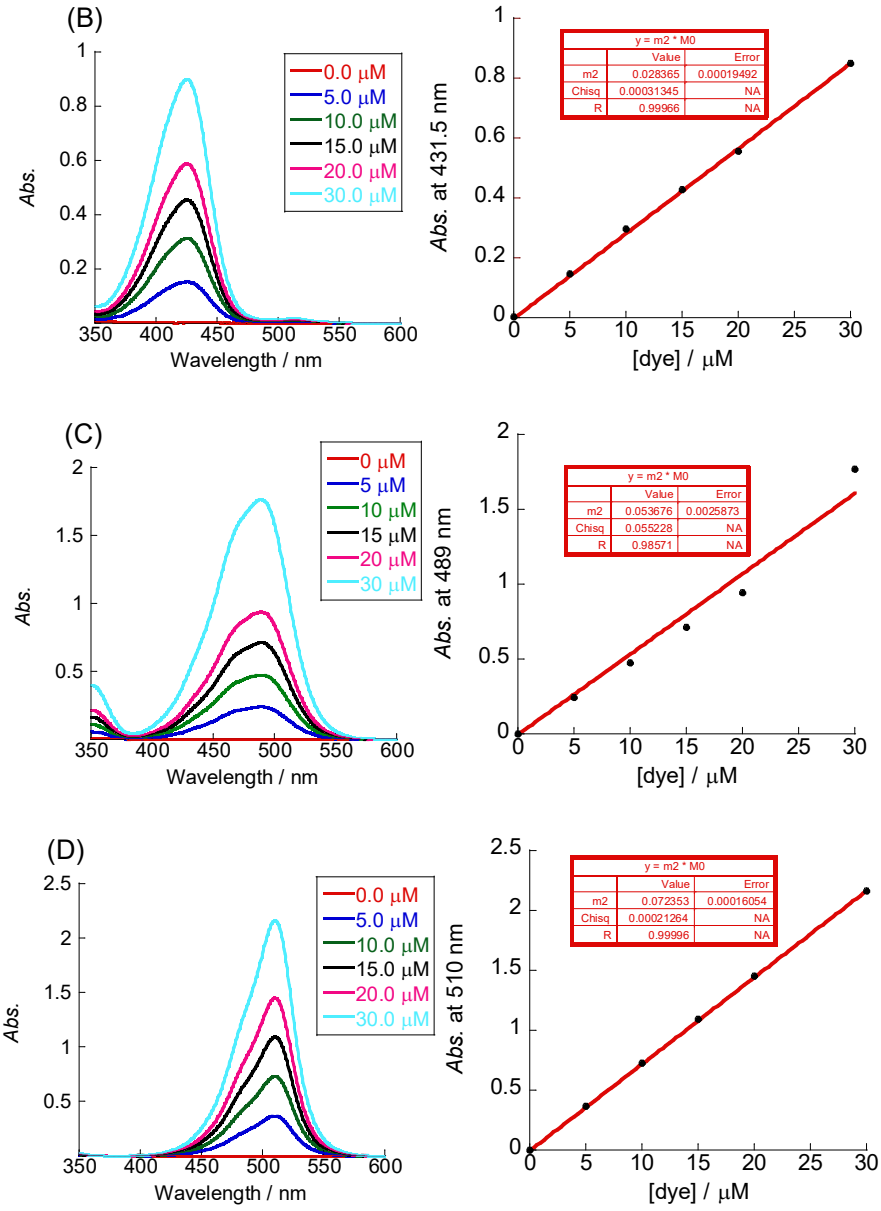

Fig. 3.1-1 Absorption spectra of four TOs in DMSO and their curve fit line. (A) TO, (B) TO-H, (C) 2TO, (D) TO-C_4. Experimental condition: [dye] = 0 - 30 μM, sensitivity: medium, data interval: 0.5 nm, scan rate: 100 nm/ min, temperature: 25 ℃, cell: 1.0 × 0.2 cm, optical path: 10 mm.

Molar absorption coefficient (ε): TO, 6.6×10^4; TO-H, 2.8×10^4; 2TO, 5.4×10^4; TO-C_4, 7.2×10^4.

3.2 Absorption spectra of TOs in phosphate buffer

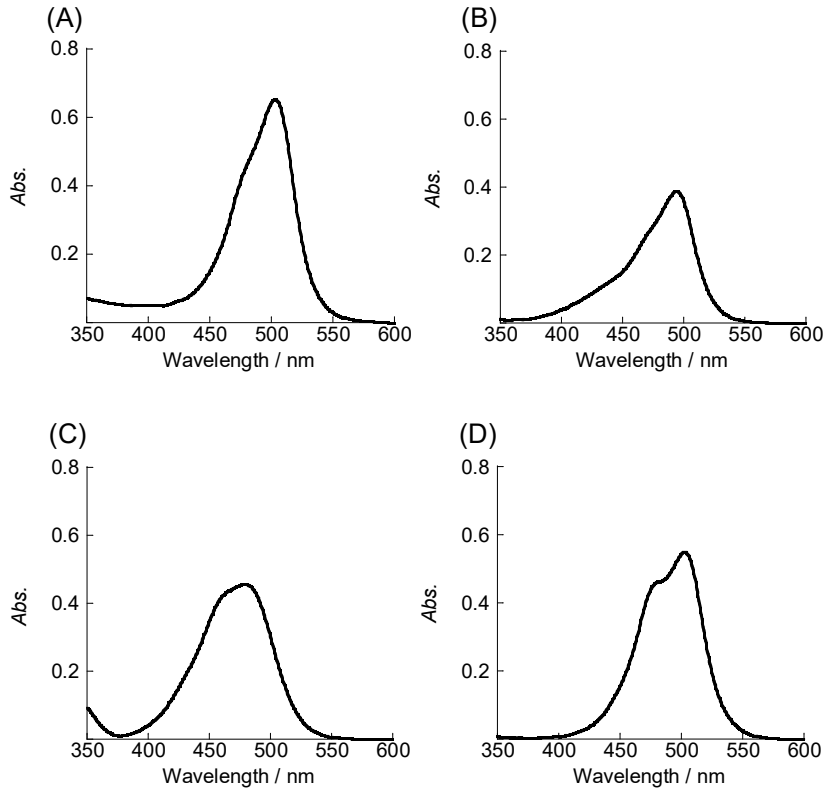

Fig. 3.2-2 Absorption spectra of four TOs in 10 mM sodium phosphate buffer (pH 7.0) containing 100 mM NaCl 1.0 mM EDTA. (A) TO, (B) TO-H, (C) 2TO, (D) TO-C_4.

Experimental condition: [probe] = 10 μM, sensitivity: medium, data interval: 0.5 nm, scan rate: 100 nm/ min, temperature: 25 ℃, cell: 1.0 × 0.2 cm, optical path: 10 mm.

The max absorption wavelength: TO, 503 nm; TO-H, 493.5 nm; 2TO, 479 nm; TO-C_4, 503 nm.

4. Reference

S1 K. Higuchi, Y. Sato, N. Togashi, M. Suzuki, Y. Yoshino and S. Nishizawa, *ACS Omega*, **2022**, *7*, 23744-23748.

S2 Y. Yoshino, Y. Sato and S. Nishizawa, *Anal. Chem.*, **2019**, *91*, 14254-14260.

S3 Y. Sato, Y. Igarashi, M. Suzuki, K. Higuchi and S. Nishizawa, *RSC Adv.*, **2021**, *11*, 35436-35439.

S4 G. Tyagi, S. Pradhan, T. Srivastava, R. Mehrota, Biochim. *Biophys. Acta, Gen. Subj.*, **2014**, *1840*, 350-356.

S5 J. D. Puglisi, I. Tinoco, *Methods Enzymol.*, **1989**, *180*, 304-325.

S6 A. Abdelhameed, X. Liao, C. A. McElroy, A. C. Joice, L. Rakotondraibe, J. Li, C. Slebodnick, P. Guo, W. D. Wilson, K. A. Werbovetz, *Bioorg. Med. Chem. Lett.*, **2020**, *30*, 126725.

S7 M. V. Sonar, M. E. Wampole, Y-Y. Jin, C-P. Chen, M. L. Thakur, E. Wickstrom, *Bioconjug.*

Chem., **2014**, *25*, 1697-1708.

S8 S. Ikeda, A. Okamoto, *Photochem. Photobiol. Sci.*, **2007**, *6*, 1197-1201.

S9 C. T. Martins, M. S. Lima, O. A. E. Seoud, *J. Phys. Org. Chem.*, **2005**, *18*, 1072-1085.

S10 J. Sun, M. Tian and W. Lin, *Analyst*, **2019**, *144*, 2387-2392.

Chapter 3

Quinoline blue and its regioisomer as fluorogenic probes for nucleolar RNA imaging in living cells

1. Introduction

Quinoline blue (QB), as the Fig. 1-1 shown, consisting of two same quinoline hetercycles through a monomethine bridge, is a typical symmetrical monomethine cyanine dye. QB was known as the first synthesized cyanine dye in 1856. Charles Hanson Greville Williams obtained this dye by distillation of cinchonine and then heated the distillate with amyl iodide and an excess of ammonia. This reaction resulted in the formation of a compound that exhibited a "magnificent blue color, which he named 'Quinoline Blue'.[1] His discovery marked a significant advancement in the field of cyanine dyes[2-7] and had a profound impact on the development of the dye for industrial applications.[8-12] So far, QB has been widely used as a forced intercalation (FIT) probe[13,14,15] and triplex-forming forced intercalation (tFIT) probe[16,17] for RNA sensing. However, to the best of my knowledge, such a RNA selective probe has never been used for nucleolar RNA imaging in living cells.

Nevertheless, 2QB (Fig. 1-1), also known as quinoline violet (QV), the regioisomer of QB, were utilized for further experiment.

Therefore, both QB and its regioisomer, 2QB, were synthesized and the nucleolar RNA selectivity in living cells were examined.

In this chapter, firstly, QB and 2QB were successfully synthesized and their properties were evaluated and compared, especially their performance in RNA selectivity. Then, QB and 2QB were applied for nucleolus imaging in living and fixed and permeabilized cells to check their staining ability.

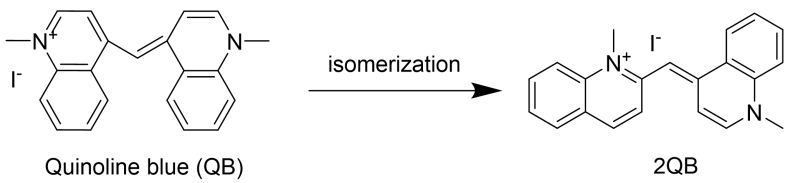

Fig. 1-1 Structure of QB and 2QB.

2. Synthesis of QB and 2QB

2.1 Synthetic scheme for the preparation of QB

QB was synthesized as the following routine. Finally, the synthesized and purified compound were characterized by ESI-MS and ^{1}H-NMR. For detailed information on synthesis and related experiments, please refer to supporting information in this chapter.

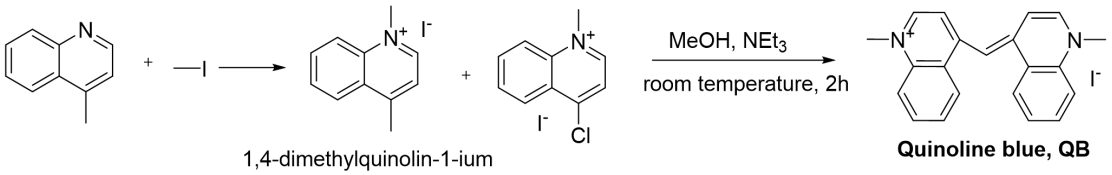

2.2 Synthetic scheme for the preparation of 2QB

2QB was synthesized as the following routine. Finally, the synthesized and purified compound were characterized by ESI-MS and ^{1}H-NMR. For details on synthesis and characterization, please see supporting information in this chapter.

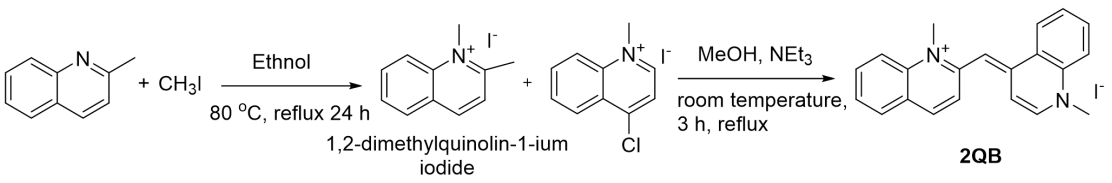

3. Photophysical properties and fluorescence signaling abilities of QB and 2QB for RNA sensing

3.1 Absorption spectra of QB and 2QB

Firstly, I examined the absorption spectra of 1. 0 μM QB and 2QB in the absence and presence of 1.0 mM ct DNA or 1.0 mM *E. coli* total RNA. In order to make it easier to observe the spectral changes, Fig 3.1-1 shows the normalized data, as shown, the maximum absorption wavelengths of both QB and 2QB are red-shifted upon binding to the nucleic acid compared to the free probe, suggesting that both probes bind to the nucleic acid by intercalate into the base pairs. Since the intercalation of the probes into the base pairs leads to the formation of a π-π stacking, this kind of stacking method extends the conjugation system and therefore a red shift occurs in the absorption spectrum.

Similar to TO and 2TO group, the red-shift in the absorption spectra indicate the binding of QB and 2QB to nucleic acid as a monomer. Again, the shoulder peak at shorter wavelengths of 2QB is more significant compared to QB, implying that more 2QB forms dimer to bind to nucleic acids.

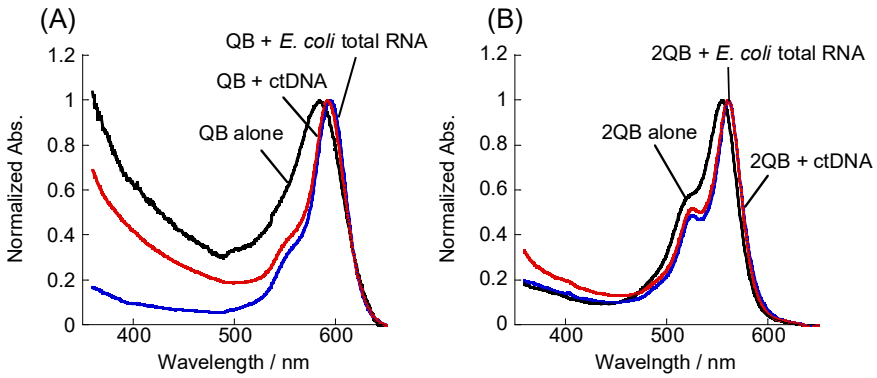

Figure 3.1-1 Normalized absorption spectra of (A) QB (1.0 μM) and (B) 2QB (1.0 μM) in the absence and presence of 1.0 mM calf thymus DNA or 1.0 mM *E. coli* total RNA. Experimental condition: [probe] = 1.0 μM in 10 mM sodium phosphate buffer (pH 7.0) containing 100 mM NaCl 1.0 mM EDTA, sensitivity: medium, data interval: 0.5 nm, scan rate: 100 nm/ min, temperature: 25 ℃, cell: 1.0 × 0.2 cm, optical path: 10 mm. Data were obtained after mixing dyes with nucleic acid solutions and subsequent incubation for 30 min.

3.2 Fluorescence response to nucleic acid solutions

3.2.1 Fluorescence response to biological nucleic acid

Also, the fluorescence spectra of QB and 2QB in the absence and presence of 1.0 mM calf thymus DNA or 1.0 mM *E. coli* total RNA were detected (Fig. 3.2.1-1) by using the same solution in Fig. 3.1-1. It's easily to observed that both QB and 2QB shows almost no fluorescence in the absence of biological nucleic acid solution, while the fluorescence intensity greatly enhanced in the yellow spectral region (λ_{em}: QB: 609.5 nm, 2QB: 578 nm) in the presence of *E. coli* total RNA.

As for the selectivity to RNA and DNA, the situation is similar to TO and 2TO group, where QB shows the selectivity to RNA over DNA (Fig. 3.2.2.-1-A, I_{RNA}/I_{DNA} = 1.8) , while 2QB, the regioisomer, shows higher selectivity to RNA over DNA (Fig. 3.2.2.-1-B, I_{RNA}/I_{DNA} = 2.6). This result indicate my speculation that the regioisomer structure has a better selectivity to RNA over DNA, not only suitable for green emissive TO and 2TO, but also applicable for yellow emissive QB and 2QB.

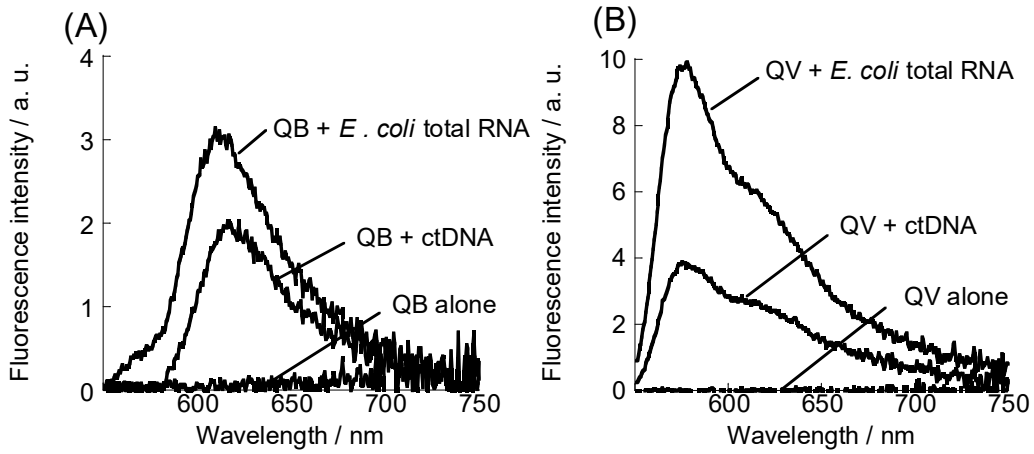

Figure 3.2.1-1 Fluorescence spectra of (A) QB (1.0 μM) and (B) 2QB (1.0 μM) in the absence and presence of 1.0 mM *E. coli* total RNA or 1.0 mM calf thymus DNA. Measurements were performed in 10 mM sodium phosphate buffer solution (pH 7.0) containing 100 mM NaCl and 1.0 mM EDTA. Excitation: 530 nm. Ex band: 3 nm, Em band: 3 nm, senseitivity: medium. Scan rate : 100 nm / min, response : 0.5 s. Temperature: 25 ℃. Data were obtained after mixing dyes with nucleic acid solutions and subsequent incubation for 30 min.

3.2.2 Quantum yield calculation

Quantum yield was determined relative to 167 nM Rhodamine 6G in EtOH (Φ = 0.95, Ex: 530 nm).[18] The calculation method was same as chapter 2. Finally, the quantum yield of QB and 2QB were calculated as the following table 3.2.2-1.

Probes	Samples	ϕ_{bound}	ϕ_{RNA}/ϕ_{free}	ϕ_{RNA}/ϕ_{DNA}	Light-up factor (I/I_0)
QB	Probe alone	＜0.001	26	1.6	320
	ct DNA	0.019			
	E coli. Total RNA	0.026			
2QB	Probe alone	＜0.001	29	2.8	640
	ct DNA	0.014			
	E coli. total RNA	0.029			

Table 3.2.2-1 Quantum yield and signaling ability of QB and 2QB.

Although both QB and 2QB have low quantum yield, about 0.026 and 0.028, respectively, it's worthy noting that, 2QB, the regioisomer of QB, exhibits a more remarkable light-up response（I/I_0 = 640) than QB (I/I_0=320). In fact, 2QB is one of the top level of yellow emissive dye with off-on signaling ability.[11]

3.2.2 Fluorescence response to synthetic nucleic acid

The fluorescence response to synthetic nucleic acid were detected as Fig. 3.2.2-1. Based on the observation of these spectra, QB prefers to bind to RNA strand (rGrC and rG) over double stranded DNA (dGdC). Similar result happens in 2QB where 2QB also prefers to bind to RNA strand over DNA, indicate that QB and 2QB are more selective to rGrC and rG bases, causing them to exhibit good selectivity to *E. coli* total RNA.

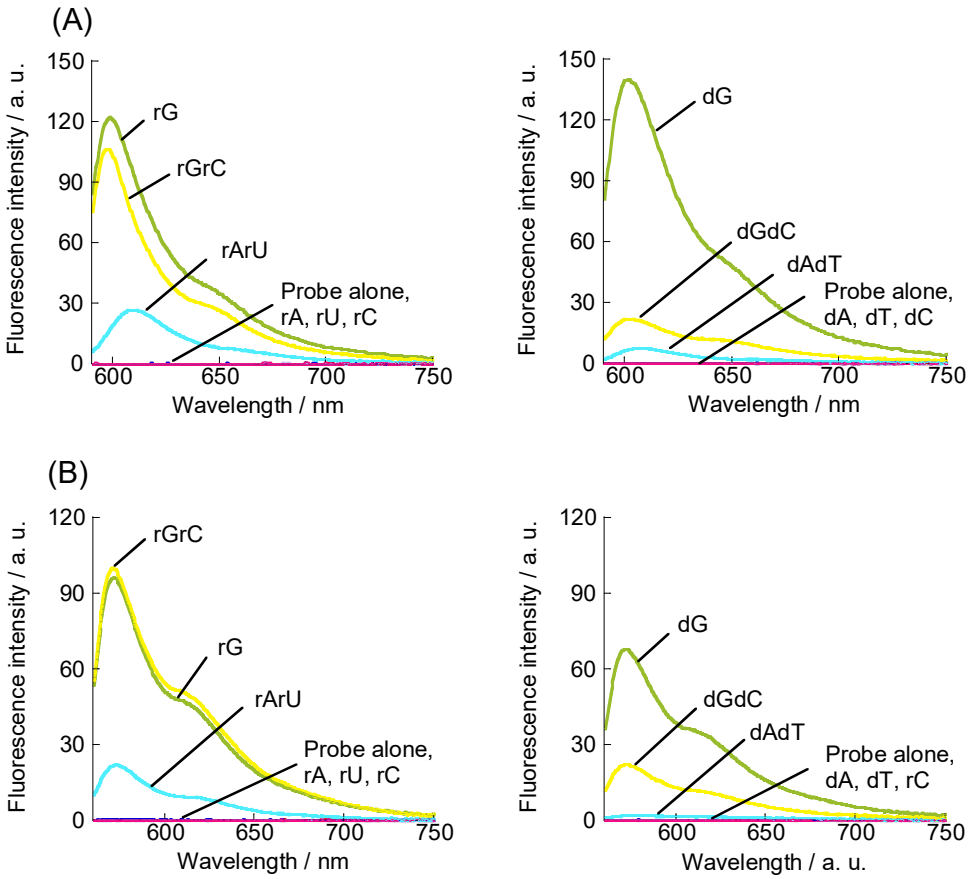

Fig. 3.2.3-1 Fluorescence response of (A) QB (1.0 μM) and (B) 2QB (1.0 μM) to synthetic nucleic acids (20 μM).

Experimental condition: Excitation: (A) 585.5 nm, (B) 555.5 nm. [dye] = 1.0 μM in 10 mM sodium phosphate buffer solution (pH 7.0) containing 100 mM NaCl and 1.0 mM EDTA. Ex band: 3 nm, Em bamd: 3 nm, senseitivity: medium. Scan rate : 100 nm / min, response : 0.5 s, temperature: 25 ℃, 3 × 3 nm quartz cell. Data were obtained after mixing dyes with nucleic acid solutions and subsequent incubation for 30 min.

The nucleic acid sequences:

rG: 5'- r(GGG GGG GGG GGG G)-3' dG: 5'- d(GGG GGG GGG GGG G)-3'

rC: 5'- r(CCC CCC CCC CCC C)-3' dC: 5'- d(CCC CCC CCC CCC C)-3'

rA: 5'- r(AAA AAA AAA AAA A)-3' dA: 5'- d(AAA AAA AAA AAA A)-3'

rU: 5'- r(UUU UUU UUU UUU U)-3' dT: 5'- d(TTT TTT TTT TTT T)-3'

3.3 Photostability of QB and 2QB

Photostability also is an important factor to evaluate the properties of probe. As evident from the Fig 3.3-1, QB shows a moderate photostability where the fluorescence intensity decreased about 37 % after 3 hours continuous irradiation after incubating QB with *E. coli* total RNA for 30 min. In the case of 2QB, the fluorescence intensity decreased 20 % after 3 hours irradiation indicating relatively better photostability in solutions compared with QB.

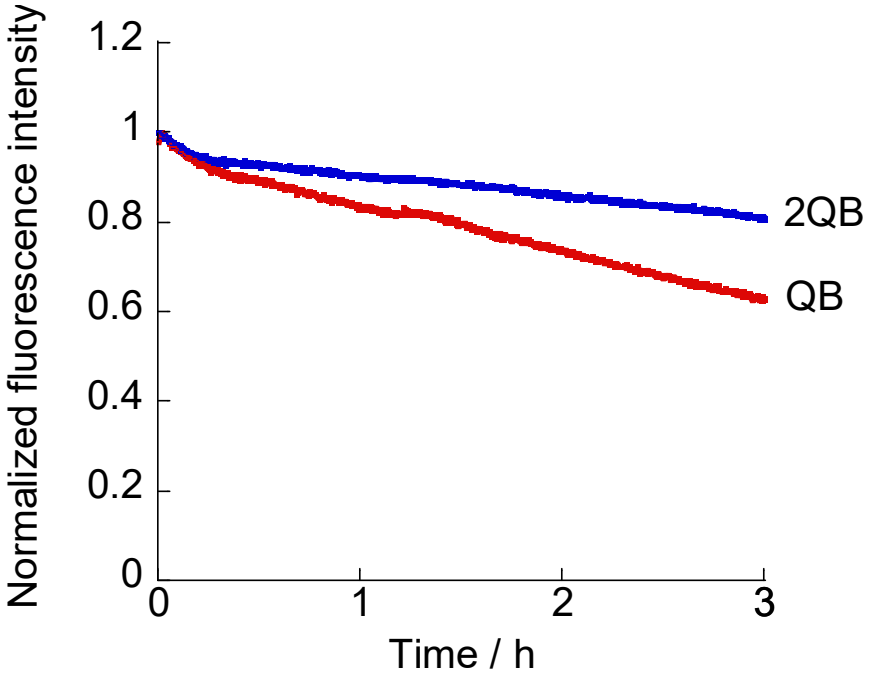

Figure 3.3-1 Changes in fluorescence intensity of QB and 2QB when bound to *E. coli* total RNA under continuous irradiation (3 h). [Probe] = 1.0 μM, [*E. coli* total RNA] = 100 nM in solutions buffered at pH 7.0 (10 mM sodium phosphate) containing 100 mM NaCl and 1.0 mM EDTA. Before the measurement, sample solutions were incubated for 30 min. Excitation: 585.5 nm (QB), 555.5 nm (2QB). Ex band: 3 nm, Em band: 3 nm, senseitivity, medium. Temperature: 25 ℃.

4. Application to cells

4.1 Living cell imaging

Then both QB and 2QB were applied to living MCF7 cell imaging. The work concentration of QB and 2QB were optimized to 3 μM.

As can be observed from the Fig. 4.1-1, QB and 2QB were co-stained with the DNA staining probe, Hochest 33342. The blue emission from the nucleus (emission filter: 435/48 nm) was in high contrast to the strong emission observed in the yellow region (emission filter: 597/45 nm) in the nucleolus. This result suggests that both QB and 2QB exhibit remarkable permeability through both the cell plasma and nuclear membrane in living cells.

Interestingly, compared to QB, 2QB shows higher contrast to the blue emission from the nucleus, as we can see in the line profile, indicating 2QB, the isomer shows better selectivity to nucleolus than QB.

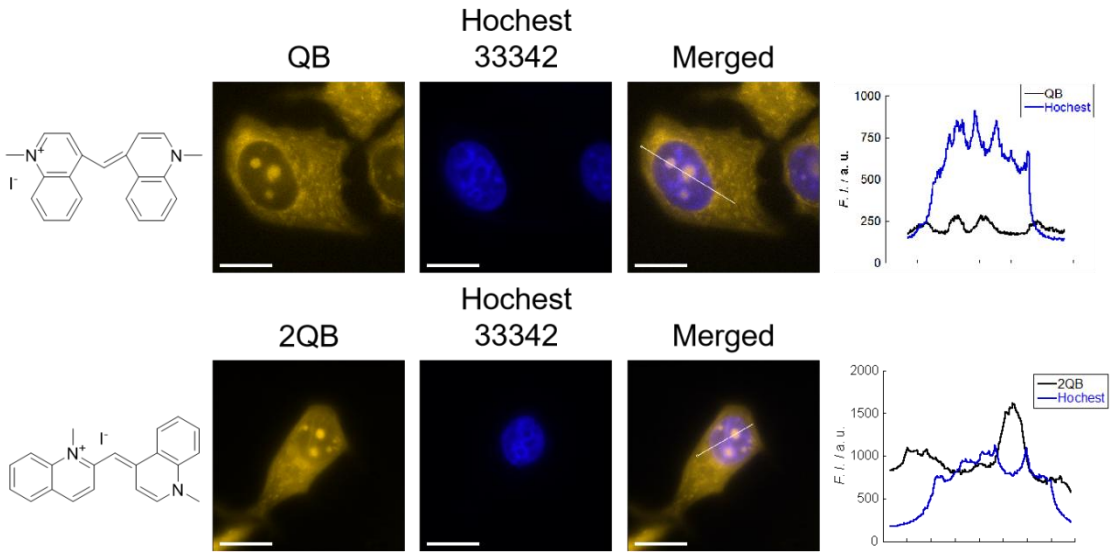

Figure 4.1-1 Fluorescence images of living MCF7 cells stained by QB (3 μM) and 2QB (3 μM) with Hoechst 33342 (176 nM). Incubation time : 20 min. Parameters: FITC, 100 %, 0.1 s for QB and 2QB; DAPI, 32 %, 0.1 s for Hochest 33342. Scale bar: 15 μm. The cells were imaged in HBSS buffer after washing with HBSS buffer twice.

4.2 Digestion experiment

The digestion experiment in the fixed and permeabilized MCF7 cells further proved both QB and 2QB shows better RNA selectivity than DNA in cells where the fluorescence signal in the nucleolus was almost disappeared after RNase treatment while strong signal remain observed by the treatment of DNase.

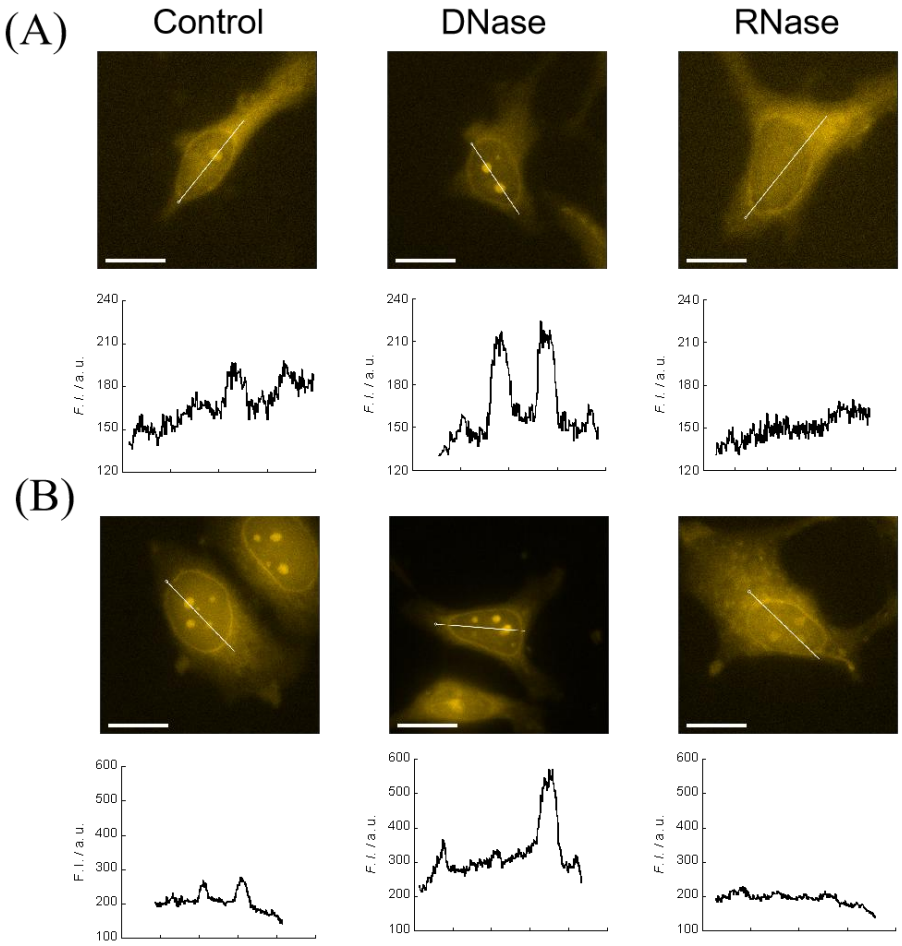

Figure 4.2-1 Fluorescence images of fixed and permeabilized MCF7 cells stained by QB (3 μM) and 2QB (3 μM) before (control) and after treatment with DNase or RNase for 3 hours. Parameters: FITC, 100 %, 0.1 s for all iamges. Scale bar: 15 μm. The cells were imaged in D-PBS buffer after washing with D-PBS buffer twice.

4.3 Fixed and permeabilized cell imaging

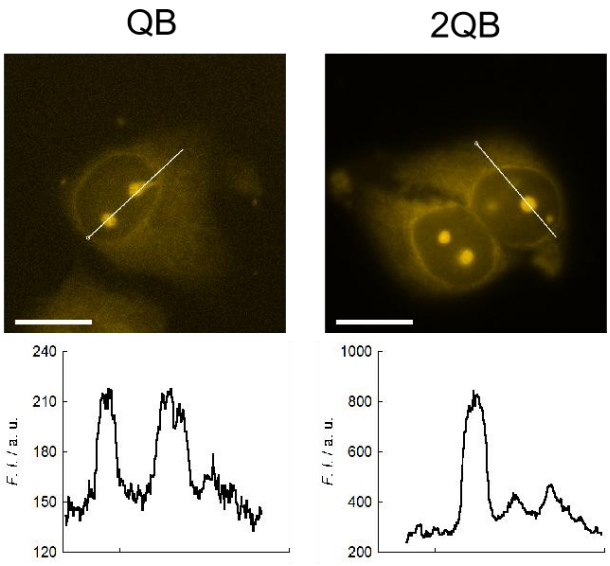

Figure 4.3-1 Fluorescence images of fixed and permeabilized MCF7 cells stained by QB (3 μM) and 2QB (3 μM) after 20 min incubation. Parameters: FITC, 100 %, 0.1 s for all images. Scale bar: 15 μm. After washing with D-PBS buffer twice, the cells were imaged in D-PBS buffer.

The staining ability of QB and 2QB in the fixed and permeabilized MCF7 cells were also checked. As it shown in the Fig. 4.3-1, strong signal in the nucleolus were observed indicate both QB and 2QB shows nucleolus staining ability in the fixed and permeabilized cells. Again, 2QB exhibits higher contrast to the nucleus as we can see in the line profile indicate that 2QB, the regioisomer works better than QB.

4.4 Living cell imaging without washing protocol

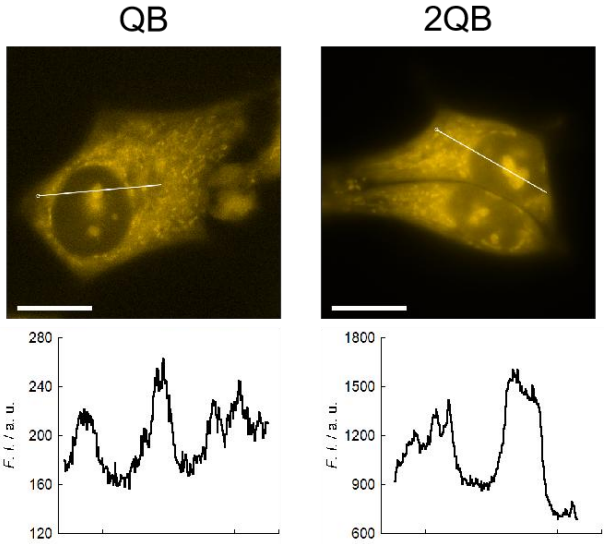

Figure 4.4-1 *No-washing* fluorescence imaging of living MCF7 cells stained by QB (3 μM), 2QB (3 μM) after 20 min incubation. Fluorescence intensity profiles along the white line are also shown. Parameters: FITC, 100 %, 0.1 s for all images. Scale bar: 15 μm. The cells were imaged in HBSS buffer.

The nucleolus staining ability of QB and 2QB in the living MCF7 cells without washing step were then confirmed. Here, the strong emission in the nucleolus and cytoplasm can be observed both in QB and 2QB. The contrast to nucleus is similar to the images obtained with washing step, while considerable emission in the cytoplasm were observed both in QB and 2QB indicate washing step is necessary for nucleolus imaging in living MCF7 cells to obtain better images.

4.5 Living cell imaging after 24 h incubation

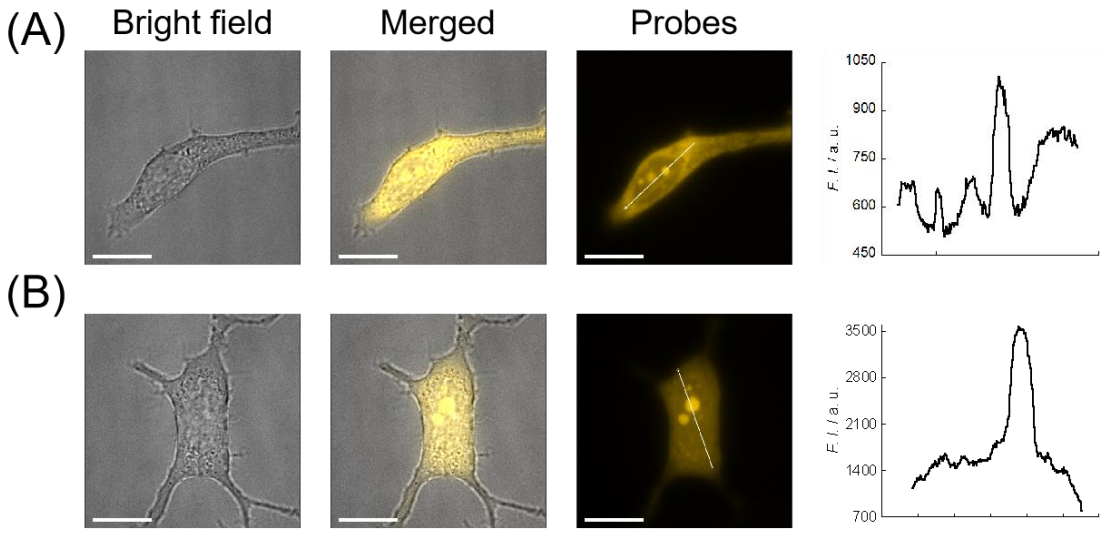

Fig. 4.5-1 Images of living MCF7 cells stained by (A) QB (3 μM), (B) 2QB (3 μM) after 24 h incubation. Fluorescence intensity profiles along the white line are also shown. Parameters: FITC, 50 %, 0.1 s for all iamges. Scale bar: 15 μm. After washing with HBSS buffer twice, the cells were imaged in HBSS buffer.

The Fig. 4.5-1 shows the images of living MCF 7 cells stained by 3 μM QB and 2QB after 24 h hours incubation. Here, no any morphological changes were observed in the cells and the nucleolus were clearly stained after 24 hours incubation indicate the two probes are working as nucleolus staining dyes applicable for long time observation and experiments. It can be found that after 24 hours of incubation, the fluorescence intensity within the cells as well as the contrast were greatly enhanced compared to 20 minutes of incubation both in the case of QB and 2QB. This suggests that longer incubation time is more suitable to obtain better images. In addition, same to the standard 20 min incubation, 2QB shows higher contrast to the nucleus and cytoplasm in the line profile, indicate 2QB, the regioisomer works much better than QB even with 24 hours incubation.

4.6 The other cell line imaging

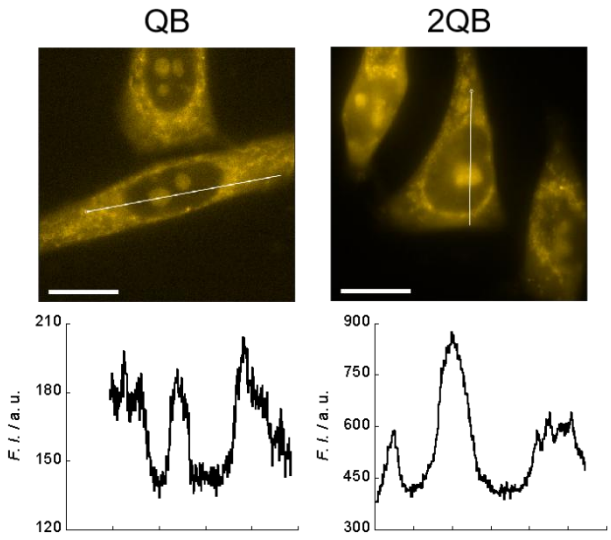

Figure 4.6-1 Fluorescence imaging of living HeLa cells stained by QB (3 μM), 2QB (3 μM) after 20 min incubation. Fluorescence intensity profiles along the white line are also shown. Parameters: FITC, 100 %, 0.1 s for all images. Scale bar: 15 μm. After washing with HBSS buffer twice, the cells were imaged in HBSS buffer.

Except for living MCF7 cells imaging, the other cell line such as living HeLa cells imaging were also performed. Fig. 4.6-1 shows the fluorescence images of living HeLa cells stained by 3 μM QB and 2QB after 20 min incubation. Here, we can observe yellow fluorescence emission in the nucleolus accompanied by strong emission in the cytoplasm. This suggests that both QB and 2QB shows nucleolus selectivity also in living HeLa cells However, as can be seen from the signal contrast between the nucleolus and cytoplasm, QB and 2QB do not stain as well as they do in living MCF7 cells, which seem to accumulate more in the cytoplasm. Such difference is probably due to the different membrane permeability of the different cell lines.

4.7 Time lapse

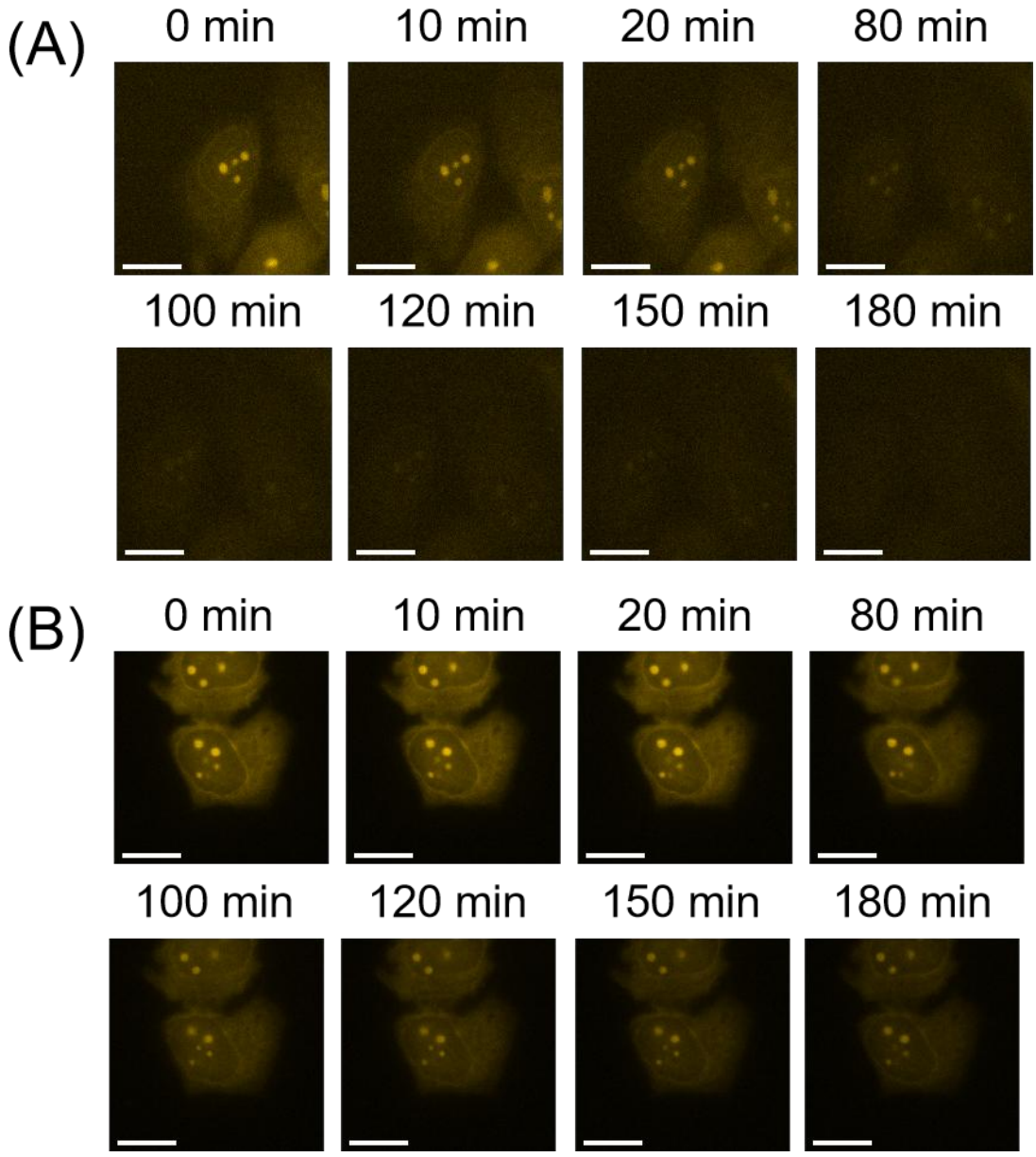

Figure 4.7-1 Changes in fluorescence imaging of fixed and permeabilized MCF7 cells stained by (A) QB (3 μM) and (B) 2QB (3 μM) after 20 min incubation for 3 h continuous irradiation with 10 min interval. Parameters: FITC, 100 %, 0.1 s for all images. Scale bar: 15 μm. After washing with HBSS buffer twice, the cells were imaged in D-PBS buffer.

The Fig.4.7-1 shows the photostability of QB and 2QB in the fixed and permeabilized MCF7 cells. After the cells were incubated for 20 min with probes and the washing step was completed, the cells were placed under a fluorescence microscope for observation. Every ten minutes for the next three hours I

recorded fluorescent images of the cells. As we can see from the images, QB shows low photostability where the fluorescence signal in the nucleolus was almost disappeared after 80 min, while the fluorescence emission still can be observed even after 180 min in the case of 2QB indicate 2QB, the regioisomer shows relatively good photostability in cells. This result is well consistent with photostability in the solutions when the two probes bind to *E. coli* total RNA.

4.8 QB works as a red-emissive dye in living cells

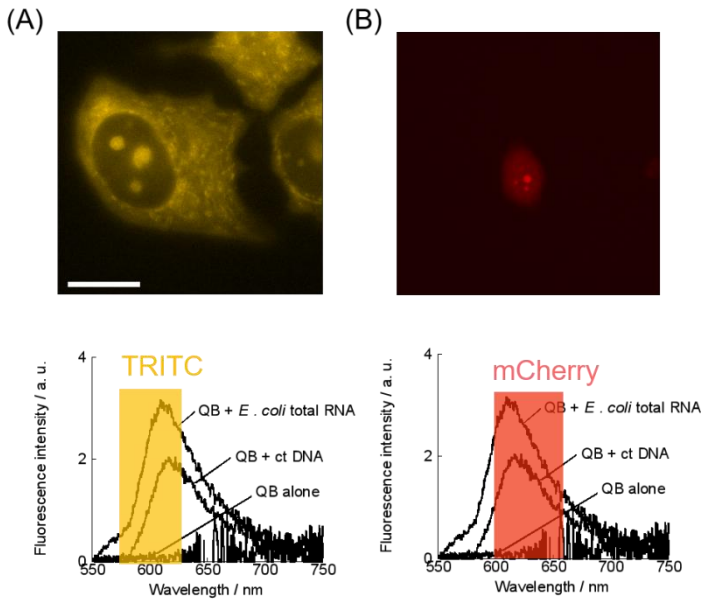

Fig. 4.7-1 Fluorescence images of living MCF7 cells stained by 3 μM QB (top) and schematic of collection regions using different filters (bottom). (A) Image was obtained by using TRITC filter, (B) Image was obtained by using mCherry filter. Incubation time: 20 min. Parameters: TRITC, 100 %, 0.1 s; mCherry: 100 ms (measured in Ohashi Lab.). Scale bar: 15 μm. The cells were imaged in HBSS buffer after washing with HBSS buffer twice.

By the emission wavelength of QB (λ_{em}: 609.5 nm), we can find that QB used for live cell nucleolus imaging can be measured not only with filters that collect electrons in the yellow region (TRITC), but also with filters that collected through the red region (above 600 nm), such as mCherry filters (emission filter: 597/45 nm). Due to the limitation of instrument and equipment in my Lab., the mCherry filters used for live cell imaging in this experiment were done in another laboratory.

The Fig. 4.7-1 shows the fluorescence images of living MCF7 cells stained by 3 μM QB after 20 min incubation by using different filters and schematic of their collection regions. Similar to using TRITC filter (emission filter: 597/45 nm), red emission can be observed in the nucleolus by using mCherry filter indicate QB even works as a red-emissive dye with nucleolus selectivity in living cells, which is a

advantage of QB because longer-emissive dye is more suitable for live cell imaging study. Since for imaging study, dyes emit in the red or deep-red region is far away from the autofluorescence emit from cellular component in 400 - 550 nm, leading to a reduced background noise and higher contrast images.

4.8 Cell toxicity

Finally, the cytoxicity of QB and 2QB in the living cells after 20 min incubation were examined. Fig. 4.8 shows the cell viability of QB and 2QB incubate for 20 min with 1 μM, 3 μM, 5 μM and 10 μM by using AlarmBlue assay reagent. It's readily to see both QB and 2QB show low cell toxicity at the work concentration (3μM) where the cell viability decreased about 20 %.

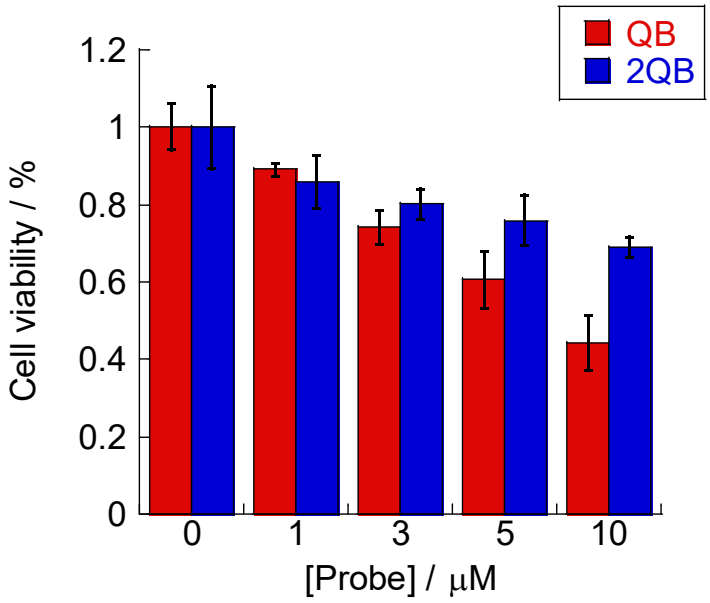

Figure 4.8-1 Evaluation of probe cytotoxicity after 20 min incubation. Buffer treatment served as a positive control. Values are means ± standard deviation of six independent experiments (N = 6). [Probes] = 0~10 μM. Ex: 570 nm, Em: 610 nm, cut off: 590 nm. Incubation time: 20 min for probes; 3 hours for AlamarBlue®.

5. Summary

In summary, the first synthesized cyanine dye QB and its regioisomer 2QB were synthesized and examined as RNA selective dyes. Both QB and 2QB shows RNA selectivity in solutions, and applicable to nucleolar RNA imaging in living cells. More impressively, 2QB, the regioisomer, worked much better than QB both in solutions and in living cells. This again remind us that isomerization is a effective way to improve probe functions such as RNA selectivity, light-up property and photostability.

6. Reference

1. K. Ilina and M. Henary, *Chem. Eur. J.*, **2021**, *27*, 4230-4248.
2. N. I. Gadjev, T. G. Deligeorgiev, S. H. Kim, *Dyes and Pigments*, **1999**, *40*, 181-186.
3. T. P. Constantin, G. L. Silva, K. L. Robertson, T. P. Hamilton, K. Fague, A. S. Waggoner, and Bruce A. Armitage, *Organic Letters*, **2008**, *10*, 8, 1561-1564.
4. L. L Zhang, X. J Liu, S. S Lu, J. Liu, S. L Zhong, Y. B Wei, T. Bing, N. Zhang, and D. H Shangguan, *ACS Appl. Bio Mater.*, **2020**, *3*, 2643-2650.
5. S. M. Yarmoluk, V. B. Kovalska, M. Y. Losytskyy, *Biotechnic & Histochemistry*, **2008**, *83(3-4)*, 131-145.
6. T. G. Deligeorgieva, S. Kaloyanova, and J. J. Vaquero, *Recent Patents on Materials Science*, **2009**, *2*, 1-26.
7. I. Timtcheva, V. Maximova, T. Deligeorgiev, D. Zaneva, I. Ivanov, *Journal of Photochemistry and Photobiology A: Chemistry*, **2000**, *130*, 7-11.
8. R. M. Abdel Aal, M. A. Gitru, Z. M. Essam, *Chemistry International*, **2007**, *3(4)*, 358-367.(solar cells)
9. W. Wu, J. Hua, Y. Jin, W. Zhan and H. Tian, *Photochem. Photobiol. Sci.*, **2008**, *7*, 63-68. (solar cells)
10. A. Pertegas, D. Tordera, J. J. Serrano-Perez, E. Ortí and H. J. Bolink, *J. Am. Chem. Soc.*, **2013**, *135*, 18008-18011. (solar cells)
11. S. Zhang, B. Li, L. Tang, X. Wang, D. Liu, Q. Zhou, *Polymer*, **2001**, *42*, 7575-7582. (laser photoinitiator)
12. S. Morishima, K. Wariishi, Y. Inagaki, M. Shibata, T. Ihida and H. Kubo, *Jpn. J. Appl. Phys.*,1999, 38, 1634-1637. (optical disks)
13. F. Hovelmann, I. Gaspar, J. Chamiolo, M. Kasper, J. Steffffen, A. Ephrussib and O. Seitz, *Chem. Sci.*, **2016**, *7*, 128.
14. S. Schöllkopf, A. Knoll, A. Homer and O. Seitz, *Chem. Sci.*, **2023**, *14*, 4166.
15. O. Tepper, H. Zheng, D. H. Appella and E. Yavin, *Chem. Commun.*, **2021**, *57*, 540.
16. T. Chiba, T. Sato, Y. Sato and S. Nishizawa, *Org. Biomol. Chem.*, **2017**, *15*, 7765.
17. Y. Sato, *Bull. Chem. Soc. Jpn.*, **2020**, *93*, 406-413.
18. D. Magde, R. Wong, P. G. Seybold, *Photochem. Photobiol.,* **2002**, *75*, 327-334.

Supporting information for chapter 3

1. Material & Method

Same as chapter 2, please see p43.

2. Method

Same as chapter 2, please see p43-46.

3. Synthesis and characterize of QB and 2QB

3.1 Synthesis of QB

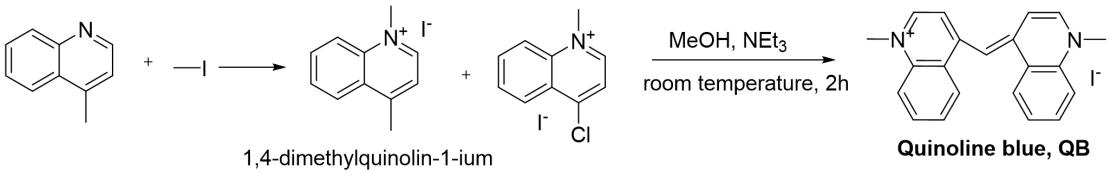

1, 4-dimethylquinolin-1-ium iodide[S1] **:** In a clean dry 250 mL flask, 4-methylquinoline(1.3 mL, 10 mmol) and iodomethane(1.25mL, 20 mmol) were added. Thereafter methyl cyanide was added to the mixture and the reaction was refluxed and stirred at 75 ℃ for 3 h. After removing the solvent by reduced pressure rotary evaporator, the yellow solid compound, 1,4-dimethylquinolin-1-ium (2.65 g) was obtained without further purification. (yield: 93 %)

^{1}H-NMR (500 MHz, DMSO-d_6): δ 9.34 (d, J = 5.8 Hz, 1H), 8.51 (dd, J = 26.4, 8.7 Hz, 2H), 8.29-8.26 (m, 1H), 8.08-8.04 (m, 2H), 4.57 (s, 3H), 3.00 (s, 3H)

***(E)*-1-methyl-4-((1-methylquinolin-4(1H)-ylidene)methyl)quinolin-1-ium iodide (Quinoline blue, QB)**[S2] **:** 1 - Methyl - 4 - chlorquinolinium iodide(305 mg, 1 mmol, 1.0 eq.) and 1,4-dimethylquinolin-1-ium (285 mg, 1.0 mmol, 1.0 eq.) were suspended MeOH (4 mL). After addition of NEt_3 (281 μL, 2.0 mmol, 2.0 eq.) The mixture was stirred at room temperature for 2 h. Then the precipitaed dye was filtered and washed with diethyl ether and air dried. Finally the quinoline blue was obtained by recrystalied from methanol. (Yield: 59 %)

^{1}H-NMR (500 MHz, DMSO-d_6) δ 8.69 (d, J = 8.5 Hz, 2H), 8.19 (d, J = 7.3 Hz, 2H), 7.91-7.91 (m, 4H), 7.67-7.63 (m, 4H), 7.25 (s, 1H), 4.05 (s, 6H). ESI-MS for $C_{21}H_{19}N_2^+$ ($[M]^+$): calcd, 299.15; found, 299.16.

3.2 Synthesis of 2QB

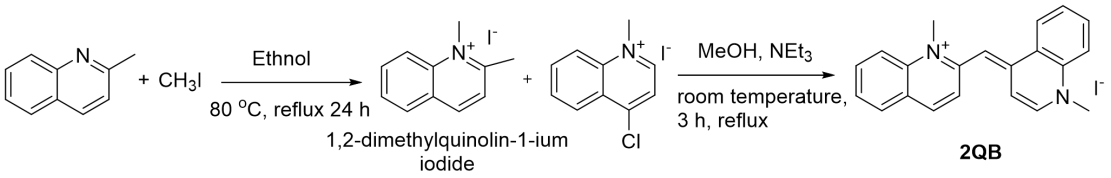

1, 2-dimethylquinolin-1-ium iodide[S3] **:** Toward a round-bottom flask with 5 mL ethanol, 1.0 mL (7.4 mmol) of 2-methylquinoline and 0.46 mL (7.4 mmol) iodomethane were added. The mixture was stirred evenly and heated to reflux at 80 ℃ for 24 h to accomplish the reaction. The system was then cooled down to room temperature, and dark yellow powder could be precipitated. The product was filtered and washed with ethanol three times without further purification, with yield of 28 %.

^{1}H-NMR (500 MHz, DMSO-d_6) δ 9.10 (d, J = 8.5 Hz, 1H), 8.59 (d, J = 8.9 Hz, 1H), 8.40 (d, J = 8.2 Hz, 1H), 8.23 (t, J = 7.2 Hz, 1H), 8.12 (d, J = 8.5 Hz, 1H), 7.99 (t, J = 7.5 Hz, 1H), 4.45 (s, 3H), 3.08 (s, 3H)

***(E)*-1-methyl-2-((1-methylquinolin-4(1H)-ylidene)methyl)quinolin-1-ium iodide (2QB)**[S2] **:** 1-Methyl-4-chlorquinolinium iodide(183 mg, 0.6 mmol, 1.0 eq.) and 1,4-dimethylquinolin-1-ium (171 mg, 0.6 mmol, 1.0 eq.) were suspended MeOH (2 mL). After addition of NEt3 (168 µL, 1.2 mmol, 2.0 eq.) The mixture was stirred at room temperature for 3 h. Then the precipitated dye was filtered and washed with diethyl ether and air dried. Finally 2QB was obtained by recrystalied from methanol. (Yield: 43 %)

^{1}H-NMR (500 MHz, DMSO-d_6) δ 8.56 (d, J = 8.9 Hz, 1H), 8.23 (d, J = 7.3 Hz, 1H), 8.08 (d, J = 9.5 Hz, 1H), 7.99 (dd, J = 14.2, 9.0 Hz, 2H), 7.94 (d, J = 3.7 Hz, 2H), 7.89 (d, J = 7.9 Hz, 1H), 7.80 (t, J = 7.2 Hz, 1H), 7.69-7.66 (m, 1H), 7.50 (t, J = 7.3 Hz, 1H), 7.41 (d, J = 7.0 Hz, 1H), 6.50 (s, 1H), 4.08 (s, 3H), 4.01 (s, 3H). ESI-MS for $C_{21}H_{19}N_2^+$ ([M]$^+$): calcd, 299.15; found, 299.16.

3.3 Characterize of QB and 2QB

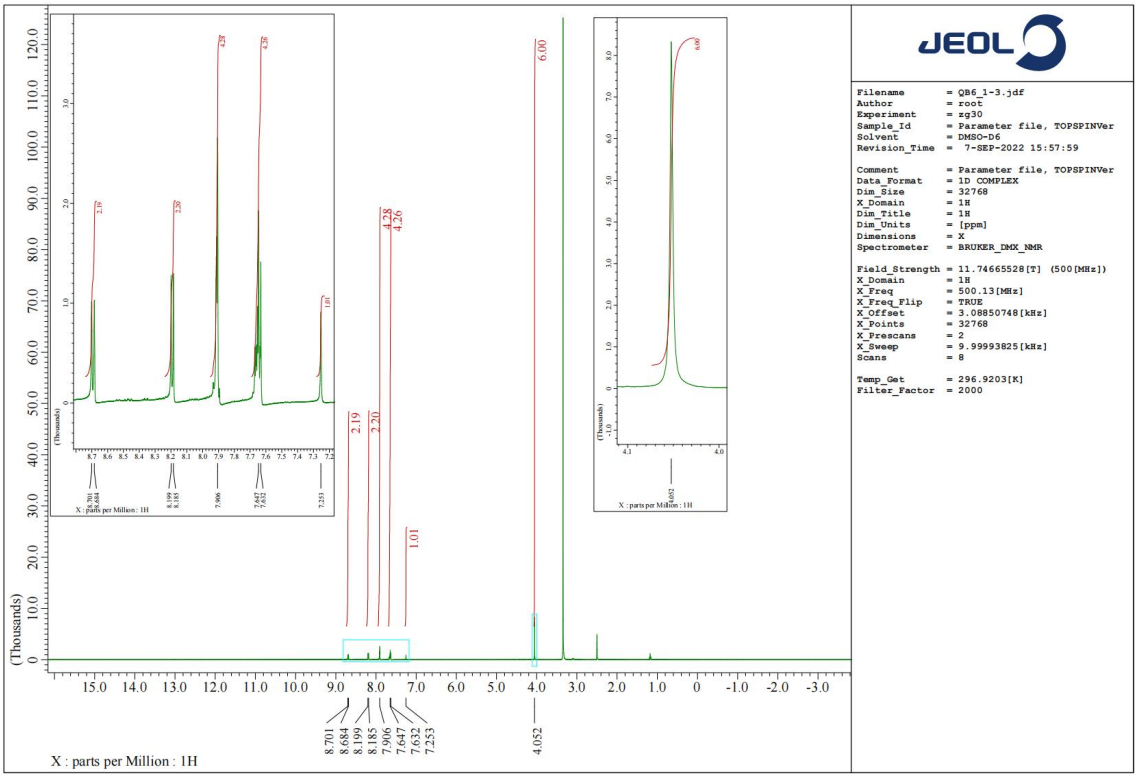

Fig. S 3.3-1 ^{1}H NMR spectrum of QB in DMSO-d_6.

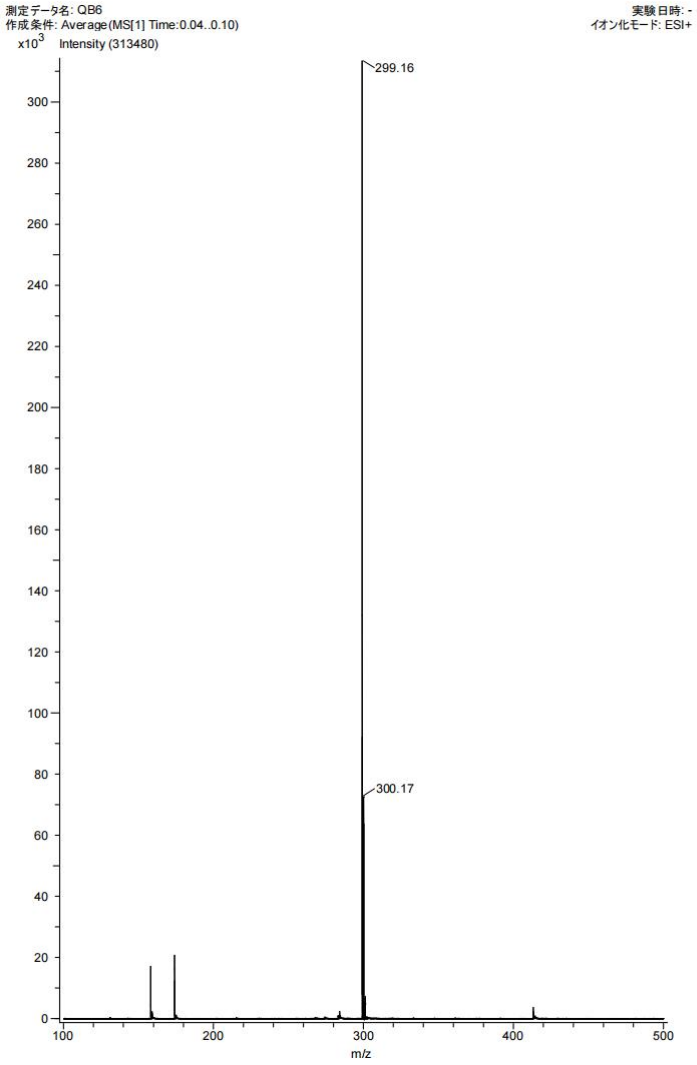

Fig.S 3.3-2 ESI-MS spectrum of QB in MeOH.

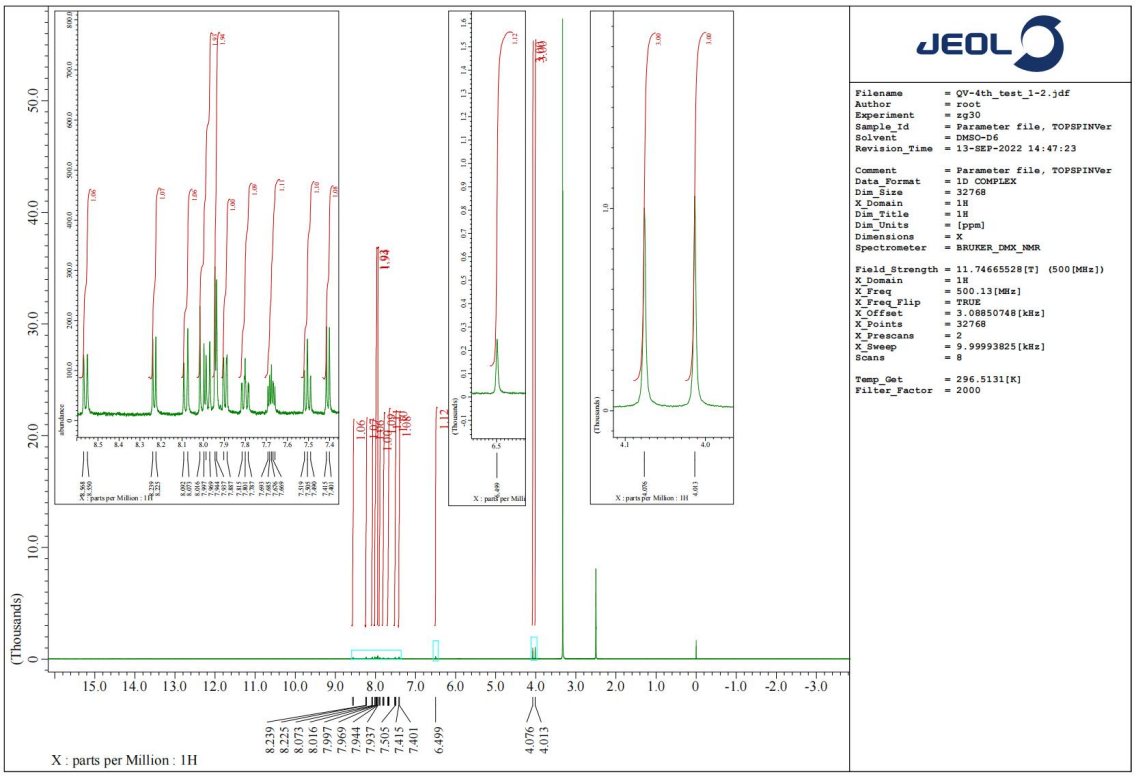

Fig.S 3.3-3 ^{1}H NMR spectrum of 2QB in DMSO-d_6.

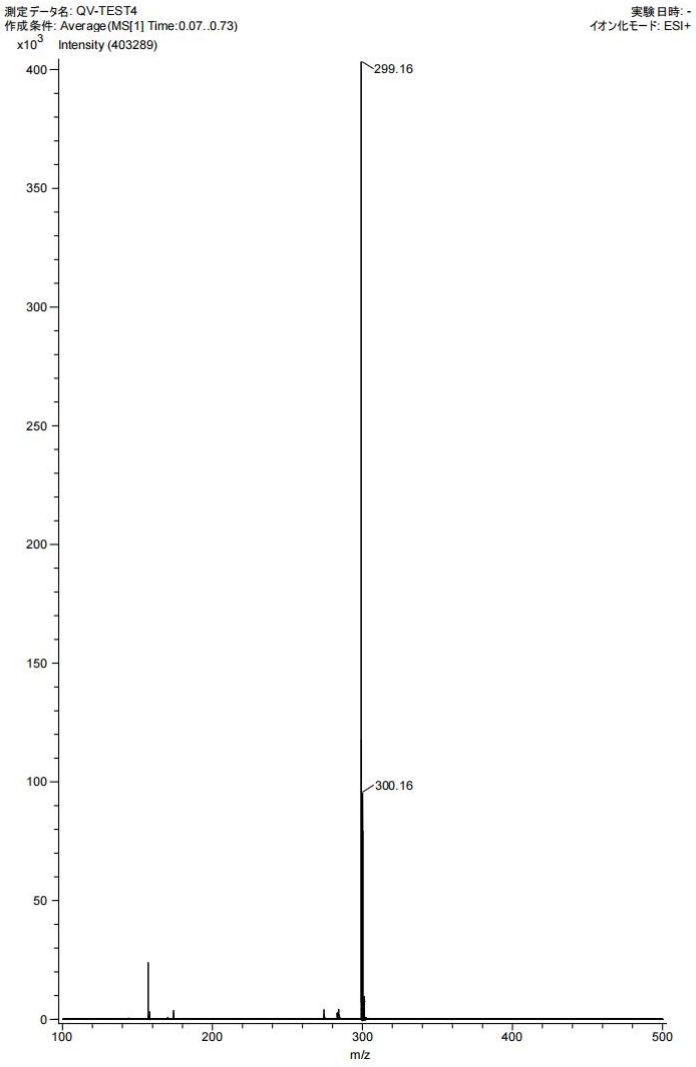

Fig. S 3.3-4 ESI-MS spectrum of 2QB in MeOH.

4. Absorption spectra of QB and 2QB

4.1 Absorption spectra of QB and 2QB in DMSO

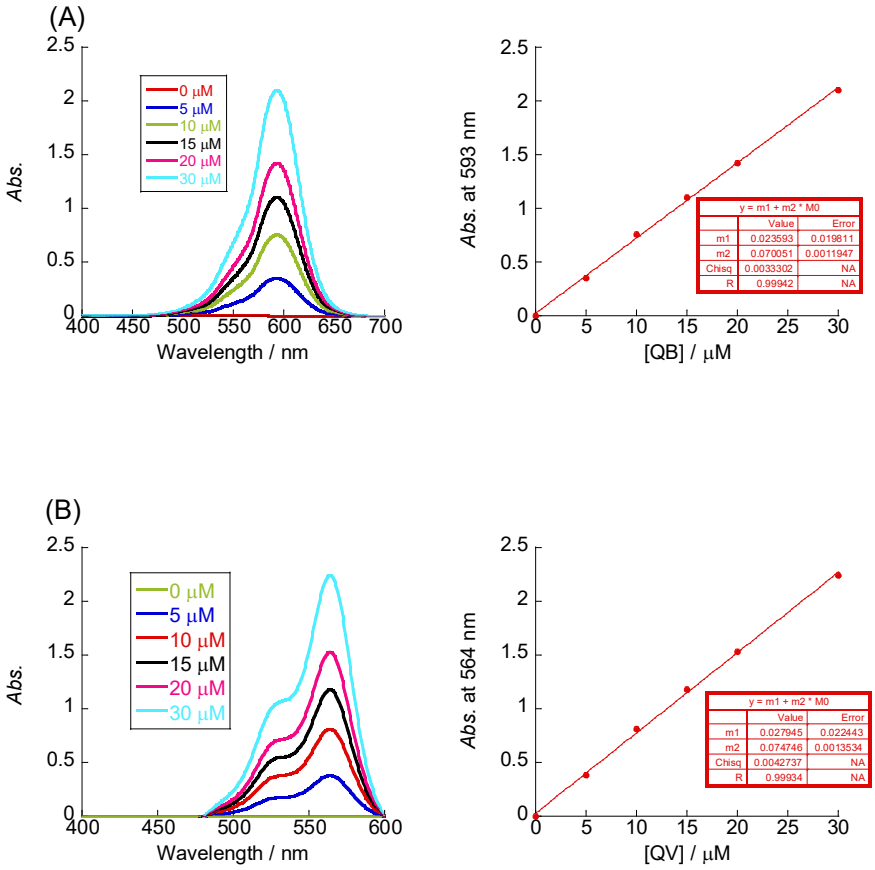

Fig. S 4.1-1 Absorption spectra of (A) QB and (B) 2QB in DMSO and their curve fit line.

Experimental condition: [dye] = 0 ~ 30 μM, sensitivity: medium, data interval: 0.5 nm, scan rate: 100 nm/ min, temperature: 25 ℃, cell: 1.0 × 0.2 cm, optical path: 10 mm.

Molar absorption coefficient (ε): QB, 2.3×10^4; 2QB, 2.7×10^4.

4.2 Absorption spectra of QB and 2QB in phosphate buffer

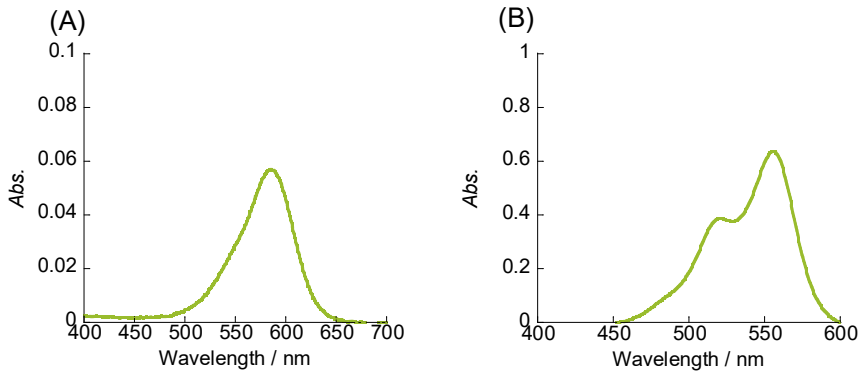

Fig. S 4.2-1 Absorption spectra of (A) QB and (B) 2QB in 10 mM sodium phosphate buffer (pH 7.0) containing 100 mM NaCl 1.0 mM EDTA. Experimental condition: [probe] = 10 μM, sensitivity: medium, data interval: 0.5 nm, scan rate: 100 nm/ min, temperature: 25 ℃, cell: 1.0 × 0.2 cm, optical path: 10 mm.

The max absorption wavelength: QB, 585.5 nm; 2QB, 555.5 nm.

4.3 Raw absorption spectra of QB and 2QB when bind to biological nucleic acid.

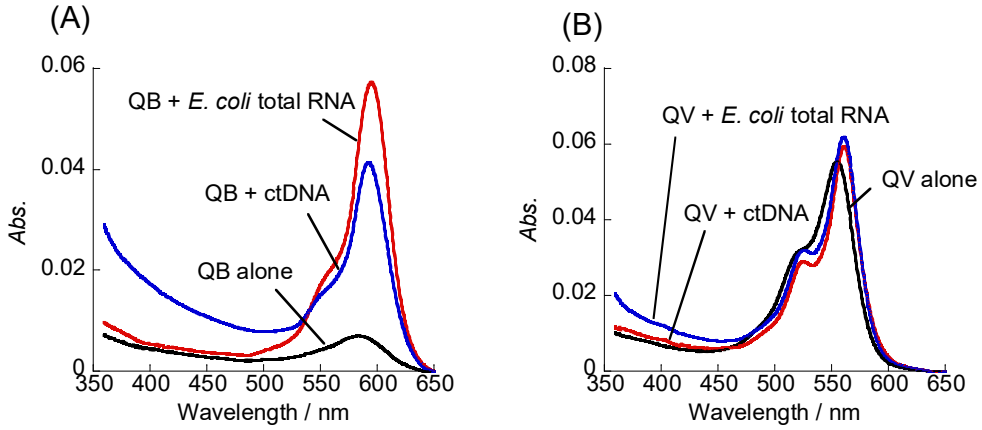

Fig. S 4.3-1 Absorption spectra of (A) QB (1.0 μM) and (B) 2QB (1.0 μM) in the absence and presence of 1.0 mM calf thymus DNA or 1.0 mM *E. coli* total RNA. Experimental condition: [probe] = 1.0 μM in 10 mM sodium phosphate buffer (pH 7.0) containing 100 mM NaCl 1.0 mM EDTA, sensitivity: medium, data interval: 0.5 nm, scan rate: 100 nm/ min, temperature: 25 ℃, cell: 1.0 × 0.2 cm, optical path: 10 mm.

5. Reference

S1 Y. Zhang, Z. Li, W. Hu, and Z. Liu, *Anal. Chem.*, **2019**, *91*, 10302−10309.

S2 T. G. Deligeorgiev, D. A. Zaneva, S. H. Kimb and R. W. Sabnis, *Dyes and Pigments*, **1998**, *37*, 3, 205-211.

S3 J. Sun, M. Tian and W. Lin, *Analyst*, **2019**, *144*, 2387-2392.

Chapter 4

Thiazole red and its regioisomer as fluorogenic probe for nucleolar RNA imaging in living cells

1. Introduction

Thiazole red (TR), as depicted in the Fig. 1-1, is an analog of thiazole orange. It is composed of benzothiazole and quinoline heterocycles connected by a trimethine bridge. TR was selected for the further experiments because it is one of the most famous asymmetrical trimethine cyanine dye. In fact, up to this point, there has been a extensive amount of research conducted on TR and TR derivatives.[1-8] However, it is commonly acknowledged that TR shows no nucleolar RNA selectivity in living cells[1] and exhibits extremely poor photostability both in solutions and in cells[1,2], which consequently limits its applications for live cell nucleolar RNA imaging.[1]

Therefore, TR and its regioisomer, 2TR, were synthesized and their RNA selectivity was examined. Hopefully, the probe functions will be improved by isomerization.

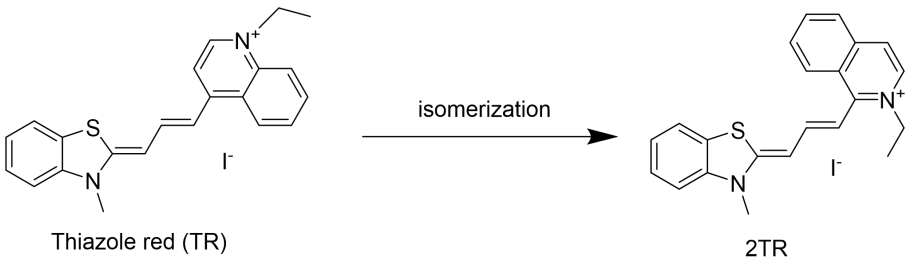

Fig. 1-1 Structure of TR and 2TR.

2. Synthesis of TR and 2TR

2.1 Synthetic scheme for the preparation of TR

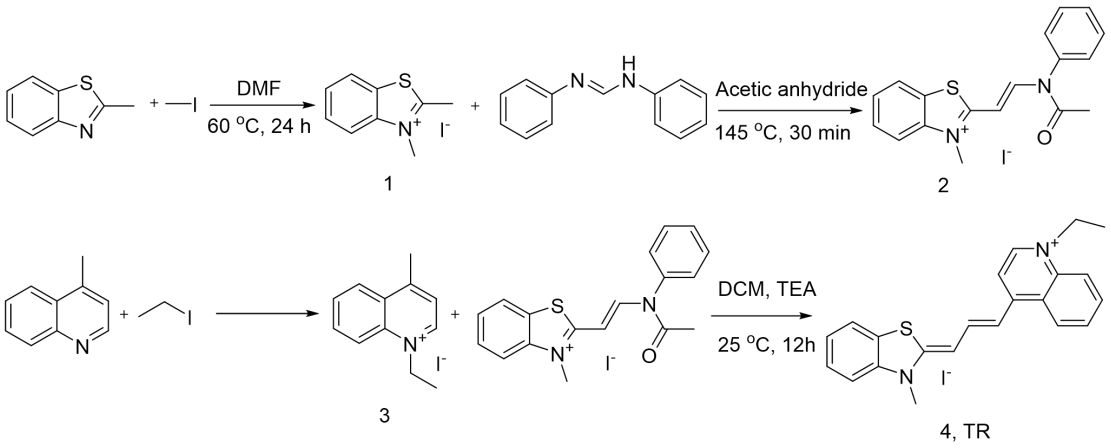

2.2 Synthetic scheme for the preparation of 2TR

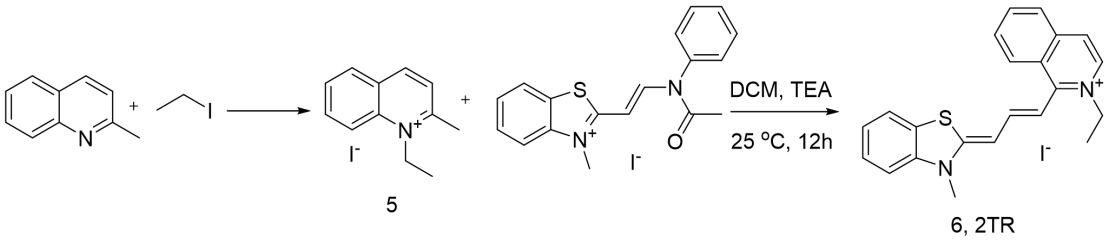

3. Photophysical properties and fluorescence signaling abilities of TR and 2TR for RNA sensing

3.1 Absorption spectra of TR and 2TR

The following Fig. 3.1-1 displayed normalized absorption spectra of TR and 2TR to biological nucleic acid. Here, a slight red shift can be observed when two probes binding to calf thymus DNA and *E. coli* total RNA indicate the two probes bind to the nucleic acid by means of intercalation, especially in a form of monomers, into the base pairs of the nucleic acid. The small shoulder in the spectra of 2TR (Fig. 3.1-1-B) implying that binding as a dimer is more significant for 2TR while no distinct blue peaks were observed in the spectra of TR (Fig. 3.1-1-A).

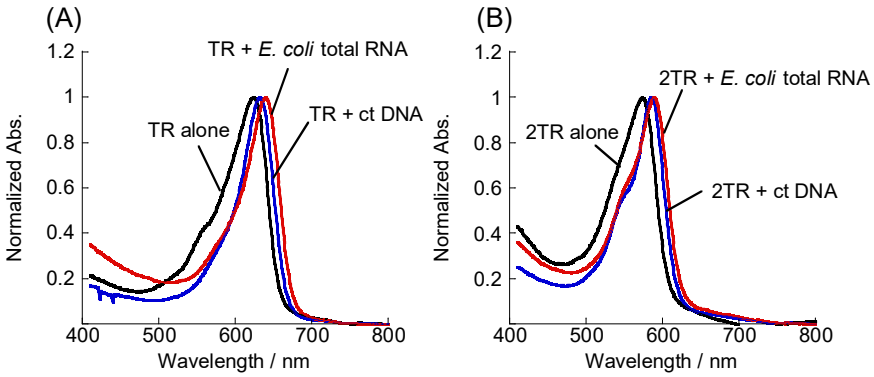

Fig. 3.1-1 Normalized absorption spectra of (A) TR (1.0 μM) and (B) 2TR (1.0 μM) in the absence and presence of 1.0 mM calf thymus DNA or 1.0 mM *E. coli* total RNA. Experimental condition: [probe] = 1.0 μM in 10 mM sodium phosphate buffer (pH 7.0) containing 100 mM NaCl 1.0 mM EDTA, sensitivity: medium, data interval: 0.5 nm, scan rate: 100 nm/ min, temperature: 25 ℃, cell: 1.0 × 0.2 cm, optical path: 10 mm. Data were obtained after mixing dyes with nucleic acid solutions and subsequent incubation for 30 min.

3.2 Fluorescence response to Nucleic acid solutions

3.2.1 Fluorescence response to biological nucleic acid

Then same sample solutions were used for the measurement of fluorescence response. As described in the following figures, the fluorescence intensity largely enhanced in the deep-red and red region (λ_{em}: TR, 661 nm; 2TR, 615 nm) after adding *E. coli* total RNA due to the restricted rotation when TR and 2TR intercalate into the base pair. Moreover, TR shows better fluorescence response to calf thymus DNA than *E. coli* total RNA (Fig. 3.2.1-1-A, I_{RNA}/I_{DNA} = 0.9). The DNA selectivity was also reported by other researcher.[1] While 2TR, the regioisomer apparently shows better selectivity to RNA over DNA (Fig. 3.2.1-1-B, I_{RNA}/I_{DNA} = 1.9). In other word, regioisomer did improve RNA selectivity in solutions.

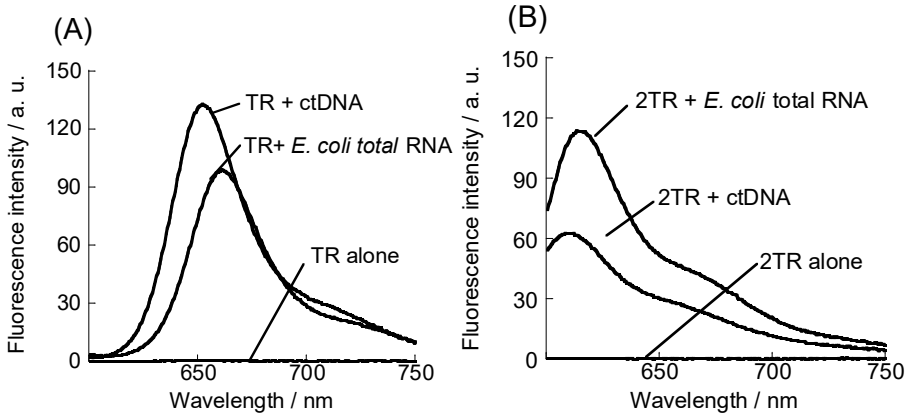

Figure 3.2.1-1 Fluorescence spectra of (A) TR (1.0 μM) and (B) 2TR (1.0 μM) in the absence and presence of 1.0 mM *E. coli* total RNA or 1.0 mM calf thymus DNA. Measurements were performed in 10 mM sodium phosphate buffer solution (pH 7.0) containing 100 mM NaCl and 1.0 mM EDTA. Excitation: 593.5 nm, Ex band: 3 nm, Em band: 3 nm, sensitivity: medium. Scan rate: 100 nm / min, response: 0.5 s. Temperature: 25 ℃. Data were obtained after mixing dyes with nucleic acid solutions and subsequent incubation for 30 min.

3.2.2 Quantum yield calculation

Quantum yield was determined relative to 200 nM cresyl violet in MeOH (Φ = 0.67, Ex: 593.5 nm).[9] The calculation method was same as chapter 2. Finally, the quantum yield of TR and 2TR were calculated and their fluorescence signaling ability were summarized as the following table 3.2.2-1, both TR and 2TR shows relatively good off-on signaling ability (TR, I/I_0 = 200; 2TR, I/I_0 = 320).

Probes	Samples	ϕ_{bound}	ϕ_{RNA}/ϕ_{free}	ϕ_{RNA}/ϕ_{DNA}	Light-up factor (I/I_0)
TR	Probe alone	0.002	165	1	200
	ct DNA	0.33			
	E coli. Total RNA	0.33			
2TR	Probe alone	0.006	35	1.5	320
	ct DNA	0.14			
	E coli. total RNA	0.21			

Table 3.2.2-1 Quantum yield and signaling ability of TR and 2TR.

3.2.2 Fluorescence response to synthetic nucleic acid

The fluorescence response to synthetic nucleic acid were measured. Different from response selectivity to biological nucleic acid, both TR and 2TR shows better selectivity to DNA strand over RNA strand, especially significant to double stranded dAdT. It again proved the intercalative binding mode of two probes. On the other hand, the significant specificity to A/T sequence may implying groove binding mode also exists.[10]

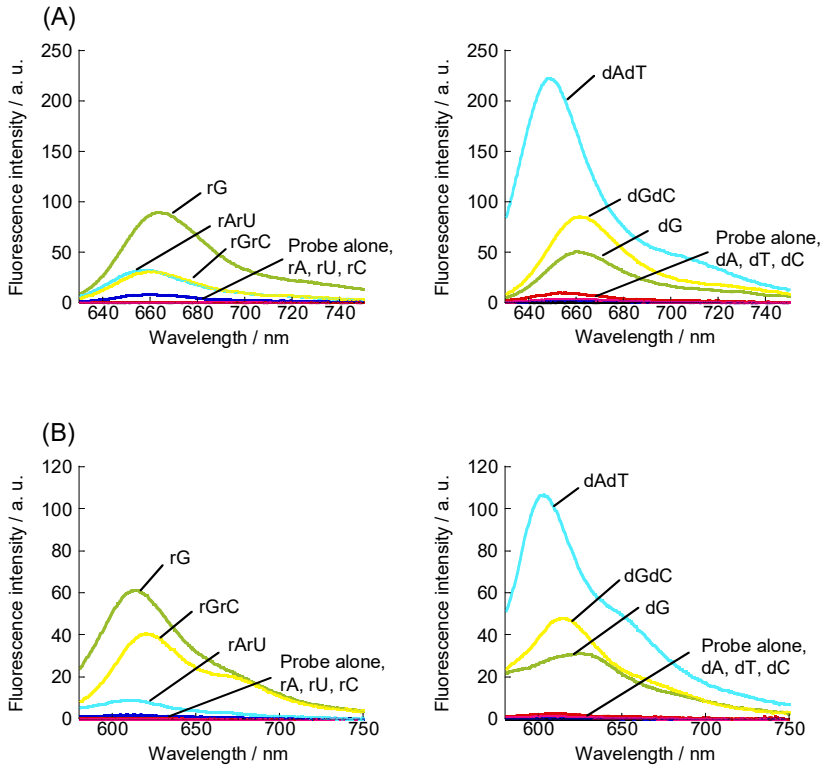

Fig. 3.2.2-1 Fluorescence response of (A) TR (1.0 μM) and (B) 2TR (1.0 μM) to synthetic nucleic acids (20 μM). Experimental condition: Excitation: (A) 624 nm, (B) 573 nm. [dye] = 1.0 μM in 10 mM sodium phosphate buffer solution (pH 7.0) containing 100 mM NaCl and 1.0 mM EDTA. Ex band: 3 nm, Em bamd: 3 nm, senseitivity: medium. Scan rate : 100 nm / min, response : 0.5 s, temperature: 25 ℃, 3 × 3 nm quartz cell. Data were obtained after mixing dyes with nucleic acid solutions and subsequent incubation for 30 min.

The nucleic acid sequences:

rG: 5'- r(GGG GGG GGG GGG G)-3'	dG: 5'- d(GGG GGG GGG GGG G)-3'
rC: 5'- r(CCC CCC CCC CCC C)-3'	dC: 5'- d(CCC CCC CCC CCC C)-3'
rA: 5'- r(AAA AAA AAA AAA A)-3'	dA: 5'- d(AAA AAA AAA AAA A)-3'
rU: 5'- r(UUU UUU UUU UUU U)-3'	dT: 5'- d(TTT TTT TTT TTT T)-3

3.3 Photostability of TR and 2TR

Photostability of TR and 2TR were checked by monitoring the fluorescence intensity change when probes binding with *E. coli* total RNA under 3 hours continues irradiation. It's obvious that TR show extremely low photostability where the fluorescence intensity decreased over 80 %, which is even worse than the commercial probe, SYTO RNA Select.[11] Fortunately, 2TR, the regioisomer of TR, improved photostability compared with TR, even though still not so good where the fluorescence intensity decreased around 45 %.

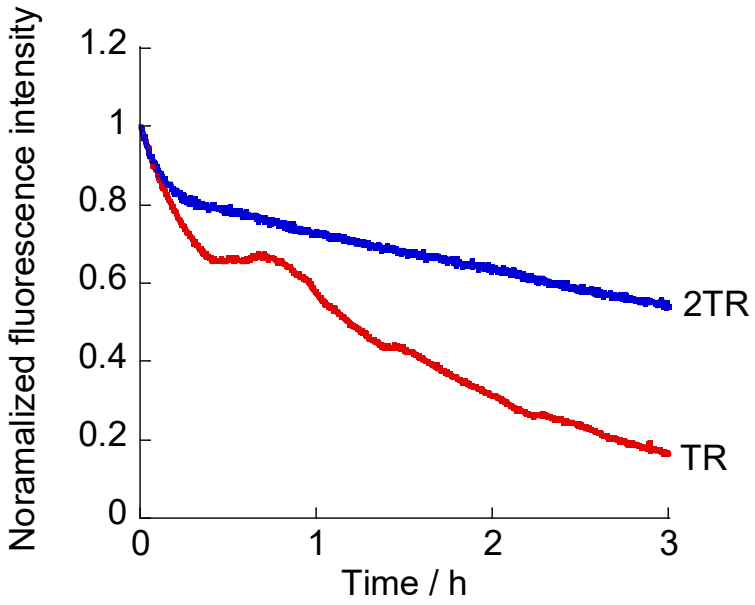

Figure 3.3-1 Changes in fluorescence intensity of TR and 2TR when bound to *E. coli* total RNA under continuous irradiation (3 h). [Probe] = 1.0 μM, [E. coli total RNA] = 100 nM in solutions buffered at pH 7.0 (10 mM sodium phosphate) containing 100 mM NaCl and 1.0 mM EDTA. Before the measurement, sample solutions were incubated for 30 min. Excitation: 624 nm (TR) , 573 nm (2TR). Ex band: 3 nm, Em bamd: 3 nm, senseitivity: medium. Scan rate : 100 nm / min, response : 0.5 s. Temperature: 25 ℃, quartz cell: 3 × 3 nm.

4. Application to cells

4.1 Living cell imaging

Then, TR were applied for living MCF7 cell imaging. The figures shows the fluorescence images of living MCF7 cells stained by 2 μM TR after 20 min incubation (Fig. 4.1-1-A-top) and also described the electrons collection region of TR by using Cy5 filter (Fig. 4.1-1-A-bottom, emission filter: 676/34 nm). Here we can see deep-red emission in the nucleus with negligible signal in the cytoplasm indicate TR shows no RNA selectivity in the living cells.

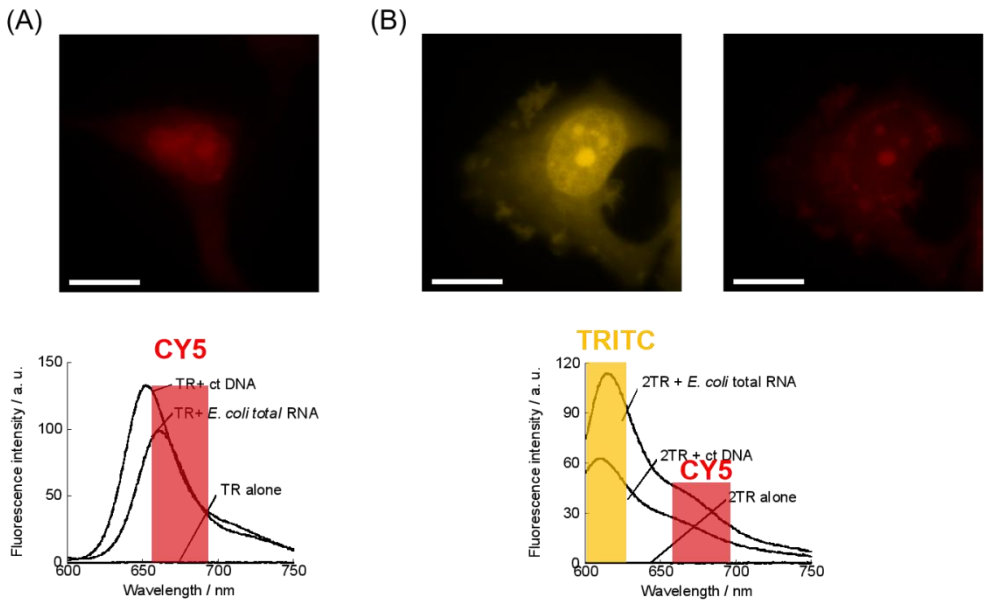

Fig. 4.1-1 Fluorescence images of living MCF7 cells stained by 2 μM TR and 2TR (top) as well as schematic of electrons collection regions using different filters (bottom). (A) Image was obtained by using TRITC filter, (B) Image was obtained by using Cy5 filter. Incubation time: 20 min. Parameters: Cy5, 10 %, 0.01 s for TR; TRITC, 10 %, 0.05 s and Cy5, 100 %, 0.1 s for 2TR. Scale bar: 15 μm. The cells were imaged in HBSS buffer after washing with HBSS buffer twice.

Significantly, much better images were obtained by 2 μM 2TR with same incubation time (Fig. 4.1-1-B-top). Here, strong yellow emission in the nucleolus can be observed by using TRITC filter (Fig. 4.1-1-B-bottom, emission filter: 597/45 nm). With greater significance, 2TR even works as a deep-red emissive dye with nucleolus selectivity in living cells where the nucleolus can be clearly observed with deep-red emission by using Cy5 filter (Fig. 4.1-1-B-bottom). Even though the fluorescence intensity decreased a lot compared with using TRITC filter because less electrons were collected.

Here the observed less accumulation in the nucleus and higher contrast to the nucleus by using Cy5 filter is due to the deconvolution computation, which automatically calculated by the computer to obtain better images. The computation is more significant to lower quality images, which is the deep-red emissive images in my case. In fact, the contrast and staining ability won't be changed by using different filter.

Since longer-wavelength emissive dye is more suitable for imaging study, Cy5 filter was used for further experiments.

4.2 Digestion experiment

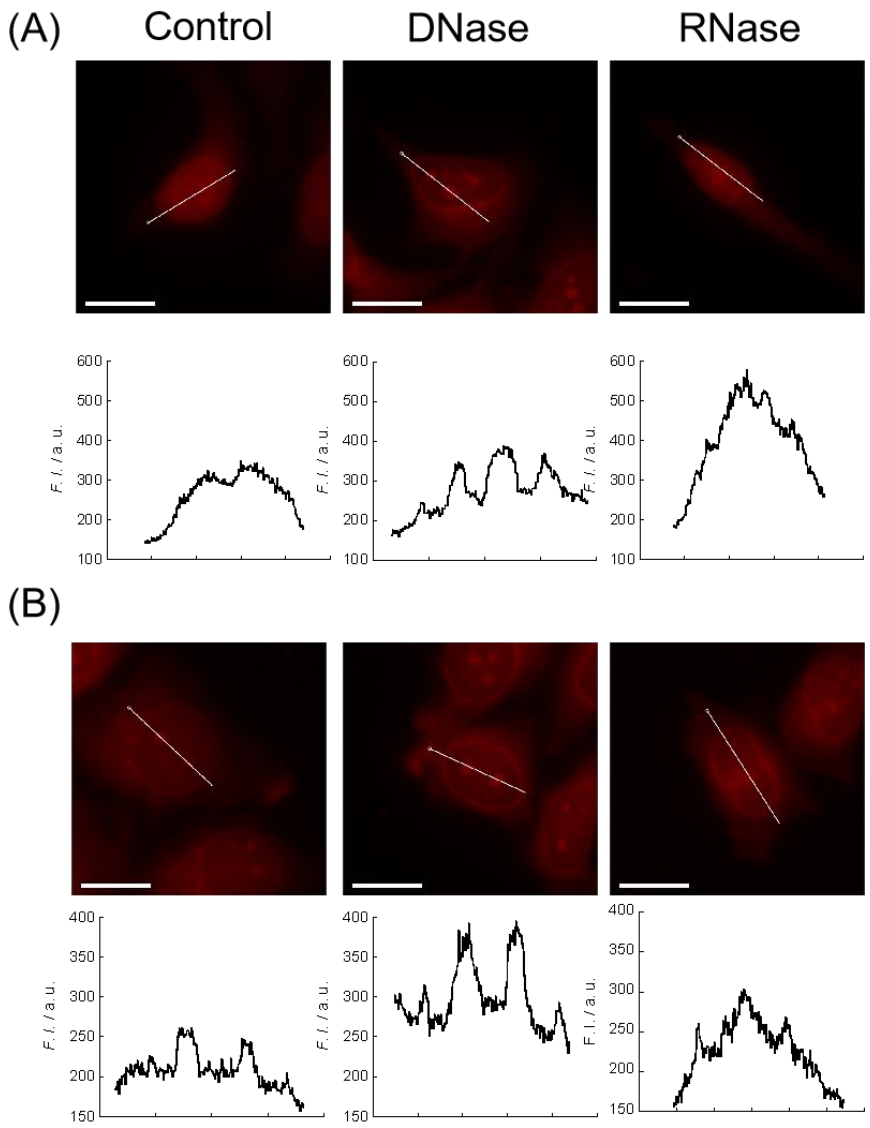

Fig. 4.2-1 Fluorescence images of fixed and permeabilized MCF7 cells stained by TR (2 μM) and 2TR (2 μM) before (control) and after treatment with DNase or RNase for 3 hours. Parameters: Cy5, 10 %, 0.01 s for TR; Cy5, 100 %, 0.2 s for 2TR. Scale bar: 15 μm. The cells were imaged in D-PBS buffer after washing with D-PBS buffer twice.

Next, the observed emission in the nucleus and nucleolus were examined by using DNase (Deoxyribonuclease) and RNase (Ribonuclease) reagent in fixed and permeabilized cells. Strong red emission in the nucleolus remained observed after 3 h incubation of DNase, while the red signal in the

nucleus seems more significant after RNase treatment (Fig. 4.2-1-A) indicate TR shows better selectivity to DNA in the nucleus in cells. However, fortunately, the situation is different in the case of 2TR. Strong red emission in the nucleolus can be observed after treatment of DNase, while the nucleolar emission was decreased after RNase treatment (Fig. 4.2-1-B) indicate 2TR has better nucleolar RNA selectivity than DNA in cells. Even though some weak signal cannot be ignored because 2TR also interacts with DNA in cells, which is good consistent with fluorescence response to biological nucleic acid in solutions (Fig. 3.2.1-1-B). Therefore, 2TR, the regioisomer is a promising probe for nucleolar RNA imaging in cells.

4.3 Fixed and permeabilized cell imaging

Having learned about the staining ability of TR and 2TR in living cells, two probes were used for fixed and permeabilized MCF7 cells. The images were obtained after incubation with 2 μM TR and 2TR for 20 min. As demonstrated in the images, TR stains the nucleus with some extent selectivity to nucleolus due to the better membrane permeability in the fixed and permeabilized cells. Similar to living MCF7 cell imaging, 2TR, the regioisomer works much better than TR where the nucleolus can be clearly observed with deep red emission.

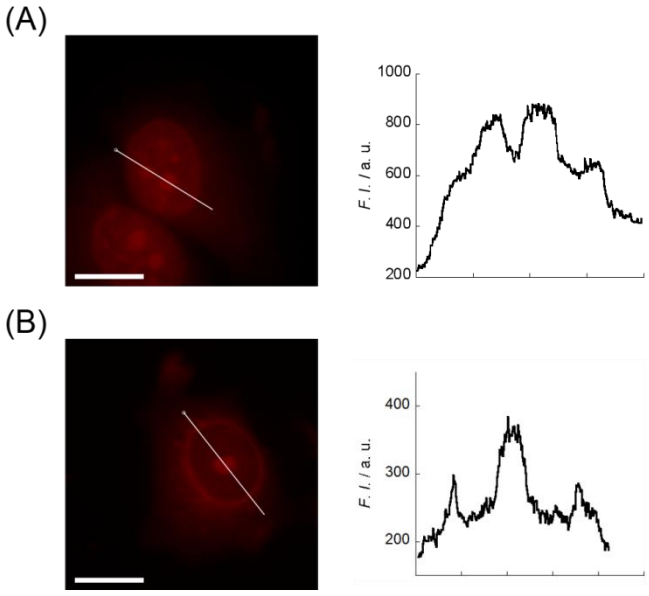

Fig. 4.3-1 Fluorescence images of fixed and permeabilized MCF7 cells stained by TR (2 μM) and 2TR (2 μM) after 20 min incubation. Parameters: Cy5, 10 %, 0.01 s for TR; Cy5, 100 %, 0.1 s for 2TR. Scale bar: 15 μm. After washing with D-PBS buffer twice, the cells were imaged in D-PBS buffer.

4.4. Living MCF7 cell imaging co-stained with mitochondria staining probe

To investigate the emission in the cytoplasm, the living MCF7 cells were co-stained with the green-emissive mitochondria staining probe, MitoTracker green. The images were obtained by firstly 20 min incubation of the commercially available mitochondrial staining probe, MitoTracker green, and then 20 min incubation of my probes, TR and 2TR. It's readily to know that the observed strong emission in the cytoplasm comes from 2TR accumulate in the mitochondria where the pearson's coefficient value reached 0.89.

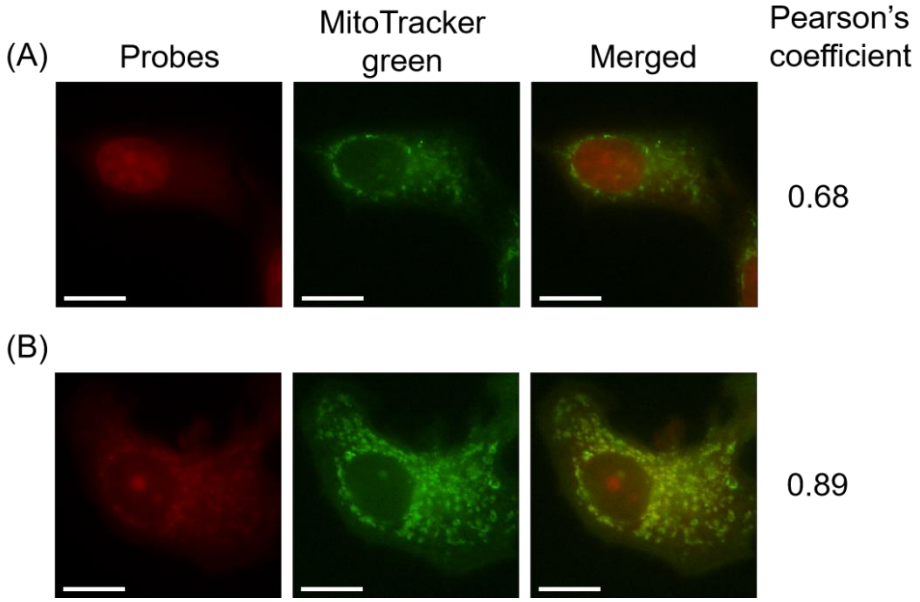

Fig. 4.4-1 Co-staining of living MCF7 cells with TR (2 μM) and 2TR (2 μM) and mitochondria-staining probe (MitoTracker green, 20 nM). Parameters: Cy5, 10 %, 0.01 s for TR; Cy5, 100 %, 0.1 s for 2TR; FITC, 50 %, 0.2 s for MitoTracker green. Scale bar: 15 μm. After washing with HBSS buffer twice, the cells were imaged in HBSS buffer.

4.5 Living cell imaging without washing protocol

The staining ability of living MCF7 cells without washing step were examined. As we can see from the images, TR stains the nucleus after 20 min incubation while 2TR stains the nucleolus, even though the signal to background ratio is not good as the images obtained with washing step indicate washing step is unavoidable to obtain better images.

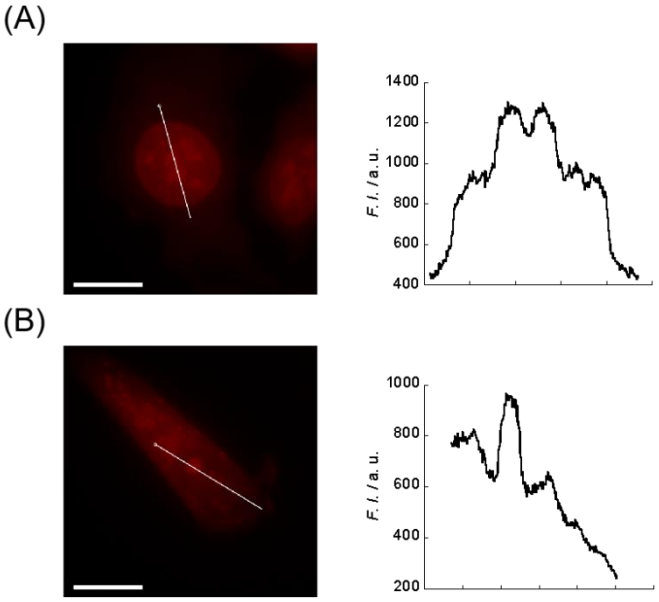

Fig. 4.5-1 *No-washing* fluorescence imaging of living MCF7 cells stained by TR (2 μM), 2TR (2 μM) after 20 min incubation. Fluorescence intensity profiles along the white line are also shown. Parameters: Cy5, 10 %, 0.01 s for TR; Cy5, 100 %, 0.1 s for 2TR. Scale bar: 15 μm. The cells were imaged in HBSS buffer.

4.6 Living cell imaging after 24 h incubation

TR and 2TR were applied to living MCF7 cells with 24 hours incubation to check the possibility of long time experiments. The fluorescence images stained by 2 μM probes and bright field cells as well as merged images were also exhibited as Fig. 4.6-1. Black region in the nucleus can be observed in the bright field images for TR and 2TR, seems due to excessive dye molecules were uptake by cells and accumulated in the nucleus with long time incubation. Unfortunately, 2TR, originally shows nucleolus selectivity in living cells with 20 min incubation, exhibits no selectivity to nucleolar RNA after 24 hours incubation. Therefore, both TR and 2TR are not suitable for long-time observation in living cells.

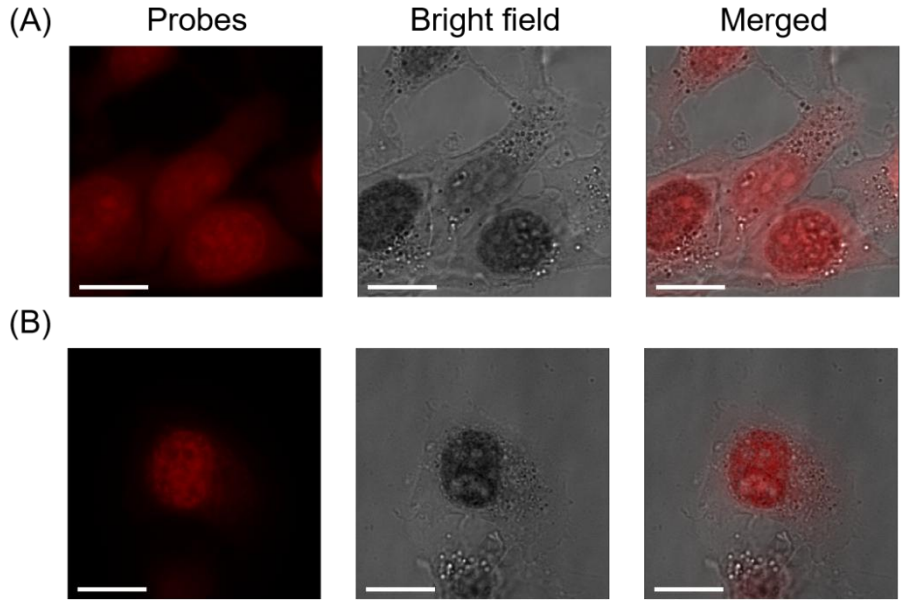

Fig. 4.6-1 Images of living MCF7 cells stained by (A) TR (2 μM), (B) 2TR (2 μM) after 24 h incubation. Fluorescence intensity profiles along the white line are also shown. Parameters: Cy5, 5 %, 0.01 s for TR; Cy5, 32 %, 0.01 s for 2TR. Scale bar: 15 μm. After washing with HBSS buffer twice, the cells were imaged in HBSS buffer.

4.7 The other cell line imaging

The staining ability of TR and 2TR were also examined in other cell line. The figures show the fluorescence images of living HeLa cells with 2 μM TR and 2TR after 20 min incubation. Same as in living MCF7 cells imaging, TR accumulates in the nucleus with negligible emission in cytoplasm. While in the case of 2TR, strong red emission in the nucleolus was clearly observed indicating 2TR also works as a nucleolus staining dye in living HeLa cells, which is much better than TR.

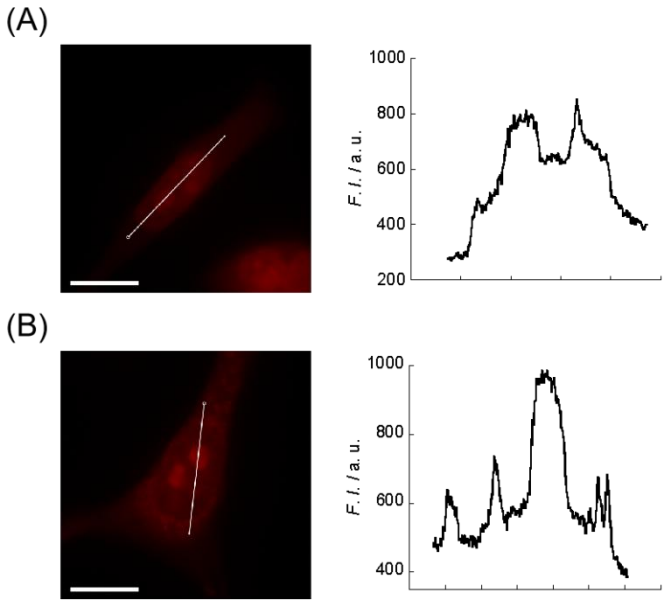

Fig. 4.7-1 Images of living HeLa cells stained by (A) TR (2 μM), (B) 2TR (2 μM) after 24 h incubation. Fluorescence intensity profiles along the white line are also shown. Parameters: Cy5, 10 %, 0.01 s for TR; Cy5, 100 %, 0.1 s for 2TR. Scale bar: 15 μm. After washing with HBSS buffer twice, the cells were imaged in HBSS buffer.

4.8 Cell toxicity

The cytotoxicity of two probes in living MCF7 cells with 20 min incubation were examined by using AlamarBlue® assay reagent. The figure shows cell viability after 20 min incubation with different concentrations. It can be seen that both TR and 2TR are low toxicity at the work concentration (TR, 2 μM; 2TR, 2 μM) to living cells where the cell viability decreased only about 10 %.

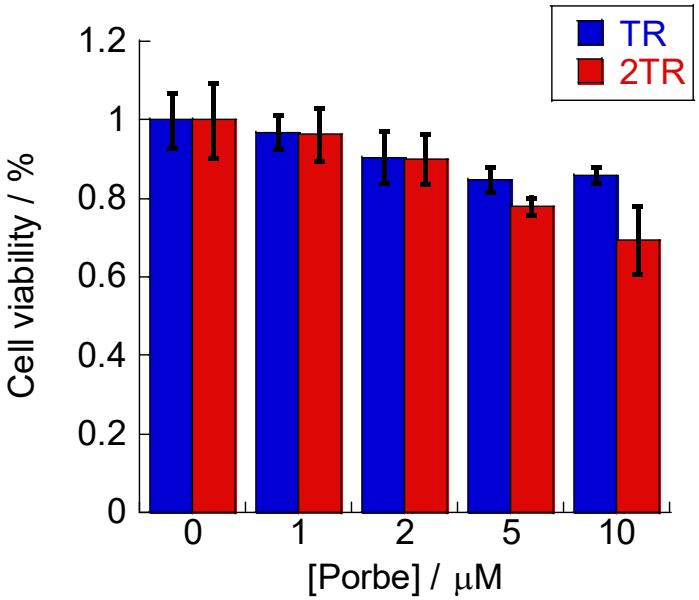

Fig. 4.8-1 Evaluation of probe cytotoxicity after 20 min incubation. Buffer treatment served as a positive control. Values are means ± standard deviation of six independent experiments (N = 6). [Probes] = 0~10 μM. Ex: 570 nm, Em: 610 nm, cut off: 590 nm. Incubation time: 20 min for probes; 3 hours for AlamarBlue®.

5. Summary

In summary, the typical unsymmetrical trimethine cyanine dye, TR and its isomer, 2TR were examined. TR shows better selectivity to DNA both in solutions and in living cells. The photostability was proved to be bad. 2TR, a regioisomer of TR, was demonstrated as a promising fluorogenic probe for nucleolar RNA imaging in living cells, showing better selectivity to RNA both in solution and living cells, compared with TR.

6. Reference

1. S. Zhang, J. Fan, Z. Li, N. Hao, J. Cao, T. Wu, J. Wang and X. Peng, *J. Mater. Chem. B*, **2014**, *2*, 2688.
2. H.-K. Walter, P. R. Bohlander, and H.-A. Wagenknecht, *ChemistryOpen*, **2015**, *4*, 92-96.
3. O. Zhytniakivska, A. Kurutos, U. Tarabara, K. Vus, V. Trusova, G. Gorbenko, N. Gadjev, T. Deligeorgiev, *Journal of Molecular Liquids*, **2020**, *311*, 113287.
4. C. Holzhauser, S. Berndl, F. Menacher, M. Breunig, A. Göpferich, and H.-A. Wagenknecht, *Eur. J. Org. Chem.*, **2010**, 1239-1248.
5. C. Holzhauser, R. Liebl, A. Goepferich, H.-A. Wagenknecht and M. Breunig, *ACS Chem. Biol.*, **2013**, *8*, 890-894.
6. Y. Sato, S. Yajima, A. Taguchi, K. Baba, M. Nakagomi, Y. Aiba and S. Nishizawa, *Chem. Commun.*, **2019**, *55*, 3183.
7. K. Ohira, Y. Sato and S. Nishizawa, *ACS Sens.*, **2023**, *8*, 522-526.
8. Y. Sato, Y. Aiba, S. Yajima, T. Tanabe, K. Higuchi and S. Nishizawa, *ChemBioChem.*, **2019**, *20*, 2752-2756.
9. S. J. Isak and E. M. Eyring, *J. Phys. Chem.*, **1992**, *96*, 1738-1742. (quantum yield)
10. J. Ghasemi, Sh. Ahmadi, A. I. Ahmad, S. Ghobadi, *Appl Biochem Biotechnol*, **2008**, *149*, 9-22.
11. K. Higuchi, Y. Sato, N. Togashi, M. Suzuki, Y. Yoshino and S. Nishizawa, *ACS Omega*, **2022**, *7*, 23744-23748.

Supporting information for chapter 4

1. Material & Method

Same as chapter 2, please see p43.

2. Method

Same as chapter 2, please see p43-46.

3. Synthesis and characterize of TR and 2TR

3.1 Synthesis of TR

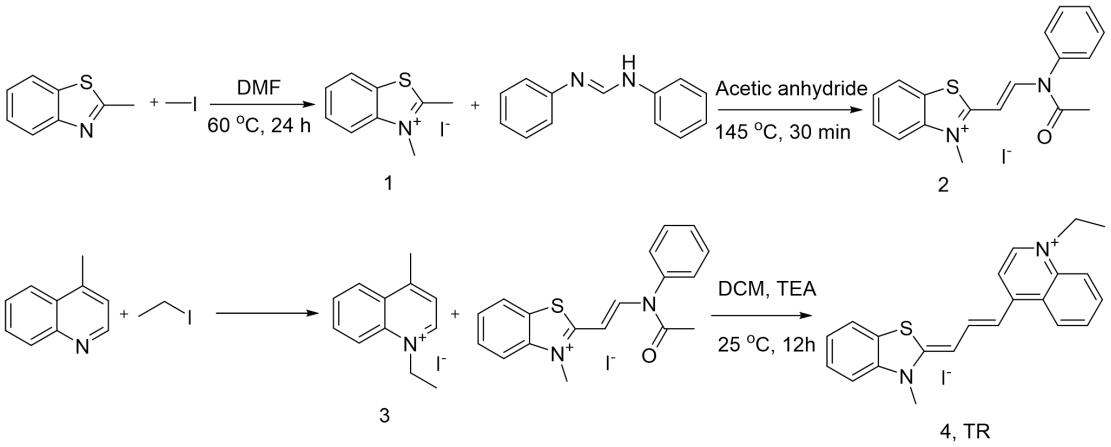

2,3-dimethylbenzo[d]thiazol-3-ium iodide (1)[S1] **:** A solution of 2-methylbenzoxazole (2.66 g, 20.0 mmol) and iodomethane (11.28 g, 80.0 mmol) in DMF (20 mL) was heated at 60 ℃ for 24 h. The solution was cooled to room temperature, and then ethyl acetate (200 mL) was added slowly. The precipitated solid was collected by filtration and washed with ethyl acetate. The product were synthesized as light pink solid. (yield: 13.31 g, 114 %)

1H-NMR (500 MHz, DMSO-d_6) δ 8.44 (d, J = 7.9 Hz, 1H), 8.29 (d, J = 8.5 Hz, 1H), 7.91-7.88 (m, 1H), 7.82-7.79 (m, 1H), 4.20 (s, 3H), 3.17 (s, 3H)

***(E)* -3-methyl-2-(2-(N-phenylacetamido)vinyl)benzo[*d*]thiazol-3-ium iodide(2)**[S2] **:** A solution of 2.91 g (10 mmol) of 2, 3-dimethylbenzo[*d*]thiazol-3-ium iodide and 2.35 g (10 mmol) of (E)-N,N'-diphenylformimidamide in 30 mL of acetic anhydride was refluxed for 30 min at 145 ℃. After cooling to room temperature, diethyl ether was added to the reaction mixture over 1 h. The purple

crystalline product so formed was collected by filtration under reduced pressure, washed with diethyl ether and water. (Yield: 3.53 g, 54 %)

1H-NMR (500 MHz, DMSO-d_6) δ 8.80 (d, J = 14.0 Hz, 1H), 8.31 (d, J = 8.2 Hz, 1H), 8.10 (d, J = 8.2 Hz, 1H), 7.80-7.77 (m, 1H), 7.73-7.64 (m, 4H), 7.55-7.53 (m, 2H), 5.69 (d, J = 14.0 Hz, 1H), 3.88 (s, 3H), 2.06 (s, 3H)

1-ethyl-4-methylquinolin-1-ium iodide(3)[S3] **:** 4-Methylquinoline (1.85 mL, 14 mmol) was dissolved in toluene (7 mL) and iodoethane (2.25 mL, 28 mmol) was added. The mixture stirred for 6 h at 120 ℃ in a sealed tube. The resulting solid was crushed, washed several times with ethyl ether and dried under vacuum to afford a yellow-green solid product without further purification. (Yield: 3.38 g, 80 %)

1H-NMR (500 MHz, DMSO-d_6) δ 9.41 (d, J = 6.1 Hz, 1H), 8.60-8.54 (m, 2H), 8.28-8.25 (m, 1H), 8.08-8.04 (m, 2H), 5.05 (q, J = 7.2 Hz, 2H), 3.00 (s, 3H), 1.58 (t, J = 7.2 Hz, 3H)

1-ethyl-4-((1E, 3Z)-3-(3-methylbenzo[d]thiazol-2(3H)-ylidene)prop-1-en-1-yl)quinolin-1-ium iodide (4, TR)[S4] **:** To a suspension of 1-ethyl-4-methyl-quinoline iodide (299.9 mg, 1 mmol) and *(E)*-3-methyl-2-(2-(N-phenylacetamido)vinyl)benzo[d]thiazol-3-ium iodide (439.3 mg, 1 mmol) in DCM (12 mL) was added Et_3N (300 mL, 2.2 mmol). The resulting dark blue mixture was stirred at room temperature for 24 h. To the mixture was added Et_2O (25 mL) over 1 h and the solid was collected by filtration and washed with Et_2O (3 × 20 mL). The crude solid was suspended in a 1: 2 (v/v) mixture of EtOH : Et_2O (21 mL) and stirred for 1 h and the solid was collected by filtration and washed with Et_2O (3 × 20 mL). The crude solid was then suspended in a 1:2 (v/v) mixture of Me_2CO : Et_2O (21 mL) and stirred for 1 h. The solid was collected by filtration and washed with Et_2O (3 × 20 mL) to afford TR as a dark blue solid. (0.4 g, yield: 84 %).

^{1}H-NMR (500 MHz, MeOD) δ 8.49 (d, J = 8.2 Hz, 1H), 8.25-8.19 (m, 2H), 8.02 (d, J = 8.5 Hz, 1H), 7.94 (t, J = 7.9 Hz, 1H), 7.72-7.68 (m, 3H), 7.49 (dd, J = 14.3, 7.9 Hz, 2H), 7.33-7.30 (m, 1H), 7.08 (d, J = 13.4 Hz, 1H), 6.45 (d, J = 12.5 Hz, 1H), 4.59 (q, J = 7.2 Hz, 2H), 3.76 (s, 3H), 1.56 (t, J = 7.2 Hz, 3H). ESI-MS for $C_{22}H_{21}N_2S^+$ ([M]$^+$): calcd, 345.14; found, 345.04.

3.2 Synthesis of 2TR

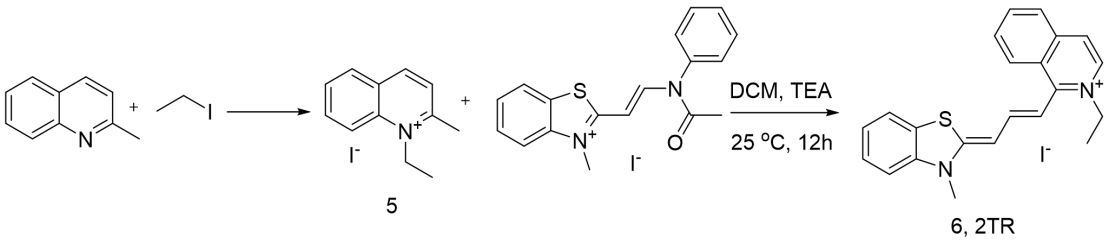

1-ethyl-2-methylquinolin-1-ium iodide (5) [S3] **:** In a clean dry 250 mL flask, 4-methylquinoline (1.3 mL, 10 mmol) and iodomethane (1.6 mL, 20 mmol) were added. Thereafter methyl cyanide was added to the mixture and the reaction was refluxed and stirred at 75 ℃ overnight. After removing the solvent by reduced pressure rotary evaporator, and then washed with ethyl, the yellow solid compound was obtained without further purification.

^{1}H-NMR (500 MHz, MeOD) δ 9.00 (d, J = 8.5 Hz, 1H), 8.57 (d, J = 8.9 Hz, 1H), 8.37 (d, J = 8.2 Hz, 1H), 8.27-8.24 (m, 1H), 8.03-7.98 (m, 2H), 5.07 (q, J = 7.3 Hz, 2H), 3.16 (s, 3H), 2.04 (s, 3H)

2-ethyl-1-((1*E*,3*Z*)-3-(3-methylbenzo[d]thiazol-2(3H)-ylidene)prop-1-en-1-yl)isoquinolin-2-ium iodide (6, 2TR) [S4] **:** To a suspension of 1-ethyl-2-methyl-quinoline iodide (298.40 mg, 1 mmol) and (*E*) -3-methyl-2-(2-(N-phenylacetamido)vinyl)benzo*[d]*thiazol-3-ium iodide (439.06 mg, 1 mmol) in DCM (12 mL) was added Et3N (300 mL, 2.2 mmol). The resulting dark blue mixture was stirred overnight at room temperature. To the mixture was added Et_2O (25 mL) over 1 h and the solid was collected by filtration and washed with Et_2O (3 × 20 mL). The crude solid was suspended in a 1: 2 (v/v) mixture of EtOH : Et_2O (21 mL) and stirred for 1 h and the solid was collected by filtration and washed with Et_2O (3 × 20 mL). The crude solid was then suspended in a 1:2 (v/v) mixture of Me_2CO : Et_2O (21 mL) and stirred for 1 h. The solid was collected by filtration and washed with Et_2O (3 × 20 mL) to afford 2TR as a purple solid. (0.4 g, yield: 84 %).

^{1}H-NMR (500 MHz, MeOD) δ 8.27 (t, J = 12.5 Hz, 1H), 8.06 (dd, J = 16.8, 9.8 Hz, 2H), 7.95 (d, J = 8.9 Hz, 1H), 7.86-7.76 (m, 3H), 7.53 (q, J = 7.2 Hz, 3H), 7.36 (t, J = 7.9 Hz, 1H), 6.55-6.51 (m, 2H), 4.61 (d, J = 6.1 Hz, 2H), 3.80 (s, 3H), 1.56 (t, J = 7.3 Hz, 3H). ESI-MS for $C_{22}H_{21}N_2S^+$ ($[M]^+$): calcd, 345.14; found, 345.08.

3.3 Characterize of TR and 2TR

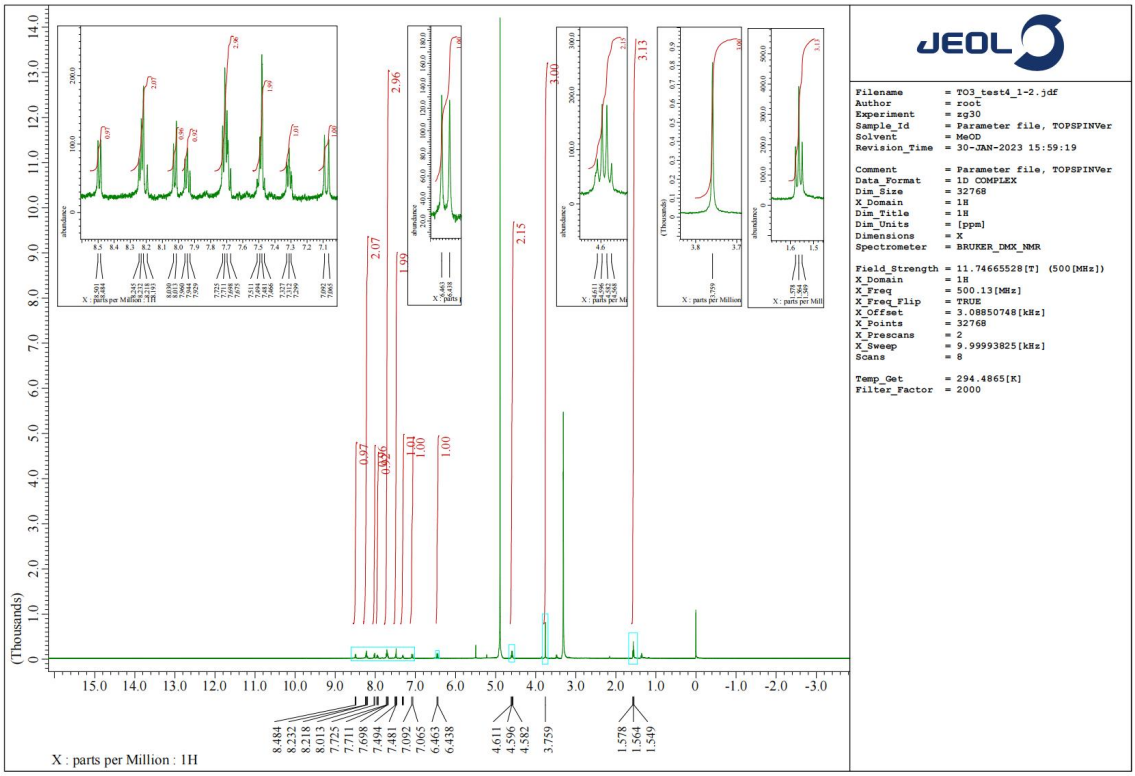

Figure 3.3-1 ^{1}H NMR spectrum of TR in MeOD.

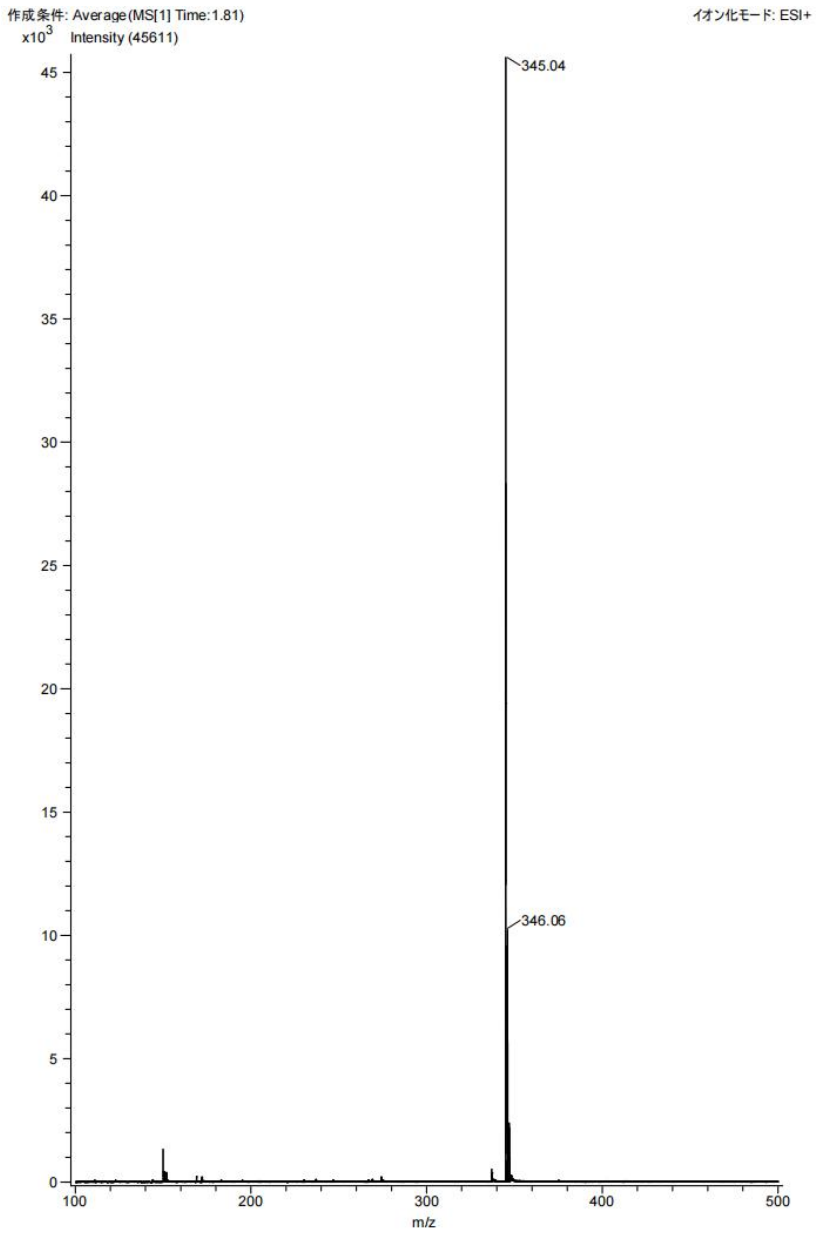

Figure 3.3-2 ESI-MS spectrum of TR in MeOH.

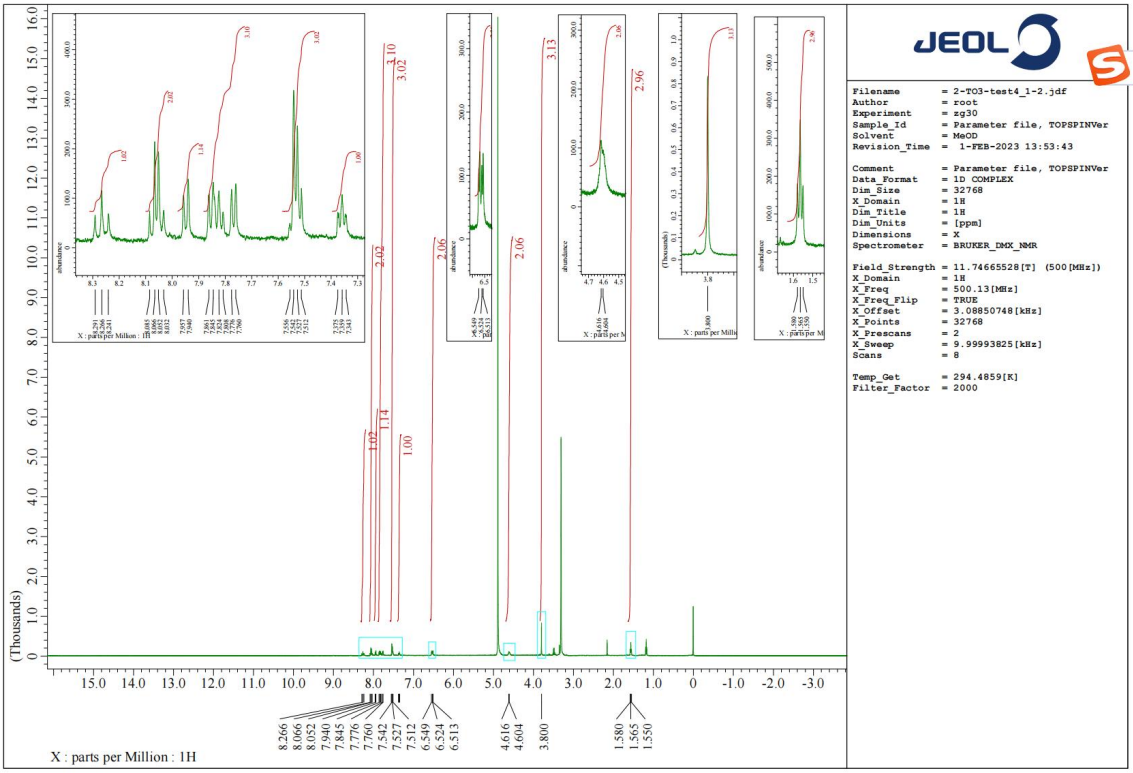

Figure 3.3-1 ^{1}H NMR spectrum of 2TR in MeOD.

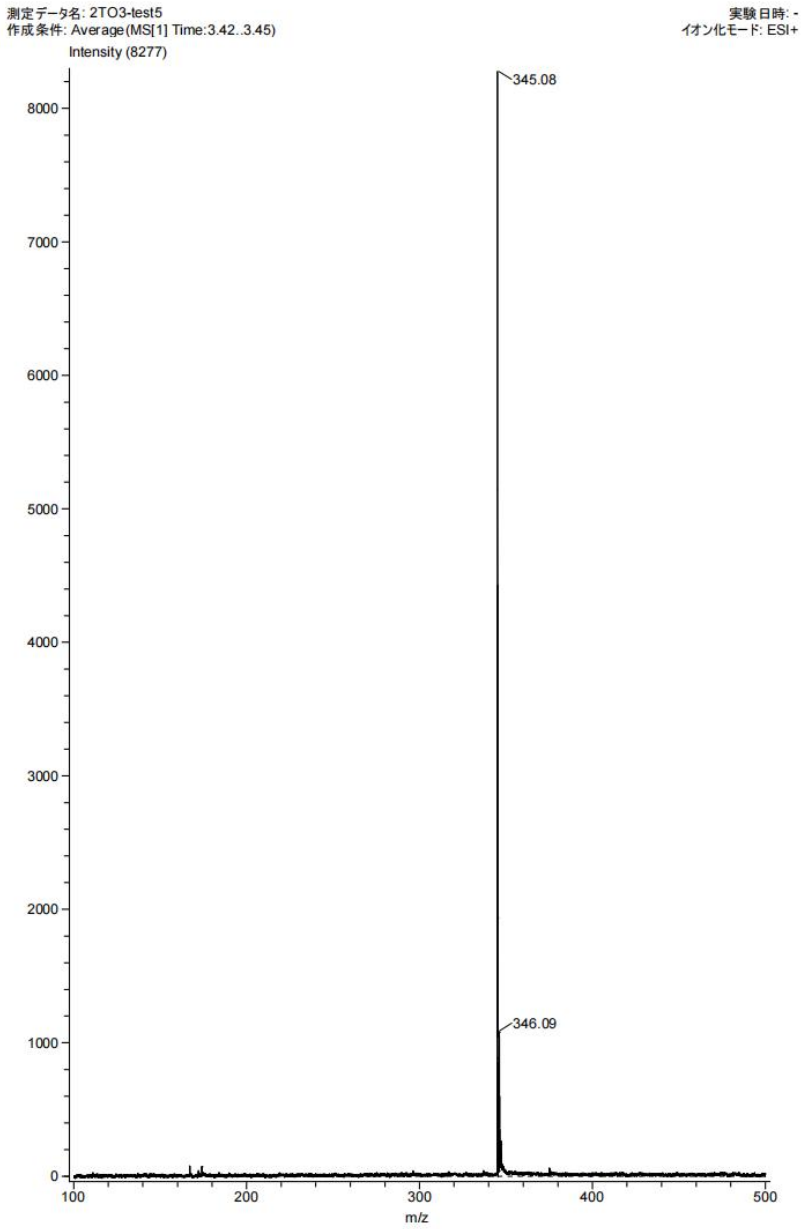

Figure 3.3-2 ESI-MS spectrum of 2TR in MeOH.

4. Absorption spectra of TR and 2TR

4.1 Absorption spectra of TR and 2TR in DMSO

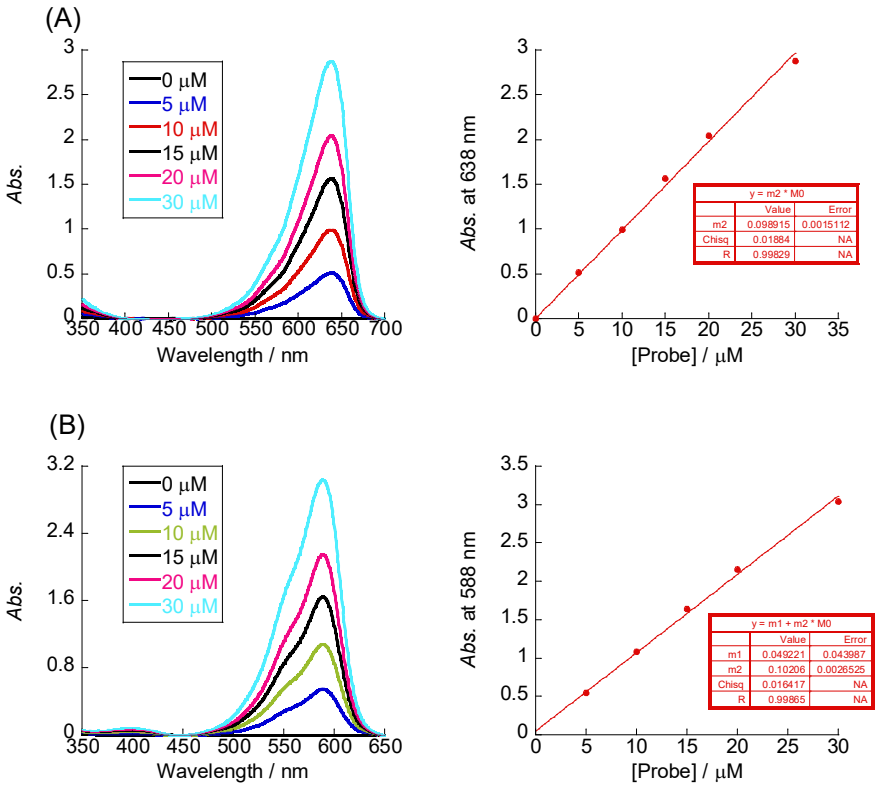

Fig. 4.1-1 Absorption spectra of (A) TR and (B) 2TR in DMSO and their curve fit line.

Experimental condition: [dye] = 0 - 30 μM, sensitivity: medium, data interval: 0.5 nm, scan rate: 100 nm/min, temperature: 25 ℃, cell: 1.0 × 0.2 cm, optical path 10 mm.

Molar absorption coefficient (ε): TR, 9.9×10^4; 2TR, 4.9×10^4.

4.2 Absorption spectra of TR and 2TR in phosphate buffer

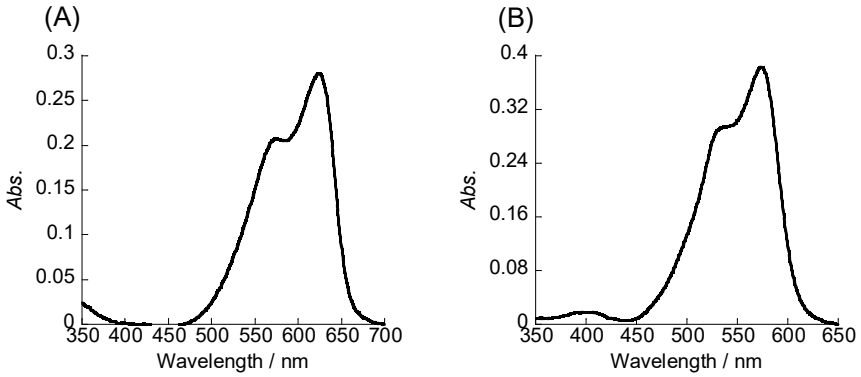

Fig. 4.2-1 Absorption spectra of (A) TR and (B) 2TR in 10 mM sodium phosphate buffer (pH 7.0) containing 100 mM NaCl 1.0 mM EDTA.

Experimental condition: [dye] = 10 μM, sensitivity: medium, data interval: 0.5 nm, scan rate: 100 nm/ min, temperature: 25 ℃, cell: 1.0 × 0.2 cm, optical path 10 mm.

The max absorption wavelength: TR, 624 nm; 2TR, 573 nm.

4.2 Absorption spectra of TR and 2TR in biological nucleic acid solutions

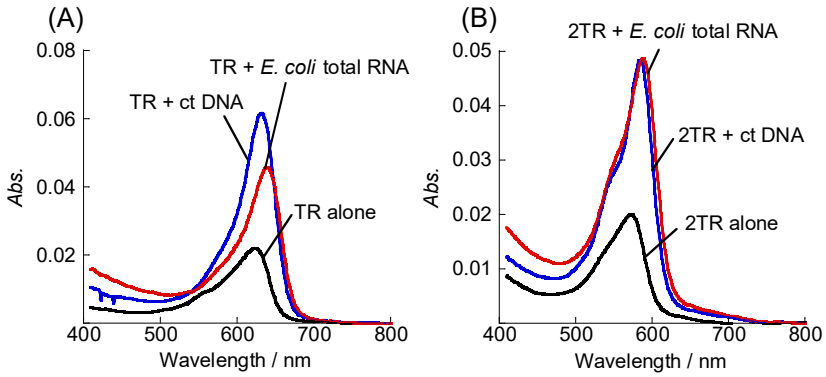

Fig. 4.3-1 Absorption spectra of (A) TR (1.0 μM) and (B) 2TR (1.0 μM) in the absence and presence of 1.0 mM calf thymus DNA or 1.0 mM *E. coli* total RNA. Experimental condition: [probe] = 1.0 μM in 10 mM sodium phosphate buffer (pH 7.0) containing 100 mM NaCl 1.0 mM EDTA, sensitivity: medium, data interval: 0.5 nm, scan rate: 100 nm/ min, temperature: 25 ℃, cell: 1.0 × 0.2 cm, optical path: 10 mm.

5. Reference

S1 Q. Shi, R. Sun, J. Ge, Q. Xu, N. Li, J. Lu, *Dyes and Pigments*, **2012**, *93*, 1506-1511.

S2 R.E.F. Boto, R. M. El-Shishtawy, P.F. Santos, L.V. Reis, P. Almeida, *Dyes and Pigments*, **2007**, *73*, 195-205.

S3 X. Han, X. Yang, Y. Zhang, Z. Li, W. Cao, D Zhang, Y. Ye, *Sensors and Actuators B: chemical*, **2020**, *321*, 128510.

S4 J. R. Carreon, K. M. Stewart, K. P. Mahon Jr., S. Shinb and S. O. Kelley, *Bioorg. Med. Chem. Lett.*, **2007**, *17*, 5182-5185.

Chapter 5

Conclusion

1. General conclusion

It is well known that nucleolus, a region that rich in rRNA, plays a crucial role in cellular activity and biological functions. However, on the one hand, current nucleolar RNA analysis methods such as molecular beacons and FISH are challenging to apply in living cells due to their large molecular weight structures, limiting their use to fixed and permeabilized cells. As a result, real-time monitoring and analysis of nucleolus are not possible with these methods. On the other hand, small molecular fluorescent probes, with their lower molecular weight and generally better cell membrane permeability, are more suitable for live cell applications. Unfortunately, commercially available and known small molecular fluorescent probes often have the limitations in terms of nucleolus imaging in living cells or low signaling ability. Therefore, developing small molecule fluorescent probes for nucleolus imaging accompanied with outstanding signaling ability is desirable. In our laboratory, we have independently developed small molecular cyanine dyes with remarkable nucleolar RNA imaging ability and outstanding light-up response, demonstrated the potential of cyanine dyes for nucleolar RNA imaging in live cells.

In chapter 2, the properties of TO itself and several TO derivatives, TO-H, TO-C_4, and 2TO were evaluated by a series of experiments. It was found that minor structural change will greatly affect probe functions. TO not only shows RNA selectivity over DNA in solutions, but also stains nucleolar RNA in the living cells and also fixed and permeabilized cells after 20 min incubation. Significantly, TO was even applicable to wash-free imaging of live cells. Apparently, TO itself is a promising fluorogenic probe for nucleolar RNA imaging in cells. More impressively, 2TO, a regioisomer of TO, worked much better. Compared to TO, 2TO showed superior selectivity for RNA in both solution and living cells, and its off-on signaling function (I/I_0 = 430-fold and $\Phi_{bound}/\ \Phi_{free}$ = 1200) was the top level among the probes developed so far for nucleolar RNA imaging in living cells.

In chapter 3, the first synthesized cyanine dye QB and its regioisomer 2QB were examined as RNA selective dyes. Both QB and 2QB were demonstrated as RNA selective dyes for nucleolar RNA imaging in living cells. Similar to TO and 2TO group, 2QB, the regioisomer worked much better with improved probe functions such RNA selectivity, signaling ability and photostability.

In chapter 4, the classical trimethine cyanine dye, TR and it's regioisomer were synthsized and their functions were examined. TR shows DNA selectivity in solutions and living cells with extremely poor photostability. Furthermore, 2TR, the regioisomer, was found to work as a promising red-emissive fluorogenic probe for nucleolar RNA imaging in living cells, showing pretty good off-on signaling ability, improved photostability and superior selectivity to RNA in both solution and living cells.

In conclusion, three kinds of typical cyanine dyes and their regioisomers were examined. Except for TR, the other cyanine dyes were found for the first time to work as nucleolar RNA selective dye in living cells, indicate that cyanine dyes are indeed good candidates as RNA selective dye. With greater significance, the regioisomers did work much better for all cases, which may provide a helpful strategy for designing RNA selective dyes in a way that regioisomer is key to improving probe functions.